ISBN: 978-81-939606-0-8

PROCEEDINGS OF

IIARP

International Conference

Date: 28th May, 2019 | Venue: Bangkok, Thailand

Co sponsored by

Conference Community.org

PROCEEDINGS OF

IIARP
INTERNATIONAL CONFERENCE

Date: 28th May, 2019

Venue: Bangkok, Thailand

Organized by

International Institute of
Academic Research & Publications

Co-Organizer

Conference Community

Corporate Address
IIARP
L/1483, HB Colony, Dumduma, Bhubaneswar, 751019
Odisha, India
www.iiarp.org

Publisher: **IIARP**

ISBN- 978-81-939606-0-8

Type set & printed by:
Pati Graphics
Bapuji Nagar, Bhubaneswar

About International Institute of Academic Research & Publications (IIARP):

The **International Institute of Academic Research & Publications** is an international non-profit academic association under 'Global Empowerment Trust®' with the stated goals of promoting cooperation among scientists, defending scientific freedom, encouraging scientific responsibility, and supporting scientific education and science outreach for the betterment of all humanity. It is the one of the world's largest and most prestigious general scientific society.

Objective of IIARP:

- To provide a world class platform to researchers to share the research findings by organizing International/National Conferences.
- To use the research output of the conference in the class room for the benefits of the students.
- To encourage researchers to identify significant research issues in identified areas, in the field of Science, Engineering, Technology and Management.
- To help dissemination of their work through publications in a journal or in the form of conference proceedings or books.
- To help them in getting feedback on their research work for improving the same and making them more relevant and meaningful, through collective efforts.
- To encourage regional and international communication and collaboration; promote professional interaction and lifelong learning; recognize outstanding contributions of individuals and organizations; encourage scholar researchers to pursue studies and careers in circuit branches and its applications.
- To set up, establish, maintain and manage centers of excellence for the study of /on related subjects and discipline and also to run self supporting projects for the benefit of needy persons, irrespective of their caste, creed or religion.

About Conference Community:

The **Conference Community**, a unit of "Global Empowerment Trust®" is known for Centre of Excellence for Technical Education, Research and development in Science, Engineering, Technology and Management in India. The Institute emphasizes on research based educational and academic deliverables which have high industrial and societal impact.

Conference Committee

Program Chair:

Dr. Mohd Helmy Abd Wahab
Dept. of Computer Engineering,
Universiti Tun Hussein Onn Malaysia

Dr. Dipti Patra
Associate Professor, Dept. of Electrical Engineering,
National Institute of Technology, India

Prof. A. Panda
Chairman, IIARP
Mail: chairman@iiarp.org

Conference Convener:

Mrs. A. Pattanayak
Mob: +91- 7328881295

Publication Head:
Mr. B. R. Mallick, IIARP, India

International Advisory Members

- **Dr. Moo Sung Kim,** College of Business, Zayed University, Dubai UAE
- **Dr. Mahboubeh Taghizadeh,** Iran University of Science and Technology, Iran
- **Prof.(Dr.)Wen-Lin Yang,** Dean, College of Science & Engineering, National University of Tainan, Taiwan
- **Dr. Pankaj Thakur,** Asst. Prof., Dept. of Tourism & Hotel Management, Arba Minch University, Ethiopia
- **Dr. Hoang Anh Tuan,** Vice Dean, Faculty of Mechanical Engineering, Ho Chi Minh city University of Transport, Vietnam
- **Dr. Dodo Yakub Aminu,** Senior lecturer, Dept. of Architecture, University Sains Islam Malaysia
- **Dr. Sunny Joseph,** HOD, Dept. of Mathematics, K. E. College, Kottayam, Kerala, India
- **Dr. Poonam Vyas,** Dept. of Humanities and Social Sciences, J K Lakshmipat University, Jaipur, Rajasthan, India
- **Dr. Ahmed A. Elngar,** Assistant Professor, Computer Science Department, Beni-Suef University, Egypt
- **Dr. Ahmad R. AlBattat,** Senior Lecturer, Management and Science University, Shah Alam, Malaysia
- **Dr. Arunachalam Kalirajan,** Senior Lecturer, Dept. of. Education of DMI St. Eugene University, Zambia
- **Mr. Yagyanath Rimal,** Lecturer, School of Engineering, Pokhara University, Nepal
- **Dr. Choen Krainara,** Office of the National Economic & Social Development Board, Office of the Prime Minister, Bangkok, Thailand
- **Dr. Nihar Ranjan Mishra,** Asst. Professor, Social Anthropology, Dept. of Social Sciences & Humanities, NIT, India
- **Prof.(Dr.)Aries Heru Prasetyo,** PPM School of Management, Jakarta Pusat, Indonesia
- **Prof.(Dr.) Narasimhaiah Gorla,** American University of Sharjah, Sharjah, UAE

TABLE OF CONTENTS

★★★

Editorial

I am delighted to welcome you all for the IIARP International Conference organized by **International Institute of Academic Research & Publications (IIARP)** in association with **Conference Community**. Good teaching emanates from Research. The teachers love for research and their experience in research are vital for the growth of the institution. Any institution is judged by the level and extent of the research work it accomplishes. This sets in a regenerative cycle of excellence. Experience of research leads to quality teaching and quality teaching imparted to the young in turn enriches the research. The campus dynamics needs such type of research teaching research environment.

The excellence of academic organizations or institutions are based on the level of their research. Research is indelible in teachers for uplifting the height of education, teaching and learning. Overall teaching faculty stands as the pillars for improving and enriching the current knowledge by adding new paradigms through innovations. The educationist utilizes his experience based on research in various facets for generating novel ideas which can ultimately elevate the system as whole.

Research and Education has thrown apart the geographical barriers and is walking on universal approach. Therefore is imperative to link technology for applications. Advancement in technology helps to reach the unreached, bringing the whole world under a roof. This will initiate a recreating progression of quality.

Intelligent minds of discoverers and inventors of the world has resulted in novel ideas and solutions. There are three unique resources to initiate discoveries, they are great books, great human beings and great teachers. Teacher's creativity, potentials and capacities will help to nurture the inventive and envisioning minds.

So this conference has been designed to stimulate the young minds including Research Scholars, Academicians, and Practitioners to contribute their ideas, thoughts and superiority in these disciplines of education/language/management/engineering. It is a pleasure to welcome all the participants, delegates and organizers to this Conference on behalf of International Institute of Academic Research & Publications.

This Publication/Seminars/Conference has received a great response from all parts of the country and abroad for the presentation and publication in the proceedings.

I sincerely thank all the authors for their valuable contribution to this conference. I am indebted towards the Reviewers and Board of Editors for their generous gifts of time, energy and effort for the Conference.

Editor-In Chief

Dr. Dipti Patra

Associate Professor,
National Institute of Technology, India

STATIC STRESS ANALYSIS OF GIRDER CROSS SECTION FOR MOBILE FOREST BRIDGE

[1]MOHD RIZUWAN M., [2]MOHD HISBANY M. H., [3]WAN MOHD SHUKRI W. A., [4]HAZRINA A.

[1,3]Forestry and Environment Division, Forest Research Institute Malaysia (FRIM), Malaysia
[2,4]Faculty of Civil Engineering, UniversitiTeknologi MARA, Malaysia
Email: [1]rizuwan@frim.gov.my

Abstract-- Forest bridge is one of the most important components in forest road network. Good forest road network allows implementation of sustainable forest management by carrying out post-harvesting activities. The bridges were needed when route without stream crossing could not being avoided. The permanent bridge structure would be easily collapsed due to storm and high velocity of water during the monsoon season. Numbers of permanent bridges are to be built along the route to the deep in the forest and high installation cost would be incurred. Therefore, a concept of modular and mobile would be the solution for the accessibility to the remote area in the forest. This proposed concept of forest bridge need a lightweight material and modular design for easy installation and handling. Design of modular and mobile forest bridge needs an optimum timber beam cross-section to be the girder in the bridge system. This cross section was the first parameter to be determined the modular design of forest bridge could be proposed. This study applied finite element method to determine the structural shape of timber beam for the forest bridge girder. The simulation was carried out with 3-point bending test under five load cases for Rectangular-shaped, I-shaped and T-shaped cross-section. Analysis of stress-strain, displacement, and volume have been carried out and recommended I-shaped cross section to be the structural shape of the timber beam.

Index Terms— Forest Bridge, Modular, FEA, Girder, Cross Section.

I. INTRODUCTION

Forest harvesting in Malaysia is currently being carried out deep inside the forest where accessibility is the main problem. This is particularly true when bridge is needed for stream or river crossing. Under the current logging road specification, temporary log stringer bridges are built for temporary usage which are removed or left to deteriorate at the end of the use period (Taylor et al., 1995). Almost any species of wood would allow usage less than three years. With a proper of culvert design and hardwood species for sill log, the service life could be extended (Chow, 2013). But this condition is subjected to site-specific soil and climatic conditions (Walbridge, Frankin, Griffiths, & Jarck, 1984). This situation leads into a problem to whoever needs to cross the stream for official or personal purposes such as Forestry Department (FD). This poses many problems when inspecting bridge timbers since often the damage is internal, leaving no visible signs of decay on the surface (Morison et al., 2002). Practically, FD will run forest and soil treatment in the logged over area for post harvesting activities in order maintains the forest health and treats the disturbed forest and soil. Most of the time upon completion of logging activities these temporary bridges are not maintained and will deteriorate and collapse due to high velocity of water flow, erosion and sedimentation (Leete, 2008).

Thus, post harvesting activities in the logged-over forests and other research activities inside the logged-over forest could not be carried out unless the bridge is repaired. As such there is a need to have a suitable cost-effective and easy to handle but durable bridge that can be used to access logged-over forest to carry out post-harvesting activities. Taylor et al., (1995) suggest for portable bridge which could be easily transported, installed, and removed for reuse at multiple sites. The ability to serve multiple installations could possible to reduce the construction cost compared to permanent structure besides of reducing potential water quality problems (Brinker & Taylor, 1997). Nowadays, there are numbers of portable bridges that have been developed in reducing the environmental impacts, but heavy machinery is needed to install and dismantle. Besides, those portable bridges are designed with limited span length and could only be applied in certain stream.

Current practice of forest road construction use native log as main structure especially as a stringer. The capability of the structure to sustain the applied loading depends on the design and material applied on it. Forest road network is generally constructed with a single lane and unpaved and exposed to the light vehicle at the early of the forest opening. However these roads exposed to extensive usage during logging operation where the heavy vehicles are used for logs transportation and may excess legal highway load. This road normally used only for a short period with a long usage cycle and this lead the management to close these roads whenever there is no logging activities (Taylor, Ritter, & Murphy, 1995).

However the disadvantages of current bridges are these bridges are designed for super heavy loads and activities which designed to use steel beam or solid timber as a stringer or girder. These structures need heavy machinery for installation and removal. Because of high installation and maintenance cost of

current bridge, there is a requirement to design a suitable and cost effective modular and mobile forest bridge that can be used to access logged-over forest for post-logging activities in this country.

This study propose the modular concept in designing the mobile forest bridge in order to solve the limitation of bridge length span and the maximum imposed loading. For normal bridge construction, size of bridge girder or deck already being earlier designed for on-site installation. These kinds of bridges are normally for permanent installation or portable bridge but with fixed bridge span. This span would not allow this bridge to be installed at other site for crossing. The expandable span of mobile bridge would give the forest manager better option of route selection for accessibility. However the design of this mobile bridge with expandable bridge span was focused on this study.

The design of modular and mobile forest bridge with lightweight material found to produce a reliable, low-maintenance bridge with capability to deliver high performance over the life of a bridge structure (Kannankutty & Flemming, 2000). The proposed bridge concept is expected to help forest manager to manage execute the post harvesting activities. The proposed bridge is installed at the stream site for crossing and the same the same bridge will be used for the next stream crossing. In this study, the span of the specimen was limited tosub-low volume category of bridges which is less than 10 m bridge span.

II. MATERIALS AND METHODS

Shape and material were the most significance factor that affected the result of the structure especially under bending. This selection was focus on cross section of the main girder which is the most important parts before further the analyses. Focus of this analysis was to select the structural shape of the beam which to be used in the next analysis. Abdollah & Hassan (2013) in the different study also use FEA to determine the suitable cross section for side door impact beam. In their study, four shape was analysed which are circular hollow, square hollow, I-type and C-type. However, only three shapes had been finalized for this study which were Rectangular-shaped, I-shaped and T-shaped (Figure 1). Analysis using finite element method had been carried out toevaluate the best cross section to be applied for timber beam.

The analysis was carried out using Autodesk Mechanical Simulation under Static Stress analysis in comparing result of stress, stain, deformations and deflections. In the Autodesk Mechanical Simulation, static stress analyses need to be defined at the beginning of setting when the program was started. The 3D model was automatically displayed with different colour to differentiate the loose parts in the model. All parts displayed in the simulation desktop should be renamed in order to ease the pre-processing process. The next activity was to mesh all parts in the model in order to create the elements and nodes. Defining the type of contact between parts would allow type of elements and nodes to be assigned for the type of connection. All parts of the specimen were set to be under surface type contact which means the models were separated and allowed to slide.

Three major steps in the simulation session were pre-processing, simulation processing and post-processing. In pre-processing, the first activities that were to be completed modelling of the geometry. In this case, 3D geometry modelling was completed using AutoCAD program before the simulation could be run. These models developed with solid modelling and assembled into a single layer. Unwanted objects in AutoCAD layer were erased and cleaned to avoid disruption during pre-processing of Finite Element Analysis (FEA). Volume intersection of 3D models checking were also being carried in AutoCAD program in order to display the intersection occur among 3D models. Final 3D models were transferred to simulation program with DWG format.

Meshing 3D models was the next activity and it should be approximate to the actual model. In processing part the process involved were mesh adaptation, numerical method and problem solver. The input required at this stage was the bounded error and the maximum iteration steps. However, for standardization in processing the iteration steps and error bounded were set to automatic which the best for that certain process. For post-processing, the result of simulation program was normally expresses in diagram, colour plots and etc. In this study the simulation result was expressed in stress, strain, deformation and displacement. These results of simulation were compiled and compare for further analysis.

Element Type

The element types that used in modelling the bridge affect the calculation of the flexural bending moment in all girders (Mabsout, Tarhini, Frederick, & Tayar, 1997). Finite element analysis program had offered options on element types, material behaviour and numerical solution controls. Besides, the program also offered an auto-meshers with graphic user interfaces, and sophisticated postprocessors and graphics to speed the analyses (Queiroz, Vellasco, & Nethercot, 2007). (Queiroz et al., 2007) in their study had used solid type of elements for the steel section and the concrete slab. The solid element is used for 3D dimensional modelling of solids. The nodes in solid element could vary from four-node tetrahedron to the 27-node brick element and eight-nodes brick element is the most common version (Tore,

Hopperstad, & Langseth, 2001). This type of element has eight-nodes and three degrees of freedom (translations) at each node. A suitable elements and appropriate solution techniques are important to obtain reliable results up to failure. In this study, solid type of brick element was used to be the main element type as (Minalu, 2010) who modelled girder flanges were as space frame elements, and flange-to-deck eccentricity as modelled by imposing a rigid link with isotropic, eight-nodes brick type of elements while (Jawad & Mohamad-ali, 2010) had modelled using a combination of eight-nodes shell elements and 3-node beam elements. (Uddin, Abro, & Vaidya, 2007), (R. M. Lin, 2011) and (Cheng, Zhao, Karbhari, Hegemier, & Seible, 2005) also in their study used eight-nodes brick type of elements.

The basic output generated from finite element analysis is the displacements which depended on the type of the element. The displacements which are translations and rotations are varied for each element and these referred as ‘degrees of freedom” (Modjeski & Masters, 2003) which were longitudinal displacement, transverse displacement, vertical movement, rotation about the longitudinal axis, rotation about the transverse axis, and rotation about the vertical axis (Alper, 2005).

Element Definition

Beside of element type, element definition also had to be setting up to those 3D models transferred from AutoCAD program. Both timber and aluminium had different grain structure and different material properties. For connector the element of aluminium was defined as isotropic and homogeneous as assumed by Aslam, (2009). This is because of this material properties were identical in all direction. This material model will only experience deflections in the elastic region of the stress-strain curve. A single modulus of elasticity and Poisson's ratio will be the requested material properties. While for timber beam the element was defined as orthotropic where the material properties are not same in all direction. This material model will only experience deflections in the elastic region of the stress-strain curve. The part may have different material properties in certain directions. Specifically, the material properties may be different in one or more of the three orthogonal directions in a rectangular coordinate system. The element properties for both aluminium and timber are as in Table 1.

Table 1:
Element properties for simulation (Eugene Kim & Andrawes, 2017).

Component	Material	Element type	Element Definition
Connector	Aluminium 6160-O	Brick	Isotropic
I-Beam	Timber	Brick	Orthotropic

After the meshing process completed the nodes and elemental propertiescould be calculated. Those generated elements and nodes was assigned and used in calculating the applied analyses. By meshing activity also the elements and nodes between connected parts could be defined. These elements and nodes would allow for setting up support condition and loading conditions at the individual element positions. The material properties could then be specified.

Material Properties

Most of analyses carried out in this study used timber as the main material for segmented beam. Western White Pine was selected to be the main material for the finite element analysis because the bending test for this species had been carried out earlier in a separate study.Material properties of timber that were used in the simulation are as in Table 2.

Table 2:
Material Properties for Western White Pine (Maloney et al., 2016)

Mass Density (kg/m^3)		425.338
Modulus of Elasticity (MPa)	Local Axis 1	11100.559
	Local Axis 2	868.739
	Local Axis 3	420.580
Shear Modulus of Elasticity (MPa)	Local Plane 12	577.091
	Local Plane 13	532.965
	Local Plane 23	55.848
Poisson's Ratio	Local Plane 12 (Major)	0.329
	Local Plane 13	0.344
	Local Plane 23	0.41
Thermal Coefficient of Expansion (1/℃)	Local Axis 1	3.06E-06
	Local Axis 2	2.21E-05
	Local Axis 3	3.06E-05

Second local axis of modulus of elasticity was applied for the calculation of allowable deflection. The result calculated for only comparison purposes.

Specimen description

In order to start the analysis, a few common structural shapes were finalized such as Rectangular, I and T shape. Dimensions of the beam were modelled with a standard size using AutoCAD program. The outer dimension cross sections were 80mm x 240mm which was the cross section geometry for the first 3D model. The other two models for I and T cross section, the geometry was based on the outer dimension of rectangular cross section (Figure 1).

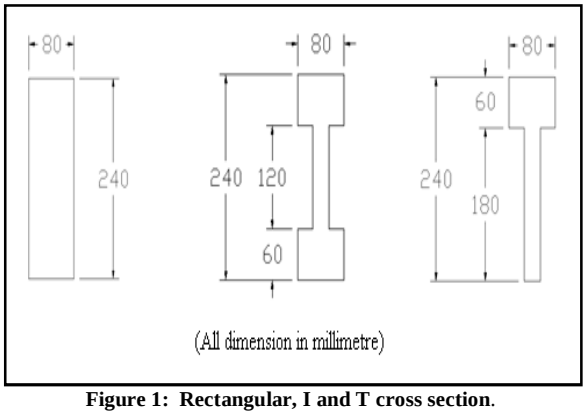

Figure 1: Rectangular, I and T cross section.

Three unit of 3D model specimen with different cross section with 10m beam span built using AutoCAD are as Figure 2. The unwanted objects in the AutoCAD desktop to finalize the 3D model before transferred to simulation program. These models would undergo the simulation of bending test under static stress analysis in Autodesk Mechanical Simulation program.

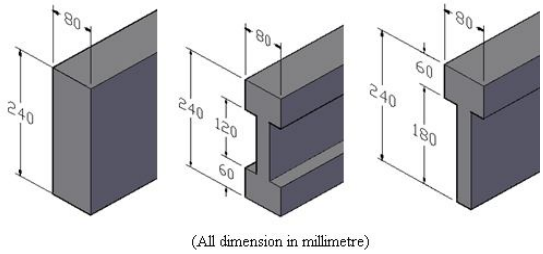

Figure 2: 3D model of Rectangular, I and T shape.

Element details

The clean model transferred to simulation program for meshing process and setting up the boundary condition. One of the most important parts dealing simulation was the meshing process. Meshing created element throughout the 3D CAD model which to be used in simulation process. These elements were bounded by number of nodes which interconnected with in the elements. Table 3 shows the information of the model for different cross section after the meshing process completed.

Table 3:
Detail information of the elements

Criteria	REC	I	T
Total nodes	3623	9379	5994
Volume (m^3)	0.192028	0.129619	0.098414
Total elements	2000	17006	8620

Test setup and loading

Three specimens were prepared in AutoCAD program with different cross sections which were Rectangular-shaped, I-shaped and T-shaped with 10 beam span. The model was exported into Autodesk Mechanical Simulation program under static stress analysis for the simulation of bending test. Loading was applied at the mid-span of the specimen as a nodal point force with downward direction. The simulation was repeated with 5 different load case started with 10.301kN, 20.602kN, 30.903kN, 41.204kN and ended with 51.503 kN. The result of stress, strain, deflection from the analysis with different load cases was recorded. Besides, volume parameter was also being analysed to compare the specimen with the different cross section. Schematic diagram for the static stress analysis in this section is as shown in Figure 3.

Beside of material selection, assignment of loading is one of the important steps in pre-processing. In this study, the assignment of loading is based on the 3-points bending test(Foster et al., 2017); (Ghazijahani, Jiao, & Holloway, 2017). Static load(Zheng & Fox, 2017) was assigned at the desired nodes on top of the specimen as nodal force with downward direction.Based on forest road and terrain condition from the main road to deep inside the forest, four-wheel drive vehicle is the best selection for transporting modular and mobile forest bridge for installation and dismantling for each stream crossing. The load design is based on four-wheel drive Toyota Hiluxwith double cabin which the Gross Vehicle Weight is approximately 3000 kg.

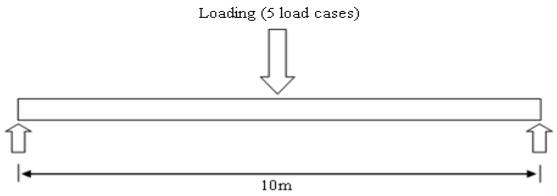

Figure 3: 3-point bending test on static stress analysis

For live load factor in load design is referred to ASSHTO HS20 which is 1.75 (Liu, 2007). The imposed load for the simulation is 51.503 kN (3000kg x 1.75 x 9.81 m/s^2). From Autodesk Mechanical Simulation, the maximum result of stress, strain and deflection could be extracted. Thus, in order to project the trend of the result five different load cases had been tabulated for simulation purposes. Those five load cases are 10.301 kN, 20.602 kN, 30.903 kN,41.204 kN and 51.503 kN were tested on the specimen in each section of the analysis. From these different load cases, the result of stress, strain and deflection were analysed.

The elements were bounded by nodes that were assigned to the boundary condition. Nodal point of loading is set at the mid-span of the beam. In this particular analysis, the selected support is at the surface of the beam end where these surfaces were set as fixed during the bending simulation. A setting of this boundary condition is standardized for all cross section. Different number of nodes in which assigned for support caused by the different cross-section of the beam and meshing processing completed with automatic mode (Figure 4).

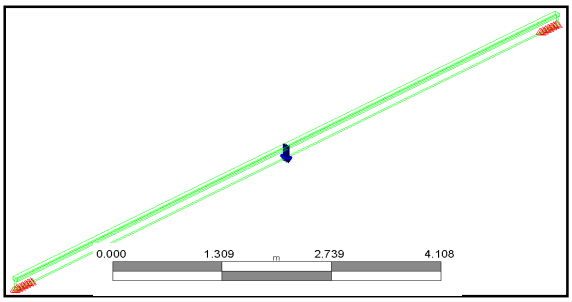

Figure 4: Boundary condition set up for the simulation.

However in completing the simulation a few assumptions were made, namely (i) the 3D models developed are assumed to be geometrically linear and responds to the system with linear elasticity (Minalu, 2010; Weaver, Davids, & Dagher, 2004;Bhashyam, 2002), (ii) the reinforcement between timber and CFRP laminates are perfectly bonded (Almusallam, Elsanadedy, & Salloum, 2015;Lin & Zhang, 2013;Park et al., 2010) and the results generated by the Static Stress analysis is not sensitively dependant on the selected mesh size (Park et al., 2010).

III. RESULT AND DISCUSSION

This study was to evaluate the respond of flexural bending on the beam with different cross sections. The analyses were completed finite element method under static stress analysis using Autodesk Mechanical Simulation program. The parametersevaluated were stress, strain, displacement and volume. The selected cross section for timber beam was determined for modelling the specimen. Three cross sections had been identified and the specimens were prepared with 10m beam span.

Stress strain analysis

Selection of timber beam cross section was based on the simulation result which was modelled with 10m beam span. Results of stress and strain were recorded with 5 different load cases. The results for Rectangular-shaped, I-shaped and T-shaped cross section were summarized into stress-strain graph as in Figure 5.

The result shows that the specimen with T-shaped cross section recorded the highest stress and strain vale among all cross section at 51.503 kN loading and followed by I-shaped and then Rectangular-shaped cross-section.

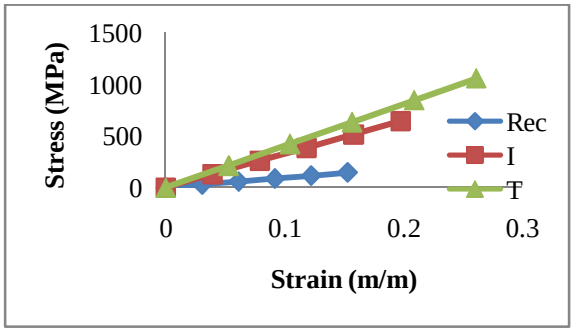

Figure 5: Stress-strain plot for Rectangular, I and T shape cross section.

Rectangular-shaped cross section recorded the lowest value of stress and strain among all of cross section. The simulation result also showed that stress distribution of a loaded beam that the greatest stress occurs at the top and bottom edges of the beam. Abdollah & Hassan (2013) has selected square hollow cross-section because of the capability of the specimen to sustain at the highest bending load before yielding. Amany & Pasini (2009) mentioned that the strain response of a beam strongly depends on the type of applied load. This led to the improvement on a rectangular section by introducing the I-section in which the large flanges were situated at a distance from the neutral axis. Therefore, I-shaped was preferred for the timber beam cross section.

Displacement analysis

Deflection analysis was the second evaluation to justify the selection the cross section for timber beam Rectangular-shaped, I-shaped or T-shaped. The simulation was based on 3-point bending set up to considered a centrally loaded and simply supported beam undergoing small and linear-elastic deformation (Amany & Pasini, 2009). Due to material and geometry, the slender of beam cross-section causes the deformation to be under non-uniform bending. In this analysis, the zero value of deflection was recorded at the support location on the 3D model. Therefore, only the maximum values of deflection which occur at the center of beam span were compared for cross section selection.

Figure 6 shows the deflection results from the simulation program and the allowable deflection calculated for reference purposes. The result showed that the highest deflection from T-shaped cross-section followed by I-shaped and then the Rectangular-shaped of the specimen.The deflection resulted from the simulation for51.503 kN loading was 0.3211m, 1.1521m and 1.7465m for Rectangular-

shaped, I-shaped T-shaped cross-section consecutively. The allowable deflection recorded for Rectangular-shaped, I-shaped T-shaped cross-section was 1.6752, 1.8234, 3.0602m consecutively. It is found that, all simulated deflections are within the allowable deflection. The beam cross-section is assumed to be uniform along its length with a homogeneous and orthotropic material.

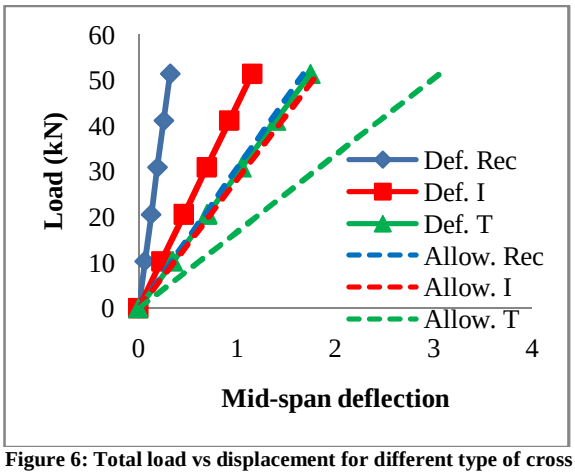

Figure 6: Total load vs displacement for different type of cross section.

The deflection result for I-shaped cross-section shows in the range between Rectangular-shaped and T-shaped cross section. In order to meet required stiffness, the minimum mass of a beam that yielded from cross-section size and shape, beam slenderness, and material govern were considered. The selection of the slenderness, shape and material is optimized the lightweight structure design(Amany & Pasini, 2009). Therefore, I-shaped cross section was suggested to be the structural shape for timber beam.

Volume analysis

As the study mainly to propose a modular and mobile concept of forest bridge, volume of timber beam is one of the main criteria should be considered during design stage because of linear relationship to the weight. The heavier structure would need number of manpower for installation of forest bridgeat the stream crossing site. Structural geometry and material are factors that would affect deformation and mass efficiency.Megson(2005)mentioned in that the yield lines are assumed to be plane and therefore the cross-section of the structure must possess a geometric compatibility. Abdollah & Hassan(2013)also choose the higher strength to weight ratio of material selection for their study. Therefore, the lighter weight of the parts in bridge structure would be prioritized.

Figure 7 shows the volume comparison of specimen for all different cross-sections. Rectangular-shapedcross section recorded the highest volume of timber beam followed by I-shaped and then T-shaped cross section T-shaped cross section contributes the lightest wright of timber beam among all cross section however, T-shaped cross section is not recommended based on stress-strain and deflection analysis. Thus, I-shaped cross section which the second choice in this volume analysisis recommended for girder cross section to ease in handling and installation processes.

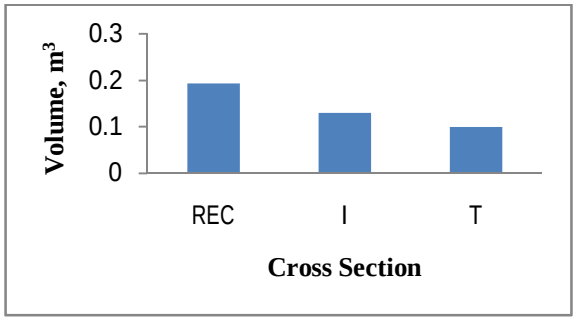

Figure 7: Volume comparisons for different cross section.

CONCLUSION

In conclusion, selection of structural shape for timber beam could affect the structural strength of the proposed modular and mobile bridge. Three different structural shapes had been analysed which are Rectangular-shaped, I-shaped and T-shaped cross section. The analysis shows that the specimens with different cross sections differently behave during the applied loading. Generally the Rectangular-shaped cross section show the strongest and the stiffest compared to other cross section. However, in order to implement the modular and mobile concept for forest bridge, I-shaped cross section was selected because of reasonable result of strength and stiffness result with lighter weight of the structure. This proposed modular mobile forest bridge is expected to solve accessibility problem and allow the forest manager to carry out post harvesting activities such as replanting activities and research activities after logging operation completed.

REFERENCES

[1] Abdollah, M. F., & Hassan, R. (2013). Preliminary Design of Side Door Impact Beam For Passenger Cars Using Aluminium Alloy. Journal of Mechanical Engineering and Technology, 5(1), 11–18.

[2] Almusallam, T. H., Elsanadedy, H. M., & Salloum, Y. (2015). Effect of Longitudinal Steel Ratio on Behavior of RC Beams Strengthened with FRP Composites : Experimental and FE Study. Journal of Composites for Construction, 3(2002), 1–18. https://doi.org/10.1061/(ASCE)CC.1943-5614.0000486.

[3] Alper, J. B. (2005). Rep roduced with permission of the copyright owner. Further reproduction prohibited w ithout perm ission.

[4] Amany, A., & Pasini, D. (2009). Material and shape selection for stiff beams under non-uniform flexure. Materials and

Design, 30(4), 1110–1117. https://doi.org/10.1016/j.matdes.2008.06.029
[5] Aslam, a. (2009). Finite Element Analysis of Stiffened Beam Column Connection. In Structures Congress 2009 (pp. 1–7). https://doi.org/10.1061/41031(341)291
[6] Bhashyam, G. R. (2002). ANSYS Mechanical — A Powerful Nonlinear Simulation Tool, (September).
[7] Brinker, R. W., & Taylor, S. E. (1997). Portable Bridges for Forest Road Stream Crossings. Alabama Cooperative Extension System, 6.
[8] Cheng, L., Zhao, L., Karbhari, V. M., Hegemier, G. A., & Seible, F. (2005). Assessment of a Steel-Free Fiber Reinforced Polymer-Composite Modular Bridge System. Journal of Structural Engineering, 131(3), 498–506.
[9] Chow, B. (2013). Engineering Manual.
[10] Eugene Kim, K.-H., & Andrawes, B. (2017). Load Rating of Deteriorated and FRP-Retrofitted Bridge Abutment Timber Piles. Journal of Bridge Engineering, 22(9), 04017058. https://doi.org/10.1061/(ASCE)BE.1943-5592.0001090
[11] Foster, R. M., Brindley, M., Lees, J. M., Ibell, T. J., Morley, C. T., Darby, A. P., & Evernden, M. C. (2017). Experimental Investigation of Reinforced Concrete T-Beams Strengthened in Shear with Externally Bonded CFRP Sheets. Journal of Composites for Construction, 21(2), 1–13. https://doi.org/10.1061/(ASCE)CC.1943-5614.0000743
[12] Ghazijahani, T. G., Jiao, H., & Holloway, D. (2017). Composite Timber Beams Strengthened by Steel and CFRP. Journal of Composites for Construction, 21(2014), 1–11. https://doi.org/10.1061/(ASCE)CC.1943-5614.0000714.
[13] Jawad, D. A. M., & Mohamad-ali, A. A. K. (2010). Analysis Of The Dynamic Behaviour Of T-Beam Bridge Decks Due To Heavyweight Vehicles, 15(2), 29–39.
[14] Kannankutty, R., & Flemming, D. J. (2000). Bridge Engineering. In Bridge Engineering (p. 10). https://doi.org/10.1126/science.45.1151.66
[15] Leete, R. (2008). Malaysia Sustainable Community:Forest Management in Sabah.
[16] Lin, R. M. (2011). Identification of modal parameters of unmeasured modes using multiple FRF modal analysis method. Mechanical Systems and Signal Processing, 25(1), 151–162. https://doi.org/10.1016/j.ymssp.2010.03.002
[17] Lin, X., & Zhang, Y. X. (2013). Novel Composite Beam Element with Bond-Slip for Nonlinear Finite-Element Analyses of Steel / FRP-Reinforced Concrete Beams. Journal of Structural Engineering, 139(12), 1–6. https://doi.org/10.1061/(ASCE)ST.1943-541X.0000829.
[18] Liu, Z. (2007). Testing and Analysis of a Fiber-Reinforced Polymer (FRP) Bridge Deck.
[19] Mabsout, M. E., Tarhini, K. M., Frederick, G. R., & Tayar, C. (1997). Finite Element Analysis Of Steel Girder Highway Bridges. Journal of Bridge Engineering, (August), 83–87.
[20] Maloney, P. E., Eckert, A. J., Vogler, D. R., Jensen, C. E., Mix, A. D., & Neale, D. B. (2016). Landscape biology of western white pine: Implications for conservation of a widely-distributed five-needle pine at its southern range limit. Forests, 7(5), 1–17. https://doi.org/10.3390/f7050093
[21] Megson, T. H. G. (2005).Structural and Stress Analysis.
[22] Minalu, K. K. (2010). Finite Element Modelling Of Skew Slab-Girder Bridges.
[23] Modjeski, & Masters. (2003). Comprehensive Design Example For Prestressed Arch ived
[24] Morison, A., Karsen, C. D. Van, Evensen, H. A., Ligon, J. B., Erickson, J. R., Oss, R. J. R., Service, U. F. (2002). Timber Bridge Evaluation : A Global Nondestructive Approach Using Impact Generated FRFs, 1567–1573.
[25] Park, J., Yindeesuk, S., Tjhin, T., & Kuchma, D. (2010). Automated Finite-Element-Based Validation Of Structures Designed By The Strut-And-Tie Method. Journal of Structural Engineering, 136(February), 203–210.
[26] Queiroz, F. D., Vellasco, P. C. G. S., & Nethercot, D. A. (2007). Finite element modelling of composite beams with full and partial shear connection. Journal of Constructional Steel Research, 63, 505–521. https://doi.org/10.1016/j.jcsr.2006.06.003
[27] Taylor, S. E., Ritter, M. A., & Murphy, G. L. (1995). Portable Glulam Timber Bridge Design for Low-volume Forest Road. In Proceedings of the 6th International conference on low-volume roads (Vol. 2, pp. 328–338).
[28] Tore, B., Hopperstad, O. S., & Langseth, M. (2001). Finite Element Modeling of Beams Under Concentrated Loading. Journal of Structural Engineering, 127(February), 176–185.
[29] Uddin, N., Abro, A. M., & Vaidya, U. (2007). Design and Analysis of Thermoplastic Composite Bridge Superstructures.
[30] Walbridge, T. A., Frankin, B. D., Griffiths, R. C., & Jarck, W. (1984).Forest road engineering. Forestry Handbook (2nd Ed.).
[31] Weaver, C. A., Davids, W. G., & Dagher, H. J. (2004). Testing and Analysis of Partially Composite Fiber-Reinforced Polymer-Glulam-Concrete Bridge Girders. Journal of Bridge Engineering, 9(4), 316–325. https://doi.org/10.1061/(ASCE)1084-0702(2004)9:4(316)
[32] Zheng, Y., & Fox, P. J. (2017). Numerical Investigation of the Geosynthetic Reinforced Soil – Integrated Bridge System under Static Loading.Journal of Geotechnical and Geoenvironmental Engineering, 143(6), 1–14. https://doi.org/10.1061/(ASCE)GT.1943-5606.0001665.

★★★

REFUSE DERIVED FUEL FROM GENERAL WASTE WITH POLYVINYL ALCOHOL AS BINDERS

[1]CHANAMON WIRIYAJARU, [1,2]CHAVALIT RATANATAMSKUL

[1]Environmental Engineering Department, Chulalongkorn University, Bangkok, Thailand
[2]Research Unit on Innovative Waste Treatment and Water Reuse, Chulalonkorn University, Thailand
Email: [1]mild-cw@hotmail.com, [2]dr_chawalit@yahoo.com

Abstract— The production ofrefuse derived fuel (RDF) from general waste in Chulalongkorn University that cannot be recycled was investigated. This can be an alternative way to reduce amount of municipal solid waste (MSW) as well as to reduce amount of fossil fuel consumption from RDF utilization. Here, the various mixtures of ground coffee, plastic and paper wastes inside Chulalongkorn University for RDF production were examined with the use of polyvinyl alcohol (PVA) as a proposed binder in RDF composition. The physicochemical properties (proximate and element analysis, heavy metal content, chloride content) and heating value of RDF were analyzed to determine the most appropriate composition for RDF production. It was found that at the mixing ratio of 5:1:3, [plastic : paper : coffee ground], RDF had heating value at 32.9 MJ/kg, compressive strength at 16.3 MPa and density at 737 kg/m^3. The addition of PVA as binder can achieve higher density and heating value of RDF production (with highest heating value, density and compressive strength at 33.3 MJ/kg, 869.5 kg/m^3 and 3.8 MPa, respectively). The average gas composition of RDF with PVA as binder at H_2 7.99%, CO 16.19% and CH_4 0.38% with the average heating value of fuel at 3.04 MJ/Nm^3. The obtained RDF had suitable physicochemical properties and heating value for the RDF to be used as co-fuel in combustion.

Index Terms— Refuse Derived Fuel (RDF), General waste, Polyvinyl alcohol.

I. INTRODUCTION

From Thailand state of municipal solid waste (MSW) report in 2016, the total of MSW amount was 27.06 million tons. Approximately 9.57 million tons of MSW was managed appropriately, 5.81 million tons of MSW could be recycled. The remain part of MSW was managed incorrectly and caused environmental problem in the area [14]. The context of MSW was negative trend since amount of MSW is increasing whereas disposal site still has not been improved. The rate of waste per capita in 2008 was 1.03 kg/capita/day while in 2016 was increased to1.14 kg/capita/day. Therefore, the rate of waste generation per capita has tendency to increase.

Energy is a fundamental factor in the needs of the citizens and the development of the country, both in the business and industrial part. As it stands in 2011, Thailand imported energy from foreign countries more than 60 percent of the total energy needs [8]. Therefore, transforming waste into the form of refuse derived fuel (RDF) to be used as a fuel to combustion process at high temperatures in cement industry is an alternative way to reduce the problems of MSW, and help reduce the amount of fossil fuel or other fuel usages as well as the import from abroad.

Refuse derived fuel (RDF) typically produced from combustible waste and non-hazardous waste that cannot be recycled. To make fuel with homogeneous physicochemical composition and higher heating value than direct combustion of MSW, RDF production is challenging.For example, the raw MSW has a typical heating value of 9.1 MJ/kg while the processed RDF has a typical heating value of 18 MJ/kg [13]

This research aims to reduce MSW by production of RDF, generated from general waste inside Chulalongkorn University as a case study, including ground coffee, plastic and paper waste with the non-recyclable part. The binder used in this research wasPolyvinyl alcohol (PVA).This research proposes the alternative method for the transformation of non-recyclable waste into RDF that has suitable properties for the combustion process at high temperatures in cement industry.

II. MATERIALS AND METHODS

1) Raw materials and preparation

The waste in the research were collected inside Chulalongkorn University as a case study though the Quartering Method. The samples were collected in July to September 2017. The non-recyclable plastic and paper wastes were separated from other fraction, and ground coffee from coffee shop.The plastic and paper wastes were reduced to the desired size though Shear Shredder, with approximately size of 2 cm.

2) Refuse derived fuel production

The compression of RDF was conducted at extrusion temperature 300 ˚C and pressure 150 bar with and without binders by using a Hydraulic Press Densifieras shown in Fig. 1. The obtained RDF was cylinder shape with a dimension of 6 cm.

Figure 1: Hydraulic Press Densifier

3) RDF Procedure

Refuse Derived Fuel (RDF) typically is the management of municipal solid waste that cannot be recycled in an effort to make fuel by improving and conditioning of waste such as removing non-combustible waste, size reduction and/or dying waste, etc. The RDF procedure is shown in Fig.2

4) Experimental procedures

To study the optimal amount of binder to obtain theRDF with suitable physicochemical properties (heating value, density,compressive strength, proximate and elemental analysis, chloride and heavy metals) The plastic waste, paper waste and ground coffee were mixed though mixer" at the ratio of waste 5:1:3 and with the binder in different amount. The amount of binder was varied to 10, 20, 30 and 40 %wt.

5) RDF characterization

The heating value was analyzed using a bomb calorimeter; the compressive strength was analyzed using a universal testing machine; the chloride was analyzed using a x-ray fluorescence spectrometer; the density was determined from equation 1.

$$D = M/V \quad (1)$$

Where: D is density of RDF (kg/m^3), M is mass of RDF (kg) and V is volume of RDF (m^3).

.

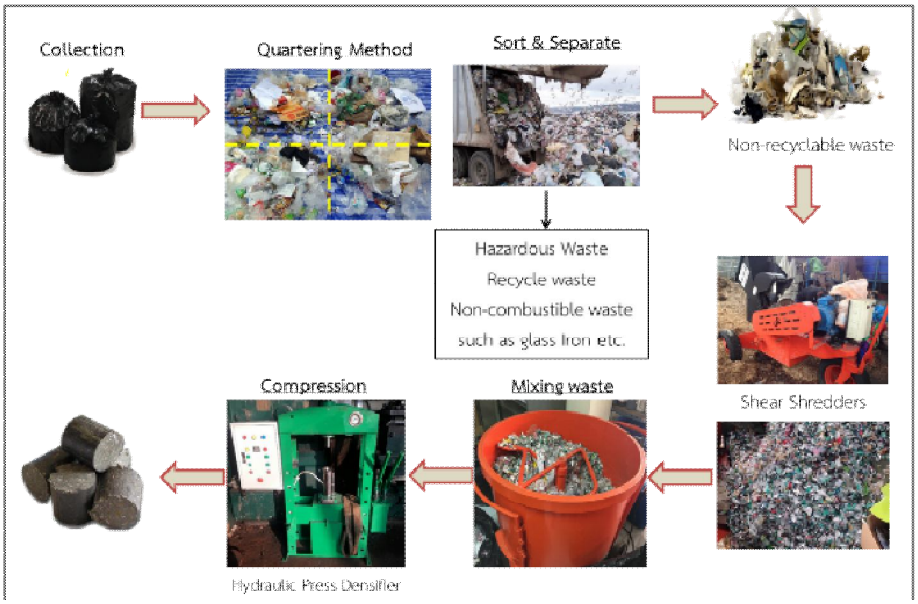

Figure 2: Flow diagram of RDF production procedure

Proximate analysis including moisture was analyzed according to ASTM E 790-87 [3], ash was analyzed according to ASTM E 830-87 [4], volatile matter was analyzed according to ASTM E 897-88 [5] and fixed carbon was determined from equation 2

$$FC = 100-(M+A+VM) \quad (2)$$

Where: FC is the percentage of fixed carbon, M is the percentage of moisture, A is the percentage of Ash and VM is the percentage of volatile matter

Elemental analysis (carbon, hydrogen, nitrogen and sulfur) was performed using a Elemental analyzer and Oxygen was determined from equation 3.

$$O\ (\%wt) = 100 - H\ (\%wt) - C\ (\%wt) - N\ (\%wt) - S\ (\%wt) - A\ (\%wt) \quad (3)$$

Where: O is the percentage of oxygen, H is the percentage of hydrogen, C is the percentage of carbon, N is the percentage of nitrogen, S is the percentage of sulfur and A is the percentage of ash.

Before heavy metal analysis, the preparation of RDF sampling was digested according to METHOD 3051 using a Microwave Digester and heavy metal was analyzed using a Inductively Coupled Plasma.

6) RDF combustion test

The combustion test of RDF through the downdraft gasifier (laboratory scale) of The Waste Incineration Research Center from King Mongkut's University of Technology North Bangkok. The air flow rate was adjusted to 300 L/min and gas sampling was collected a total of 3 samplings at a time when the temperature in the downdraft gasifier was constant. The gas composition was analyzed using a Gas Chromatography.

The heating value of fuel (G_{LHV}) is the amount of heat of fuel generated per 1 m^3 at standard temperature and pressure, G_{LHV} calculated from equation 4.

$$G_{LHV} = [(CO\%\times 12.63) + (CH_4\%\times 35.88) + (H_2\%\times 10.78)]/100 \quad (4)$$

Where: G_{LHV} is the heating value of fuel (MJ/Nm^3), CO is the percentage of carbon monoxide (g), CH_4 is the percentage of methane (g) and H_2 is the percentage of hydrogen (g).

III. RESULT AND DISCUSSION

1) Raw materials characterization

Table 1 shows elemental composition, average moisture content and heating value of raw materials used in the research. Plastic waste has the highest heating value in the range of 38.0-45.6 MJ/kg. Since plastic is a hydrocarbon compound, carbon and hydrogen are the major elements. The materials that have higher carbon and hydrogen contents; therefore, the heating values are higher. Ground coffee has the highest moisture content at 36.19 %wt. The moisture content depends on the season that collecting samples of waste. The materials that have higher moisture content and therefore, their heating values are lower.

PVA is a synthetic polymer. It has an adhesive quality and flammable as paper. The major elements of PVA are carbon and hydrogen as plastic. In this research PVA was used as a binder, it has heating value at 22.8 MJ/kg.

2) RDF physicochemical properties.

Generally, RDF binder can be divided into three (3) types: inorganic binder, organic binder and compound binder[10]. Polyvinyl alcohol can be classified as polymer-organic binder. The advantage property of PVA is its good cohesiveness. However, PVA is easy to be decomposed at high temperature, so briquette's thermal strength is poorer. Table 2 shows the properties of RDF as comparedto with and without binder at different amount of binder.The research found that RDF that non-used binder had heating value of 32.9 MJ/kg, compressive strength of 15 MPa and density of 724.4 kg/m^3. While RDF that used PVA as.

Table. 1 Elemental composition, average moisture content and heating value of raw materials.

Materials	C (%wt)	H (%wt)	N (%wt)	S (%wt)	moisture (%wt)	Heating value (MJ/kg)
Plastic waste	80.27	15.38	0.38	0.00	0.19	38.0-45.6
Paper waste	41.12	8.82	0.00	0.03	5.49	13.5-22.2
Coffee ground	23.36	9.31	0.89	0.07	36.19	21.0-21.8
PVA	50.02	9.50	0.00	0.05	6.21	22.8

Table.2 the properties of RDF as compared to with and witiout binder at different the amount of binder.

Ratio of waste (plastic : paper : coffee ground)	Amount of PVA	Density (Kg/m^3)	Compressive strength (MPa)	Heating value (MJ/kg)
5 : 1 : 3	Without binder	724.4	15.0	32.9
	10 %wt	767.5	3.8	34.2
	20 %wt	869.5	3.8	33.3
	30 %wt	806.9	3.3	30.9
	40 %wt	587.8	N/A	30.9

N/A not analysis due to RDF had lower density

Table.3 The physicochemical properties, heating value and chloride of RDF with PVA as binder.

Parameter	RDF with PVA as binder	Quality of RDF in UK	Quality of RDF in Italy
Proximate analysis			
• Moisture (%wt)	2.7	7.0-8.0	25.0
• Ash (%wt)	5.3	12.0	20.0
• Volatile matter (%wt)	89.2	68.0	
• Fixed carbon (%wt)	2.8	10.0	
Heating value (MJ/kg)	33.3	>18.7	
Chloride (%wt)	0.2	0.3-1.2	0.90
Elemental analysis			
• Carbon (%wt)	67.24		
• Hydrogen (%wt)	11.01		
• Oxygen (%wt)	16.40		
• Nitrogen (%wt)	0.05	0.50-1.00	
• Sulfur (%wt)	0.01	0.10-0.50	0.60

Figure 2:The RDF with PVA as binder at 20 %wt.

binder at 20 %wt had heating value of 33.3 MJ/kg, compressive strength of 3.8 MPa and density of 869.5 kg/m3. The addition of PVA as binder in RDF could increase density but decreased compressive strengthand heating value of RDF. Since PVA has a melting point 180 to 190 ˚C when compressed at higher melting point temperature, which resulted in PVA meltingand then after cold condition, PVA became hard and brittle. As a result, when applying the pressure to test the compressive strength, it was easily cracked. The lower compressive strength might be a consequence of non-uniform and non-homogeneous [12].

At amount of PVA 40 %wt, it inform the cylinder shape of RDF sincePVA is easily decomposed at high temperatures. When used in excess suitable amounts and compressed at temperatures above the melting point, which resulted in the melting than creating cohesiveness.

The heating value of RDF tended to decrease when increasing amount of PVA. At amount of PVA 0.1, it achieved the highest heating value at 34.2 MJ/kg.

The density of RDF affects the combustion reaction and gas production. The fuel with higher density reduced the rate of fuel consumption. Since, the RDF has resistant to combustion and long combustion time.

This RDF with PVA as binder had density of 869.5 kg/m^3. Also this RDF had density more than 600 kg/m^3 that can be classified as RDF-5 (densified RDF)

Table.4 The heavy metal content of RDF with PVA as binder

Heavy metal	RDF with PVA as binder (mg/kg)	UNI EN 15359 (Paolo et al., 2015) (mg/kg)	EURIT (2000) (Garces et al., 2016) (mg/kg)
Cu	17.1	500	200
Zn	45.4		500
Mn	15.0	250	200
Ni	7.6	30	200
Co	<0.5	18	200
Cr	9.2	100	200
Pb	3.2	240	200
Cd	0.8	4	10
Hg	<0.5		2
As	<0.5	5	10

for being used in fluidized bed combustor or multi fuel combustor (ASTM E-75). The higher density of fuel are desirable in terms of transportation, storage and handling [1]. The density of RDF depends on the density of theraw material used and the compressing temperature and pressure.

Fig. 2 shows the obtained RDF with PVA as binder at 20 %wt. And Table.3 shows the physicochemical properties, heating value and chloride of RDF with PVA as binder (20%wt) ,compared to thequality of RDF in UK and Italy.

Moisture content of RDF at 2.7 %wt, which is below the standard of quality of RDF in UK and Italy. As a result of the higher moisture content in fuel during combustion process, it generally decreases the heating value of fuel, lower quality and volume of gas produced.

Ash content of RDF at 5.3 %wt, which is below the standard of RDF quality in UK and Italy. The ash content depends on the raw materials to be compressed. The ash content of fuel tended to increase when using inorganic compound or biomass as raw materials. The fuel high ash content affects the fuel with lower heating value.

The volatile matter content of RDF at 89.2 %wt, which exceeds the standard of quality of RDF in UK. The volatile matter is the part of volatile of fuel including carbon, hydrogen and oxygen are component. The fuel with high carbon and hydrogen content tended to increase volatile matter content.The content of volatile matter affects the flammability of the fuel. If the surface molecules of fuel not remaining gas, the fuel is not flammable. As a result of high volatile matter content, it made the fuel easily ignite and highly reactive in combustion process.

Moisture, ash content and volatile matter (%wt) could provide a good indication of the combustibility of the MSW [13].

Fixed carbon is the stable part of the structure of fuel after determine moisture, ash and volatile matter. The fuel with high fixed carbon content that the fuel will have resistant to combustion. From the experiments, the RDF had fixed carbon content of 2.8 %wt, which is below the standard of RDF quality in UK. Increasing the amount of biomass as raw materials is increasing fixed carbon.

This RDF had a heating value of 33.3 MJ/kg, which exceeds the standard ofRDF quality in UK. The

heating value of fuel depend on moisture content and the heating value of raw materials to be compressed. This RDF had chloride content of 0.2 %wt., which lower than the standard of RDF quality in UK and Italy. This paper removes polyvinylchloride (PVC) plastic could cause decrease chloride content. The chloride content is key to quality of fuel. To chloride content, it is quite low in most cases, below 1 %wt.; being these wastes suitable for industrial combustion at moderate temperatures (850˚C), higher 1 %wt.; it would be necessary to raise the temperature to 1100˚C [9] to protect corrosion in furnaces and generation of acid gases emission such as hydrogen chloride (HCl) and polychlorinated dibenzodioxins (PCDDs) during combustion, which have effect on environment andhuman health.

The element composition of RDF: 67.24 %wt. C, 11.01 %wt. H, 16.40 %wt. O, 0.05 %wt. N and 0.01 %wt. S. The content of carbon, hydrogen and oxygen do not have standard limiting values. However the fuel with higher carbon and hydrogen contents have a higher heating value. While the content of nitrogen and sulfur below the standard of quality of RDF in UK and Italy. The fuels with high nitrogen and sulfur content, when used in the combustion process will result in a NO_x and SO_x as air pollution are the cause of acid rain, environmental pollution and acidic water resources. Furthermore, sulphation in the combustion chamber facilitates accumulation of HCl and vaporized salts [13].

The heavy metal contentsof RDF with PVA as binder are shown in table 4. This RDF had heavy metal content all of parameter lower than the limit of the standard UNI EN 15359 and EURIT (2000). Since this RDF was produced from general waste inside educational institution through direct random sampling with good separation and removed hazardous waste so that the waste is not significant contaminants of heavy metal.

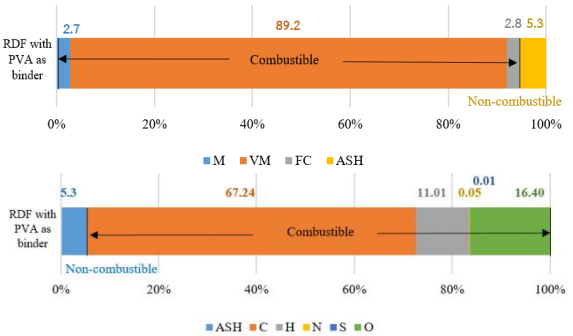

Figure 3. The composition of RDF

Where: FC is the percentage of fixed carbon, M is the percentage of moisture, A is the percentage of Ash and VM is the percentage of volatile matter O is the percentage of oxygen, H is the percentage of hydrogen, C is the percentage of carbon, N is the percentage of nitrogen, S is the percentage of sulfur.

Fig. 3 shows the composition of fuel, it can be divided into three parts as moisture part, combustible part (volatile matter and fixed carbon) and non-combustible part (ash). The RDF had combustible part at 92 % of fuel, moisture content at 2.7 % of fuel and non-combustible part at 5.3 % of fuel.

3) The combustion test of RDF

The combustion test of the RDF was performed by gasification process to produce the syngas. The gasification is generally a thermochemical process which converts fuel into gaseous components, containing carbon monoxide, hydrogen, methane and some other inert gases (ref?). Thegas sampling was collected a total of 3 sampling at time interval of 3 minutes each. Fig.4 shows the gas composition of RDF with PVA as binder and Table 5 shows the Summary of gas composition and heating value in fuel of RDF with PVA as binder.

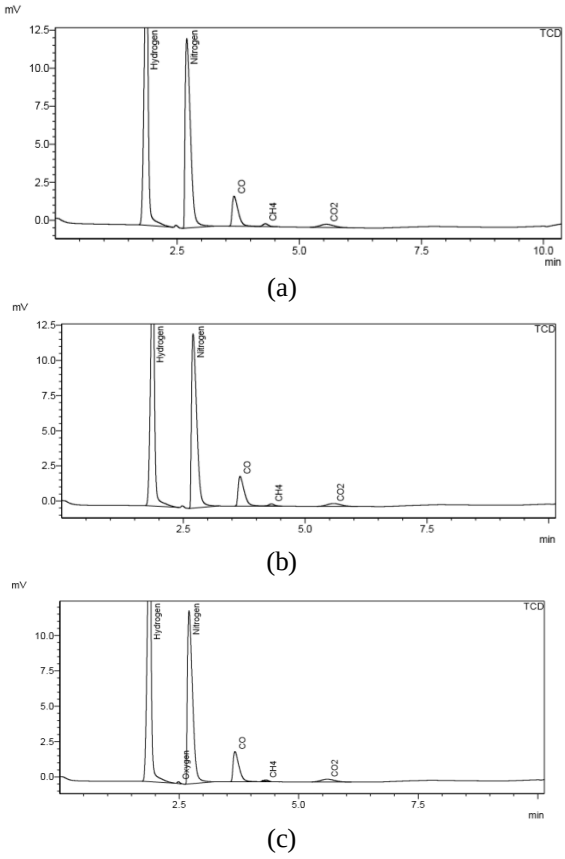

Figure 4. The gas composition of RDF with PVA as binder.
(a) 1st sampling gas
(b) 2nd sampling gas
(c) 3rd sampling gas

Table.5 Summary of gas composition and heating value in fuel of RDF with PVA as binder

Gas composition	1	2	3	Average
H_2 (%)	8.02	7.51	8.45	7.99
O_2 (%)	0.00	0.00	0.00	0.00
N_2 (%)	64.45	63.59	62.00	63.34
CO (%)	14.91	16.52	17.15	16.19
CH_4 (%)	0.53	0.44	0.17	0.38
CO_2 (%)	9.42	9.09	8.58	9.03
The heating value of fuel (MJ/Nm^3)	2.94	3.05	3.14	3.04

The syn-gas occurs within the time range of 10-110 minute of combustion time. The average gas composition of H_2 7.99%, CO 16.19% and CH_4 0.38% with the average heating value of fuel at 3.04 MJ/Nm^3.C.Chiemchaisri et al, 2010 also produced RDF from waste at open dump site applied to small scale down draft gasification process. They found that the gas composition consisted of H_2 0.02%, CO 9.86% and CH_4 0.96% with the heating value of fuel at 1.59 MJ/Nm^3 [6].S. Hirunprasertsri et al, 2014 also produced RDF from waste at landfill applied to down draft gasification process. They found that the gas composition consisted of H_2 4.00%, CO 2.59% and CH^4 1.95% with the heating value of fuel at 1.46 MJ/Nm^3 [15].

The gas composition of fuel depended on temperature in gasifier, composition of fuel, reactant with fuel and moisture content. For example,H. Boerrigter et al, 2006 found that the gas composition of gasification process depended on the gasification temperature. Syn-gas was produced by low temperature (below 1000˚C) with the syngas components of H_2 and CO typically contain only ~50% of the energy in the gas, while produced by high temperature (above 1200˚C) with completely converted into H_2 and CO [11].A. Tawitsri et al, 2016 found that when the amount of HDPE plastic in fuel high tended to increase volume of CO, CH4 and N2 but decreased volumeof H2 and CO2 [6].

4) The classification of RDF

The classification of RDF according to the standard ASTM E-75, this RDF can be classified as RDF-5 (RDF Densified) by means of the production of RDF from combustible waste through compress process with the density more than 600 kg/m^3. The RDF-5 is suited for use as fuel or co-fuel in Fluidized Bed Combustor or Multi Fuel Combustor. Furthermore, this RDF can be classified as RDF-7 (RDF Syn-gas) by means of the production of syn-gas from combustible waste through gasification process. The RDF-7 is suited for use to produce syn-gas in Burner orIntegrated Gasification-Combined Cycle (IGCC). If the RDF has high amount of plastic, it should be used in the combustion process at high temperatures in order to reduce air pollution and negative effects onto the environment.

Table.6 Summary of properties of Polyvinyl Alcohol as binder

Binder	Classification	Advantage	Disadvantage	Remark
PVA	Organic Binder-Polymer	• Good cohesiveness • High heating value • Low ash content	• High cost • Low compressive strength	Forming condition (Zhang el at., 2018) • Cold compress process • Forming pressure (300-350 bar)

CONCLUSION

Non-recyclable components of general waste has potential to produce Refused Derive Fuel (RDF). It is an alternative way to reduce the amount of MSW sent to the landfill and to reduce the amount of fossil fuel used in the combustion process at high temperatures.

The addition of PVA as binder in RDF, which resulted in RDF with low compressive strength but higher density and heating value when using PVA at 20 %wt. (most suitable amount of PVA). However, the density and heating value tended to decrease when increasing the amount of PVA higher than 20 %wt.

At the amount of PVA 20 %wt., RDF had highest compressive strength of 3.8 MPa, density of 869.5 kg/m^3 and heating value of 33.3 MJ/kg. The average gas composition consisted of H_2 7.99%, CO 16.19% and CH_4 0.38% with the average heating value of fuel at 3.04 MJ/Nm^3. The summary of properties of Polyvinyl Alcohol is shown in Table 6.

As for the physicochemical properties, overall results are satisfactory as below the standard limit.

The production of RDF from Universitywaste is feasible and the key of RDF production is collection and separation of waste by avoiding PVC plastic and heavy metal in waste. Since the quality of RDF depends on the raw material composition.

ACKHOWLEDGMENTS

This research is financially supported by Faculty of Environmental Engineering, Chulalongkorn University, Research Unit on Innovative Waste Treatment and Water Reuse, Chulalongkorn University and The Waste Incineration Research Center, from King Mongkut's University of Technology North Bangkok.

REFERENCES

[1] A. Demirbas, " Physical properties of briquettes from waste paper and wheat straw mixtures," *Energy Conversion & Management*, vol. 40, pp.437-445, 1999.

[2] American Society for Testing and Materials (ASTM),"Standard Test Method for Gross Calorific Value of Refuse-Derived Fuel by the Bomb Calorimeter E0711-87," (Reapproved 2004), 2004

[3] American Society for Testing and Materials (ASTM),"Standard Test Method for Residual Moisture in a Refuse-Derived Fuel Analysis Sample E0790-87," (Reapproved 2004), 2004.

[4] American Society for Testing and Materials (ASTM),"Standard Test Method for Ash in the Analysis Sample of Refuse-Derived Fuel E0830-87," (Reapproved 2004), 2004.

[5] American Society for Testing and Materials (ASTM),"Standard Test Method for Volatile Matter in the Analysis Sample of Refuse-Derived Fuel E0897-88, (Reapproved 2004), 2004.
[6] A. Tawitsri, and S. Sanitjai, "The study of gasification of municipal plastic waste in small scale downdraft gasifier," *The 8th Thailand renewable energy for community conference*, pp.62-65, 2016.
[7] C. Chiemchaisri, B. Charnnok, and C. Visvanathan, "Recovery of plastic wastes from dumpsite as refuse-derived fuel and its utilization in small gasification system," *Bioresource Technology*, vol. 101, pp. 1522-1527, 2010.
[8] Department of Alternative Energy Development and Efficiency, Ministry of Energy, Guideline for renewable energy from biomass gasification,2016.
[9] D. Garces, E. Diaz, H. Sastre, S. Ordonez,and J.M. Gonzalez,"Evaluation of the potential of different high calorific waste fractions for the preparation of solid recovered fuels,"*Waste Management*,vol. 47, pp. 164-173, 2016.
[10] G. Zhang, Y. Sun, and Y. Xu, "Review of briquette binders and briquetting mechanism," *Renewable and Sustainable Energy Reviews*, vol.82, pp. 477-487, 2018.
[11] H. Boerrigter, and R. Rauch, "Review of applications of gases from biomass gasification," Syngas production and utilisation, *Biomass Gasification*, pp. 211-230, 2006.
[12] J. Jamradloedluk, and C. Lertsatitthanakorn, "Properties of Densified-Refuse Derived Fuel using glycerin as a binder,"*Procedia Engineering*, vol.100, pp.505-510, 2015.
[13] L. Zhao, A. Giannis, W.Y. Lam, S.X. Lin, K. Yin, G.A. Yuan, and J.Y. Wang, "Characterization of Singapore RDF resources and analysis of their heating value," *Sustainable Environment Research*, vol. 26, pp. 51-54, 2016.
[14] Pollution control department, Ministry of Natural Resources and Environment, "Thailand state of municipal solid waste (MSW) report in 2016," 2017.
[15] S. Hirunprasertsri, and S. Booddee, "Experimental study to obtain gas production conditions from the old landfill solid waste by using gasification process," *SWU Engineering Journal*, vol. 9, pp. 16-27, 2014.

★★★

DEVELOPMENT OF PHOTOVOLTAIC HEATING SYSTEM

[1]NUR FAIRUZ MOHAMED YUSOF, [2]MAZWIN MAZLAN, [3]NOR SYAFIQAH SYAHIRAH BINTI MOHAMED

[1,2,3]Lecturer, School of Electrical System Engineering, University Malaysia Perlis, Malaysia
E-mail: [1]nurfairuz@unimap.edu.my, [2]mazwin@unimap.edu.my, [3]norsyafiqah@unimap.edu.my

Abstract— Photovoltaic (PV) is an electronic device that convert sunlight into electricity. This project was developed by using a 10 W PV as a power generator then the generated electricity is stored in a 12 V rechargeable battery. The charger control circuit is located between PV and storage element to prevent the overcharging. While the heating controlled by using Arduino Uno. This project implements a close loop temperature sensor which senses the rising of maximum temperature that can lead to loss of nutrients in the liquid. The heating control circuit is supplied with 5 V while the heating element circuit that includes a glow plug is supplied with 12 V. The heated temperature can be set to prevent liquids or water heated with overheated temperatures. This stand alone project can provide a facility for consumers to heat up liquids or water until its suitable temperature during off-grid.

Index Terms— Photovoltaic, Heating system, DC heating element, Arduino controller.

I. INTRODUCTION

Significant decrease of PV technology cost in the last decade has opened a new market with simple solar water heating systems combining the PV modules and direct current (DC) electric heating elements. Heating system is a method of heating something that has a low temperature to a high temperature. Heating methods that used solar energy have been widely used today such as generating electricity for supply to the mosque, solar water heater at home, solar energy lighting lamp and etc. The boiling point temperature of the water is 100°C. Domestically, water is traditionally heated in vessels known as water heaters, kettles, cauldrons, pots, or coppers [1].

Various of PV heating system are studied throughout these years. The method of using peltier heater for Vapour Phase Soldering (VPS) of components on printed circuit board (PCB) automated system [5]. Apart from that, method using a glow plug to increase the temperature in the diesel engine cylinder by passing electrical current through the glow light and can increase the start of the engine's characteristics. A glow plug electrically heated by a 12 V battery was used for igniting the fuel [6]. Since a glow plug is a heating device used to aid the starting of diesel engines in cold weather therefore it is suitable to be used in the heating system [4]. In 2016, a small scale Double Burner Smart Electric Stove project had been develop in Bangladesh due to it's energy crisis. The system has two burners that require a 1520 W solar power panel and two sets of 48 V lead acid batteries. The heating element used is the ordinary coil used in the AC stone with Pulse Width Modulation (PWM) controller to control the heat [8]. While in 2017, a solar thermal system for a single house family of four people is develop based on the PIC16F887 microcontroller as the system controller and coil as the heating element [9]. Based on previous method, the glow plug with Arduino controller is purposed to be used in the project due to its simplicity and low cost.

This project introduce a close loop temperature sensor which is used to detect temperature from rising to maximum temperature can lead to loss of nutrients in the liquid. In fact, the existence of this project can prevent wastage of electricity by continuously heating up. Once the water temperature reaches the level of suitable heating temperature the electricity will be automatically stopped. The heater will heat the beverage with the appropriate temperature to drink and will cut off when it reaches the appropriate temperature.

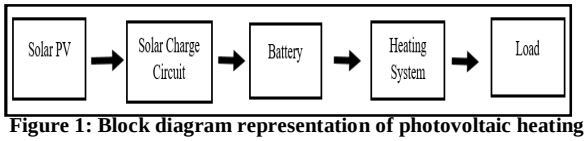

Figure 1: Block diagram representation of photovoltaic heating system.

The prototype consists of two parts which operate in different level with different characteristics, but in the same phase to produce a good working system. The first part of the prototype is the photovoltaic system that consists of solar PV module which acts as a power source by delivering the power converted from the sunlight to the energy storage. A 12W solar PV module was used. Then, the PV energy storage part is covered by two components, which are a charger control circuit and 12V rechargeable battery. The charger control circuit operates by keeping the battery properly charged by the solar PV module. As the battery is fully charged, the charge controller will cut off the current from the supply in order to prevent the battery from damaged. The second part is the heart of the prototype which is the heating system. This part consists of the temperature sensor to detect the temperature inside the container, the Liquid Cristal Display (LCD) displays which its function is to display the temperature detected by the sensor and

several Light Emitting Diode (LED) that indicated on and off heating process. Then the heating element in used is a glow plug. While the main controller within the input and output of heating system is Arduino Uno. Meanwhile, the load of this system is water or liquid.

II. SOFTWARE TESTING

Software Proteus 8 is used to assist in designing and simulating electronic circuits. This project also used Arduino Uno as the main component for controlling the system and respond to relays. The circuit contains several components such as LCD, LEDs, temperature sensor, relay, resister and Arduino Uno. The schematic diagram of the heating system circuit is shown in Figure 2.

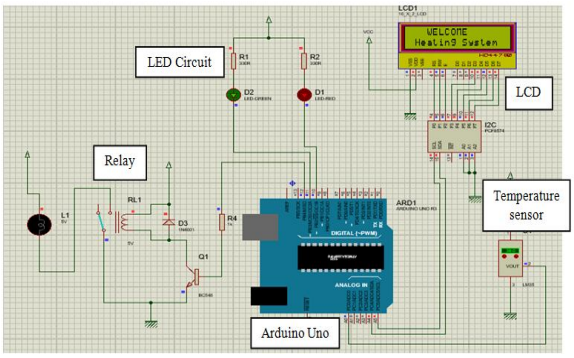

Figure 2: Simulation diagram of heating system.

In this project, Arduino Uno used port D for connection to 2 x 16 LCD through i2C, port B for LEDs connection and relay and port C for temperature sensor. The temperature sensor, LM35 is connected to Arduino Uno at pin A0 and act as the input to heating controller. The temperature can be calculated based on the ratio between the voltage capacities that can be counted by the Arduino analog pin (1024 or 10 bit) and the LM35 capability of measuring the temperature. The temperature can be determined based on equations (1). The 5V voltage change to 5mV and multiply with the reading from sensor. During prototype testing, the reading of LM35 sensor detect during the heating process is 81.92□. Therefore, the temperature is equal to 40 □.

$$\text{Temperature } (^{\circ}\text{C}) = \text{Reading (sensor)} \times \frac{5}{1024} x \frac{1000}{10} \quad (1)$$

Additionally, the LCD components using 5V supply are connected to Arduino pins 9, 8, 5, 4, 3 and 2. The LCD will display the temperature in the Celsius unit after getting input from the temperature sensor. The project also used LED that acts as the output of the heating system and to illustrate the current heating is in process or not.

Then, the main part is the Arduino coding process as shown in Figure 3. The initial coding part stated the fundamental integer in the coding for every component that contained in Protest 8 which connected to Arduino. To send signals from input to output, “digitalWrite” is used and determined by the setting HIGH or LOW. The "if (C <40)” coding states that the value below 40□ will follow the instruction in the " if () " bracket and if the value obtained other than the under 40□ will be directions under "else" coding. Each received signal will take one second to complete the next instruction. “analogRead” is used to read the sensor input located on the analog part of the Arduino since its read the sensor in analog form.

```
void loop()                          //method to run the source code repeatedly
{
 reading = analogRead(sensor);       //READ VALUE SENSOR
 C = (reading *(5.0/1024.0)*100);    //FOMULA READING TEMPERATURE
 lcd.setCursor(5,1);                 // 5-COLLUMN 1-ROW
 lcd.print(C);                       //LCD DISPLAY VALUE FROM C

if (C<40)                           // VALUE BELOW 40
{
  digitalWrite(LED_RED,HIGH);        // LED RED OFF
  digitalWrite(LED_GREEN,LOW);       // LED GREEN ON
  digitalWrite(RELAY,HIGH);          // LED GREEN ON
  delay(1000);                       //Update at every 100m Seconds
 }

 else                                //VALUE ABOVE 40

 {
  digitalWrite(LED_RED,LOW);         //LED RED ON
  digitalWrite(LED_GREEN,HIGH);      //LED GREEN OFF
  digitalWrite(RELAY,LOW);          //HEATER OFF
  delay(1000);                      //Update at every 100m Seconds
 }
```

Figure 3: Arduino main Coding

III. HARDWARE IMPLEMENTATION

The hardware prototype development is divided by two main parts which is the PV system and heating system. For the PV system, the battery as energy storage is controlled by the charger control circuit that control the voltage of the battery from overcharging and over-discharging by the voltage from the 12V PV module. When the voltage of the battery is below 12.5V, the PV module will charge the battery. Meanwhile, if the voltage of the battery surpasses 14.5V, the charger control circuit will cut off the supply from the PV module in order to prevent overcharging. This state indicates that the battery is fully charged. However, the battery can either be in charge or dump condition when the voltage level is in the range between 12.5V and 14.5V. The acceptable voltage of the battery for the system usage is between the range of 12.5V and 14.5V since the battery operating at normal condition in this range. The DC voltage of the battery is used to supply to the heating system. In addition, this battery has a capacity of 12 Ah that can accommodate to heat the heating element.

The second part is heating system, a glow plug in used as the heating element for this project. The 12 V relay is used to accommodate the voltage available on the glow plug connection and the flowing voltage will be cut off and render the state of relay from normally open to normally close or vice. In able to get the desired output, the power of the output reserves must be higher than the power required by the glow plug. Therefore the 12V glow plug with 60W power rating is selected. The rated current of the load can be obtained from the equation (2) which equal to 10A. Thus, to accommodate the calculated load current two glow plug being used in the prototype development.

$$\text{Load Current} = \frac{\text{Power}}{\text{Rated Voltage}} \quad (2)$$

Figure 4 shows the main circuit of the project that begins with the battery as the energy storage that generated from the PV module, followed by the charger control circuit as the controller to prevent overcharging. Then follow by the Arduino that control the input and outputs heating circuit.

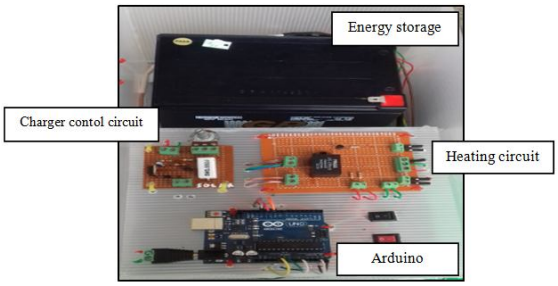

Figure 4: Hardware prototype of the overall system.

A T-shape metal stand was installed on the solar PV module for ease of testing process. The PV module will act as external power supply to the heating system and connect to the control charger circuit and battery. The heating chamber is used to facilitate the heating process, the material to be heat is place in the heating chamber. The overall view of the hardware prototype of the project is shown in Figure 4.

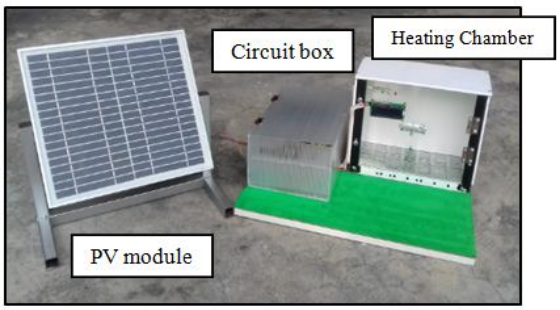

Figure 4: Overall view of the project.

IV. SIMULATIONS AND HARDWARE RESULTS

Simulation testing is done by using Proteus 8 software, at the beginning of the project, the LCD displayed words "WELCOME" and "Heating System". Then the temperature sensor displayed temperatures such as detecting temperature in the environment after the circuit works. Relays in the Proteus 8 only need to press the "+, -" symbol to detect the temperature to illustrated the real relay function. Once the LCD displays the value found sense by the LM35 temperature sensor, the main controller which is Arduino analyzed the received data and identified the value of the sensor either exceed the set value or less than the set value. If the analyzed data is less than 40□, Arduino will direct to turn on the green LED. All this process is shown in Figure 5.

When the green LED is on, indicating the heating process is happening and the relay operated according to instructions from Arduino to run the heating process. The relay will change from Normally Close (NO) to Normally Close (NC). The heating process continued until the sensor detects the temperature value reaches 40□. In the simulation, the used of the lamp as a symbol to indicate the heating process is happening when the light goes on.

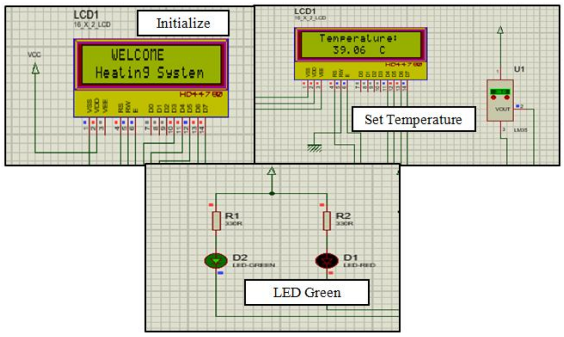

Figure 5: Simulation Testing.

After the temperature value reaches 40□, Arduino will analyzed for subsequent commands which is the red LED is on, it indicates that the heating process has been stopped. Thus, the relay changed the condition from NO to NC and the lamp symbol switch off. Figure 6 shows the heating process is in a state of condition working and not working. However at all times, the LCD will constantly displays the temperature values detected during that time.

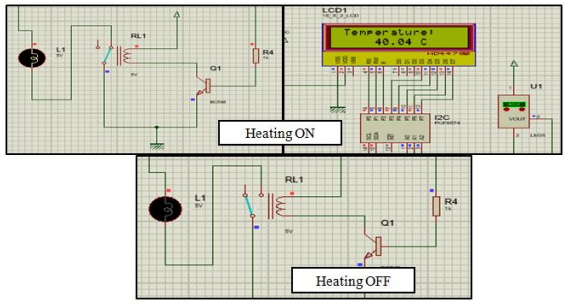

Figure 6: Simulation heating process.

The PV module generates electricity well when charging the battery. The charging process depends on the PV output generated on that day. When the weather is cloudy, PV is not efficient to charge the battery due to its low output of PV. In addition, the charging process runs fast when hot weather and PV can produce higher output. The charger control circuit works well during charging and discharging the battery. The rated voltage can be adjusted by using the potentiometer on the charger control circuit. The charger control circuit cutting off the power supplied from PV to the battery when the voltage rise above 14.5 V. Meanwhile, the battery is charged as the voltage fall below 12.5 V. The heating system circuit also produces a satisfactory output. The glow plug as heating element due to several factors and is

connected to the bottom of the prototype for heat absorbing from the bottom of the container and the heat can be delivered faster.

The complete hardware prototype is used in analyzing the heating process for a different material as shown in the Figure 7. The first testing is done by using a container of iron material. The container is insert in the heating chamber. Once the switch is on, the heat that being generated by glow plug is detected by the temperature sensor and displays the temperature on the LCD screen. The green LED light up to indicate the container containing the liquid being heated to reach the warm temperature. The container is heated at the bottom to ensure the heat is heated from the bottom and absorbed into the liquid. Then the second testing is done using a container of glass material. The used of different containers also affects the time for the fluid to become warm. The heating process is completed when the temperature in the heating chamber is detected has reached a warm level. After the heating process stops, the LCD display the temperature that detected by the sensor when the container in warm conditions. The red LED light up to indicate that the relay has changed from NO to NC.

Analysis is carried out on two different container materials which are glass containers and iron containers. The quantity and type of the liquid tested is the same for both containers in able to record the time allocated for the heating process. The time for each container heating is recorded in Table 1 and Table 2 respectively.

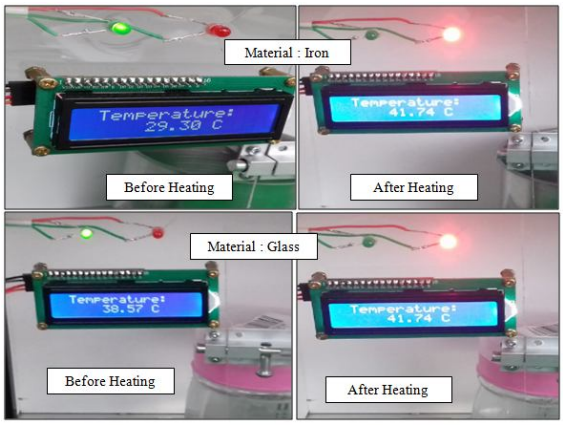

Figure 7: Hardware prototype testing for a different material.

Based on the tabulate data, the iron containers need a shorter time than glass containers. This is because the iron is a good conductor material for heating systems. Besides, the iron container quickly absorbs the heat from the heating element located at the bottom of the container. In addition, the container's thickness level also affects the heating time. When the container is heated, the temperature on the container increases and the heat from the container is transferred to liquid. Heat energy flows from higher temperatures to lower temperatures until the container and liquid reach the same temperature. Therefore, this testing shows that the increase in liquid heating time depends on the quantity of liquid.

Figure 8 shows the relationship between the heating time and the liquid quantity. In addition, the analysis is carried out using different diameter of iron container. The small container is used with a diameter of 4.8 cm while the large container has a diameter of 9.3 cm. The results obtained show small containers take shorter time for water to turn the condition into warm. Hence, different container sizes affect the time to heat the water.

Table 1: Heating time data using the iron container

Quantity of liquid (mL)	Temperature (°C)		Time (minute)
	Before	After	
50	29.75	42.23	10
100	28.99	41.35	18
150	29.45	42.15	25

Table 2: Heating time data using the glass container

Quantity of liquid (mL)	Temperature (°C)		Time (minute)
	Before	After	
50	29.54	41.74	12
100	29.75	41.22	20
150	30.23	41.12	32

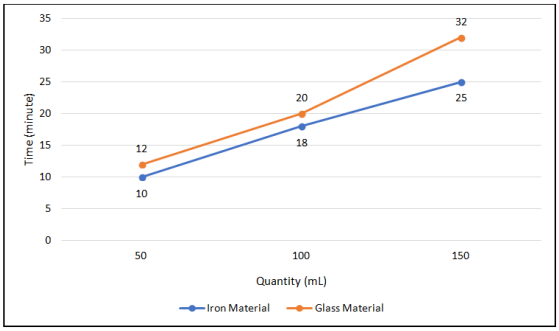

Figure 8: Data tabulate for a different material.

CONCLUSION

In this paper, a photovoltaic heating system was develops and analyze through hardware and software. The simulation was performed using Proteus 8 software while the hardware prototype consists of the PV module, charger control circuit, battery, Arduino as main heating system controller, glow plug as heating element. From the hardware testing, the prototype manages to heat both glass and iron container with same type and quantity liquid to a desired warm needed. Analyzes are carried out to determine the relationship between the heating temperature and the type of used materials. The heating process occurs until the heating temperature is detected at the maximum temperature level. Heating the iron containers is faster than heating of the glass container. The results have been found in good agreement with the analysis presented in this paper. Therefore, this paper recommends the proposed

system to support heating process during off grid since the PV module is able to act as supply source the the whole components.

REFERENCES

[1] "Water heating," *Wikipedia*, 15 Nov 2017. [Online]. Available: https://en.wikipedia.org/wiki/Water_heating. [Accessed: 01-Dec-2017].

[2] Ferguen, "Temperature and Measurement: Termometer," *FERGUEN.COM*, 29-Apr-2017. [Online]. Available: http://www.ferguen.com/2017/04/suhu-dan-pengukuran-termometer.html. [Accessed: 01-Dec-2017].

[3] Sulaiman Shaari, Ahmad Maliki Omar and Shahril Irwan Sulaiman, "*Fundamental of Solar Photovoltaic Technology"*, Sustainable Energy Development Authority of Malaysia, 2012.

[4] "Glowplug," *Wikipedia*, 10-Apr-2018. [Online]. Available: https://en.wikipedia.org/wiki/ Glowplug. [Accessed: 22-Apr-2018].

[5] M. L. Do, M. Novak, and I. Uhlir, " Applied Electronics," *Vapour soldering system with peltier heater*, pp. 1–4, Sep. 2009.

[6] B. Karthikeyan and K. Srithar, "Performance characteristics of a glowplug assisted low heat rejection diesel engine using ethanol," *Applied Energy*, vol. 88, no. 1, pp. 323–329, Aug. 2011.

[7] R. Dott, A. Genkinger, and T. Afjei, "System Evaluation of Combined Solar & Heat Pump Systems," *Energy Procedia*, vol. 30, pp. 562–570, 2012.

[8] S. Siddiqua, S. Firuz, B. M. Nur, R. J. Shaon, S. J. Chowdhury, and A. Azad, "Development of double burner smart electric stove powered by solar photovoltaic energy," *2016 IEEE Global Humanitarian Technology Conference (GHTC)*, 2016.

[9] V. D. N. Santos, M. Cerveira, and F. Moita, "Novel safety and energy management functions to solar water heating systems," *2017 International Conference in Energy and Sustainability in Small Developing Economies (ES2DE)*, 2017.

★★★

URBAN MOBILITY: CURRENT AND FUTURE CHALLENGES

[1]ROBERTO MONTEMANNI, [2]LUCA MARIA GAMBARDELLA, [3]FRANCESCA CELLINA, [4]FABIO CARTOLANO, [5]PAOLA COSSU, [6]ANDREA EMILIO RIZZOLI

[1,2,6]Dalle Molle Institute for Artificial Intelligence (IDSIA)
[4]Institute for Sustainability Applied to the Built Environment (ISAAC)
University of Applied Sciences of Southern Switzerland (SUPSI)
[4,5]FIT Consulting
E-mail: [1]roberto.montemanni@supsi.ch, [2]luca.gambardella@supsi.ch, [4]francesca.cellina@supsi.ch, [4]cartolano@fitconsulting.it, [5]cossu@fitconsulting.it, [6]andrea.rizzoli@supsi.ch

Abstract— SocialCar integrates carpooling with existing transportation modes in urban and peri-urban areas. The system is based on algorithms that plan routes for users and rely on a considerable amount of heterogeneous data. Social networks also play a role. Autonomous vehicles are emerging and will revolutionize transport. We try to understand the impact they could have in a system like SocialCar.

Index terms— Urban mobility, carpooling, public transportation, autonomous vehicles, self/driving cars, social media.

I. THE SOCIALCAR EU PROJECT

SocialCar is an EU H2020 research project that aims to develop an intelligent transport system based on an innovative approach to transport demand management, and more specifically to carpooling (also known as lift-sharing in the UK and ride-sharing in the US) in urban and peri-urban areas.
The overall objective is to develop a new communication network for intelligent mobility, sharing information on car-pooling integrated with existing transport and mobility systems. The SocialCar network is natively integrated into existing real-time public transport information and carpooling systems, ensuring an effective, high-quality, and enriched multimodal travel planning system for travelers. The platform takes advantage of social media and crowdsourcing practices to communicate, share information, and exchange useful transport data by means of innovative algorithms in order to allow the best just-in-time notifications to travelers.

During its lifetime, the SocialCar project has integrated multiple (public/private/social) data sets by means of powerful planning algorithms as leverage for promoting an effective carpooling service for citizens, making it a complementary transport mode that extends public transport networks. The integration of carpooling with the public transport network has proven that a social and intelligent mobility network deployment is feasible and effective. Big Data related to public transport, carpooling, and crowdsourcing are integrated in a livable environment in order to provide final users with a positive travel experience allowing comparison and choice between multiple options/services. The Route Planner and Ride Matching components of the architecture are described in Jamal et al. (2017). Interaction between users and the SocialCar system is managed through social media and the mobile app, both of which support the living community of users, as depicted in Figure 1. A conceptual architecture of the project is depicted in Figure 2, while an example of the solutions proposed can be found in Figure 3.

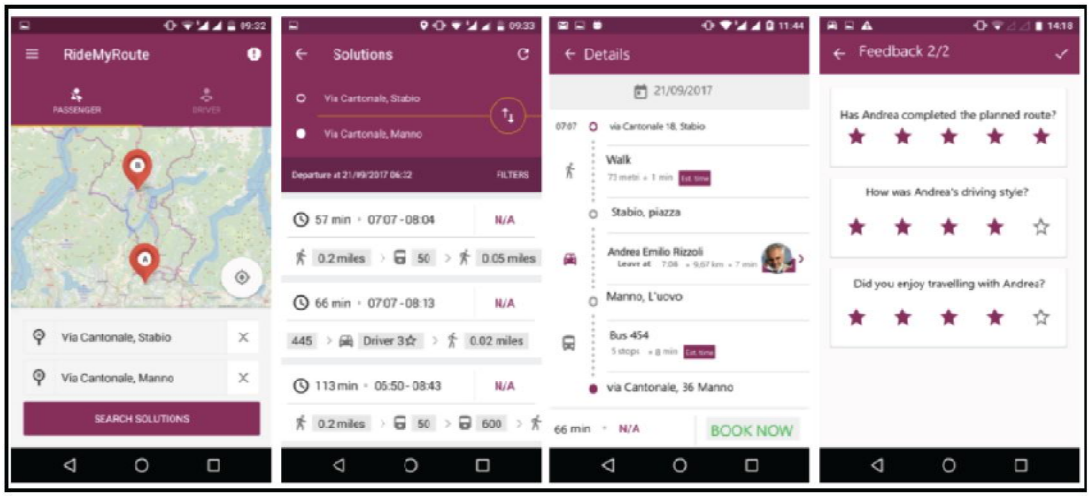

Figure 1: The SocialCar App. From left to right: the passenger indicates the desired starting and arrival points; the app outputs a list of available mobility options; the passenger selects one option and receives the full sequence of its legs; once the ride has taken place, both the passenger and the driver are requested to leave a feedback on each other.

SocialCar is not developing or establishing carpooling or on-demand car service software or services, so it is not competing with existing and established products such as UberX [3], Lyft [4], and Carma [5]. Instead, it is developing enhanced features that can be adopted by these and other existing services. These enhanced features will deploy an effective integration of public transport with carpooling and on-demand car services. Recent studies have shown that the attractiveness of carpooling has sometimes been decreasing [6] because of low fuel prices, and strong incomes [7].

The psychological barrier of riding with strangers is also likely to play a role [8]. However, the idea of integrating carpooling with existing transportation modes can potentially invert this negative trend. This is also corroborated by the very recent EU study presented in Finger et al. [9].

The involvement of 10 European urban sites – some of which already offered carpooling services at different maturity levels when the project started, and others of which have developed it during the project – allowed SocialCar to prove the concept's validity and business case, making for easier acceptance of innovative concepts and the consequent application into citizens' everyday life. Testing and validation of the SocialCar system in these sites has been coupled with the development of innovative and transferable business models for the sustainability and scalability of service provision, including their impacts on legal framework. This is the result of the joint effort and expertise of social, transport, and economic professionals within the project team, taking into account environmental, ethical, and security implications.

II. AUTONOMOUS VEHICLES AND URBAN TRANSPORTATION

The development of autonomous vehicles (sometimes referred to as *self-driving, driverless orrobotic* vehicles) has been rapid in the last few years, with remarkable progress motivated by both hardware and software improvements [10]. At the same time, intelligent transport systems are becoming increasingly cooperative and connected (C-ITS) thanks to new technologies (mobile telco, the Internet of Things, Big Data, and artificial intelligence among others and have enabled distributed computational processes in terms of locations and service provisions, all along the value chain.

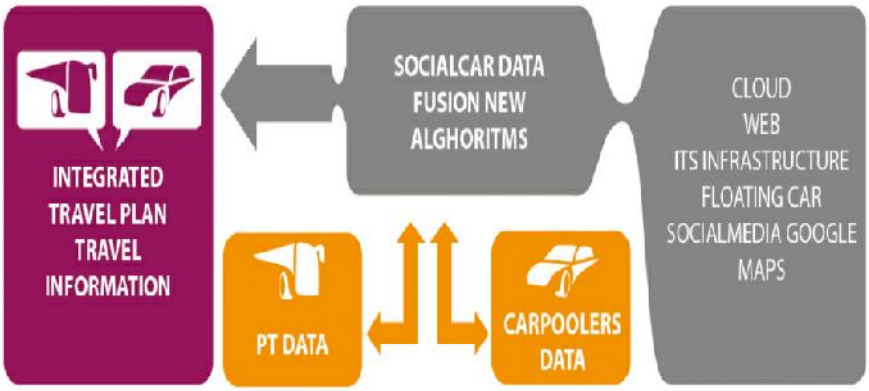

Figure 2: The SocialCar architecture.

Hence, the emergence of autonomous cars adds another relevant hint to this evolving framework, increasing the relevance of a deep interaction among infrastructure, vehicles, users; therefore, C-ITS have been declined in more specific terms referring to the digital transformation of infrastructures (smart infrastructure, C-Road) and vehicles (driverless cars, automated vehicles). The CITS wording itself has been extended in cooperative, connected, and automated mobility (CCAM), emphasizing the relevance of recent innovative features.

To date, most attention has been concentrated on the capability of autonomous vehicles to drive among human-driven vehicles, and to correctly interact with them on the road. Now the spectrum is enlarging and questions about the impact of such vehicles into general transport planning is becoming an important theme of discussion [11].

At the regulatory level, the European Commission is progressing in identifying suitable scenarios for this future mobility and industrial players (automotive, telco, infrastructure managers, telematics service providers) are strongly engaged in advancing the development of C-ITS and steering the public agenda in favour of services enabling cooperative, connected, and automated mobility, especially focusing on individual transport as key asset in respective markets. Their strategy is to reach and demonstrate effectiveness of new services in terms of traffic fluidity, safety, and comfort, and they aim to be well positioned in the future large take-up of driverless cars. For this reason, they have relevant influence toward the EU in bringing concrete demonstrations, setting standards, and promoting new regulations in favour of individual transports that can feed their markets.

Other institutional organizations (such as UITP [12] and Polis [13]) that are traditionally more inclined to promote the sustainable mobility through reducing land use and car ownership and encouraging collective transport, have shown a certain degree of caution, and even fear, regarding a potential unmanaged uptake of commodities of individual transport and in the future of driverless cars that, by changing the way people will "consume their travel experience", may have dramatic negative effects in multiplying individual transports and at the expenses of public transport [14, 15]. For this reason, they are strongly warning EU and national agendas about activating strategies and long-term policies for an integrated vision of future mobility.

Therefore, it is evident that there is a creeping conflict between the two categories above presented both trying to influence the position of Member States and therefore the EU agenda.

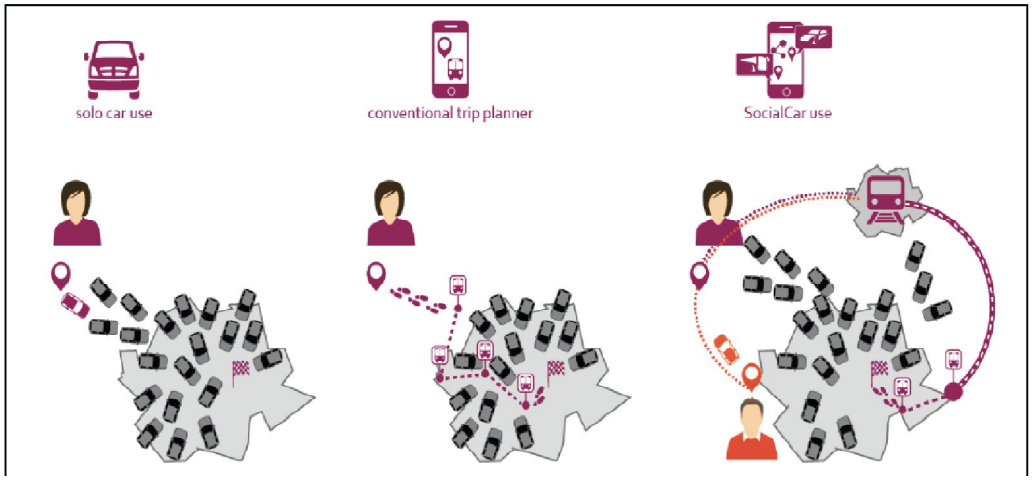

Figure 3: Example of the benefits of the use of the SocialCar App.

In addition, some authors have raised concerns about such an impact [16], and support the thesis that autonomous vehicles can be a benefit only if such vehicles are *electric* and *shared* among users.

In the optic of the present article, we are mainly interested in the latter condition: carpooling is an intrinsic form of sharing vehicles. We move further and combine the results of these studies [11,16] with those of [9], where it is forecasted that carpooling in urban areas is likely to be a reality only if integrated into other modes of transportation, in a Mobility-as-a-Service (MaaS) fashion. From an operational perspective, autonomous vehicles could be integrated in a platform like SocialCar as an *ondemand* transportation service. In the long term – studies refer to a period of approximately 30 years [11] – autonomous vehicles are likely to be the only ones left on the road, and in that case the role of applications like SocialCar, with their crucial carpooling component, will be likely to lose meaning. But before this relatively distant future, we believe that integrating carpooling into existing transportation modes (also including autonomous vehicles in the near future) is likely to be the only way to improve the liveability of our cities, while proving efficient transportation solutions for commuters.

CONCLUSION

The EU Project SocialCar has shown that integrating carpooling services with existing transportation modes can lead to concrete advantages for commuters in urban and peri-urban areas. The integration plays a key role in the success of such a system, together with the development of an appealing and intuitive interface able to also interact with modern social media platforms.

Experts forecast that the advent of autonomous vehicles into our everyday lives will happen relatively soon. They will definitely have an impact into urban transportation, and we believe their integration into a MaaS model could lead to something even more attractive and convenient for the users. Especially in a transition phase lasting for at least a few decades, the role of a system like SocialCar is likely to be extremely central.

REFERENCES

[1] "SocialCar = Public Transport + Carpooling = Social Media".http://socialcar-project.eu

[2] J. Jamal, R. Montemanni, D. Huber, M. Derboni, and A.E.Rizzoli, "A multi-modal and multi-objective journey planner for integrating carpooling and public transport," *Journal of Traffic and Logistics Engineering* 5(2), 2017, pp. 68–72.

[3] "UberX – Affordable, everyday rides". https://www.uber.com/ride/uberx/

[4] "Lyft – A ride when you need one". https://www.lyft.com

[5] "Carma – Mobile Technology for Verified Rides". https://www.gocarma.com

[6] N.D. Chan, and S.A. Shaheen, "Ridesharing in North America: Past, Present, and Future," *Transportation Reviews* 32, 2012, pp. 93–112.

[7] H. Park, and R. Gebeloff, "Carpooling Declines as Driving Becomes Cheaper," *The New York Times*, January 29th 2011.

[8] G. Correia, and J.M. Viegas, "Carpooling and carpool clubs: Clarifying concepts and assessing value enhancement possibilities through a Stated Preference web survey in Lisbon, Portugal," *Transportation Research Part A* 45, 2011, pp. 81–90.

[9] M. Finger, D. Kupfer, J.J. Montero, and M. Woled, "Research for TRAN Committee – Infrastructure funding challenges in the sharing economy," *European Parliament, Policy Depertment for Structural and Cohesion Policies*, Brussels, 2017.

[10] M. Ostrovsky, and M. Schwarz, "Carpooling and the Economics of Self-Driving Cars," *Technical report.* Stanford School of Business, 2018. https://web.stanford.edu/~ost/papers/sdc.pdf

[11] T. Litman, "Autonomous Vehicles Implementation Predictions: Implications for Transport Planning", *Victoria Transport Policy Institute*, 2018. https://www.vtpi.org/avip.pdf

[12] "UITP – Advancing Public Transport". http://www.uitp.org/

[13] "POLIS – Cities and Regions for Transport Innovation". https://www.polisnetwork.eu/

[14] The International Association of Public Transport, "Policy brief. Autonomous vehicles: a Potential game changer for urban mobility," *UITP* 2017. http://www.uitp.org/news/autonomous-vehicles-urbanmobility

[15] S. Hoadley, "Road Vehicle Automation and Cities and Regions", *The Polis Traffic Efficiency and Mobility Working Group*, 2018. https://www.polisnetwork.eu/uploads/Modules/PublicDocuments/polis_discussion_paper_automated_vehicles.pdf

[16] J. Leslie, "Will Self-Driving Cars Usher in a Transportation Utopia or Dystopia?," *Yale Environment* 360, 2018. https://e360.yale.edu/features/will-self-driving-cars-usher-ina-transportation-utopia-or-dystopia

★★★

INFLUENTIAL FACTORS TO CREATE AND STRENGTHEN THAI ELDERLY'S HEALTH EMPOWERMENT CLUB

[1]SUTHEP DACHACHEEP, [2]KANYARAT WORACHAT, [3]BORILUX BOONYARATTAPAN

[1]Assistant Professor, Ph D.,
[1,2,3]Faculty of Communication Arts, KasemBundit University, Thailand
E-mail: [1]suthep.dac@kbu.ac.th, [2]kanyarat.wor@kbu.ac.th, [3]borilux.boo@kbu.ac.th

Abstract— Aging society becomes a big issue in many countries including Thailand. Elders staying healthy to achieve successful aging is a key concern for government health promotion. There are elderly clubs created for the purpose of exercising together in public parks. Few clubs, however, remained for a long time. This study investigated influential factors that strengthen the elders' exercise club. Data was collected through in-depth interview of14 members from two selected exercise clubs. To indicate influential factors the concepts of Thai community empowerment indicators were modified. The factors then comprise of group leader, group members, group relationship structure, group management ability, and group activities.

Index Terms— Elderly, Elders, Health Empowerment, Exercise Club, Elderly Exercise, Successful Aging.

I. INTRODUCTION

Aging society becomes the big issue in many countries including Thailand. By 2035, the country's aging population is expected to reach 20 million, accounting for 30 percent of the population (Population Studies Center Research Report, 2015). Generally, in Thai family there has been 3 generations living under the same roof. This allows them to look after other members. However, the Thai family unit is being changed because of the modern way of life and aging society. There is an increase in Thai elders living alone or with spouse, but without their children. Elders are forced to be more self-reliant with longer life spans due to progress in medical science.

Staying healthy is a key concern for elders for long survival. There are several health promotion projects created from the government to encourage elders to take care of their health. Exercise and physical activity have been identified as a key public health strategy to improve both physical and mental health in the old age. There are elderly groups that have been set up for the purpose of exercising together in public parks. Types of slow dance exercise such as 'Tai Chi' and 'Qi Gong' are suitable and become favorites among those elderly's exercise groups (or health empowerment club in this research). However, only few groups have remained active today while others disbanded shortly after.
It is interesting to learn how those elderly's physical exercise groups continue actively. This research attempts to figure out factors behind the success. The research therefore was conducted to answer the question:

What are the factors influencing the creation and the longevity of Thai elderly's physical exercise (or health empowerment) clubs?

II. RELEVANT THEORIES AND RELATED STUDIES

There are relevant concepts and theories that are employed in this research, which are the definition of elderly people, The Activity theory, The Disengagement theory, and community empowerment concepts.

Definition of Elderly People

Although the Britannica encyclopedia states that most Western countries set the age of 60 to 65for retirement, the Thai Act on Older Person 2003 marks 'Older person' as a person who has attained the age of at least sixty years. Therefore, this research will use the Thai Act on Older Person 2003 to define 'elderly people'.

The Activity Theory

Academics try to explain the situation of 'growing old'. One popular theory is 'The Activity Theory' (Havighurt,1963), which is favored in the field of gerontology. The theory states that elderly people feel happy to join their activities as similar as they did in their middle age. [1] Therefore, to gain successful aging, "people should maintain the activities and attitudes of middle age as long as possible and the find substitutes for the activities which they must give up—substitutes for work when they are forced to retire; substitutes for clubs and associations which they must give up; substitutes for friends and loved ones whom they lose by death." [2]

The Disengagement Theory

Cumming and Henry (1961), meanwhile, proposed Disengagement Theory which states that in the process of aging people slowly withdraw themselves from society and activities they used to involve in the middle age. They generally curtail their social environment into what they feel is their comfort zone.

The disengagement process occurs universally, inevitably, and intrinsically.[3][4]

The disengagement theory has been criticized as it failed to explain the despair felt by some of the elders who are involuntarily disengaged. [5] However, it gradually regained the credibility as some research has proved that the theory is suitable for explaining the research result. Johnson & Barer (1992) proposed that some elements of Cumming and Henry's disengagement theory are relevant in understanding the social world of the very old. The theory was employed to discuss about elders with poorer health who redefine their level of social integration and are satisfied with a narrower and more constricted social world. [4]

Community Empowerment Concept

World Health Organization (WHO) defines Community empowerment as the process of enabling communities to increase control over their lives. Meanwhile "Communities" is referred as groups of people that may or may not be connected, but who share common interests, concerns or identities. In this context, the elderly's physical exercise club may be assumed as a 'community'.

Pointing specifically to the to Thai community, PrawaseWasi (1998) stated that the empowerment of Thai community means the ability of community members to continuously manage all kinds of situation. [6]

There were few thoughts of community empowerment indicators which have been used to express the strength of community. Among them, KanjanaKaewthep (2000) focuses on people (both in terms of quantity and quality), wisdom, property and group moral. [7] On the contrary, UtaiDulayakasem and OrasriNgamwitayapong (1997) determine empowerment indicators from horizontal social structure, self-sufficiency economic system, close relationship system, life learning process, etc. [8]

This research modified the concept of community empowerment and Thai community empowerment indicators to shape factors that may influence on the creation and strength of elderly's health empowerment clubs. The factors to be studied are; group leader, group members, group structure, group management ability, and group activity.

Table 1

Factor	Indicators
Group leader	trustworthiness, creativity, management ability, devotion, open-mindedness, etc.
Group members	cooperation on thinking and decision making, action, interaction, relationship system, etc.
Group structure	group balance and equality, knowledge exchanging, etc.
Group management	role and duty, norm, funding, group rule, etc.
Group activities	Exercising, economic activities, culture and society, etc.

III. METHODOLOGY

This research 'Influential Factors to Create and Strengthen Thai Elderly's Physical Exercise Club' was conducted as a part of the main research project 'Development of Communication Process to Create Strength for Elderly People Club of Health Empowerment in Bangkok'. It is a qualitative research aiming to study factors that influence the creation and the strength of elders' physical exercise club in public parks around Bangkok.Two long-standing exercise clubs from two public parks were selected to conduct the research. The two clubs are 'Qi Gong Suan Seri Thai Club' and 'TukMor Club at SuanLuang Rama 9 Park'.

Data was collected via in-depth interviews together with participant observations. The interview format combined structured and open-ended questions in a setting to allow interviewees to discuss freely. We interviewed 8 female members (age 62, 65, 69, 69, 71, 73, 80 and 86) and 6 male members (age 62, 64, 67, 71, 79 and 87) from the two selected clubs. Topics of interview questions included personal information, health questions, history of the clubs and the five influencing factors following the concepts of Thai community empowerment indicators.

Duration of participant observations and in-depth interview process took place at Suan Seri Thai public park and SuanLuang Rama 9 public park from January to June 2017.

IV. RESEARCH RESULT

After interviewing with 14 seniors from TukMor Club at SuanLuang Rama 9 and Qi Gong Suan Seri Thai Club, the results of the interview can be explained in five topics: group leader, group member, group structure, group management, and group activities.

Group leader: The study found that trainers or exercise leaders (or TukMor teacher and Qi Gong teacher) of both groupsare unofficially elected through respect from community members. Currently, there is only one exercise leader from each club and they both have been the club members for more than 10 years. The two leaders have been accepted as an important factor to create and strengthen the clubs from the past until now. The most admirable traits are self-discipline, devotion to coach at the public park without holiday, and willingness to teach or explain.

"The teacher is never absent. When we have problem with the exercise, he is willing to explain."
(member, 65 years old)

"She is really devoted and self-discipline"
(member, 69 years old)

Group members: The majority members of TukMor club at SuanLuang Rama 9 and Qi Gong Suan Seri Thai Club are retired from their work. Therefore, they spend more time exercising. Most of them are concerned with their health and accepted that exercising in public park allow them to enjoy a fresh environment. Some elders admitted that they prefer exercising with people at the same age group which they feel comfortable to talk to. However, through participant observation technique we found there were only small talk among elderly members. Mostly they come for exercising and then separate to go back home. Only small close group remain to talk to each other.

"exercise is good for health. I like TukMor slow dance. It is very fresh when we exercise in the park and have a little talk with friends"
(member, 64 years old)

"We never make a phone call for appointment. There is no need appointment. Teacher never stop so we can come every day"
(member,73 years old)

"I sometimes hang out with friends in the club. But not often because we have something to do"
(member, 61 years old]

Group structure: Apart from appointing exercise leader to be unofficially group leaders. There is another similarity between TukMor Club at SuanLuang King Rama 9 and Qi Gong Suan Seri Thai, in which they were both unofficially set up by a group of seniors. The objective of the clubs is to exercise together to empower their health. Therefore, the relationship among members involve equality and respect for each other. Though there are some members that gather in small groups and occasionally get together outside the club area, as a whole group the members' relationship is not very tightly knit.

"Actually, there is no leader. But I am the one who teacher them. So they give me respect."
(exercise leader, 80 years old)

"There is no hierarchy. Mostly people come to make their life better. They already think about healthy. Someone comes with friend, other comes and meet each other here"
(exercise leader, 67 years old)

Group management: According to the unofficial setting, the two clubs have nomanagement standard form. The decision making, therefore, depend mostly on the exercise leaders of the clubs.However, there are volunteer coordinators (selected from the club members) to help manage activities apart from group exercise, such as to distribute news and extra information.

"I leave it to the teacher to make any decision. She is senior and stay with the club since the beginning"
(member, 62 years old)
"Qi Gong club we have the teacher's secretary to cooperate."
(member, 71 years old)

Group activities: The main activity of the two clubs is physical exercising. Apart from this there is only one activity that allows members a chance to develop relationships. TukMor club manages 2-day trip together once a year in March. While Qi Gong club prepares lunch party at the club founder's house.

"We have a party once a year. Around March we stop for days and went out together. There is no compulsory. It you want to go then buy a ticket."
(Member, 79 years old)

"We get together once a year and go to the temple together"
(member, 87 years old)

CONCLUSION AND DISCUSSION

After analyzing the influential factors to create and strengthen Thai elderly's health empowerment club, we found that the clubs' members consider exercise leader is considered important to the club. Self-discipline, devotion to lead the group exercise without holiday make member confidence in the club, aligned with the concept of community empowerment indicators. By Kaewthep (2000) in term of quality people.

Regarding the club members, as most members are elderly with the age over 60 and retired from work, they have extra time on their hands. These elderly members pay more attention to their health and exercise. Interestingly, the relationship among members is that they do keep some space between each other. Polite words are used to communicate.

The club members mostly come to join the exercise. They have little talk to each other then split to go home. There are only few small groups that stay longer to meet with their groups. Besides, the two clubs have other activities that allow all member to join and getting to know more about each other, but only once a year. This situation may be explained by Activity theory combining with Disengagement theory. The research demonstrates that elderly members of the two group are willing to join the activities. This harmonizes with the Activity theory of Havighurst [1,2]. On the other hand, elderly members prefer to keep close relationship among their small group while keep some distance to other members. This can be explained by Disengagement theory that when people get older, they redefine their level of

social integration and are satisfied with a narrower and more constricted social world (Johnson & Barer, 1992). As they are getting older, elders gradually withdraw themselves from the previous society and satisfy of staying in the same environment. (Cummings & Henry, 1961)

The loose nature of the group structure, among other factors like the lack of an official leader and the lack of a standard form, might lead to an environment with little in pressure, which may explain why such loosely-knit groups were able to stay together for years despite lacking in unity as a whole.

SUGGESTION

The research was conducted in the two public parks in Bangkok with two exercise club. Therefor the result may not be generalized. We suggest an extra investigation in other locations.

REFERENCES

[1] R. J. Havighurst,"Successful aging,"*Processes of aging: Social and psychological perspectives*, vol.1, pp.299–320. 1963.

[2] R. J. Havighurst, "Successful aging," Presidential address given to the Division of Maturity and Old Age," American Psychological Association, Chicago, Ill, September 2, 1960.

[3] E. Cumming, and W. Henry, "Growing Old. New York: Basic Books. 1961.

[4] C. L. Johnson, and B. M. Barer, "Patterns of engagement and disengagement among the oldest old,"Journal of Aging Studies, 6(4), 351-364.1992

[5] J. F. Gubrium, "Toward a socio-environmental theory of aging," The Gerontologist, Vol. 12(3_Part_1), 281-284. 1972.

[6] P.Wasi, "PrachakhomTambon: Strategy for Sufficiency economy moraland health. Edition no 2. Bangkok: Matichon. 1998.

[7] K. Kaewthep, "Media for Community," Knowledge Processing. Bangkok: The Thailand Research Fund. 2000

[8] U. Dulayakasem and O. Ngamwitayapong, "Education System and Community," Conceptual Frameworkand Research Proposal. Bangkok: The Thailand Research Fund. 1997

★★★

COOPERATIVE SPECTRUM SENSING USING RMT FOR COGNITIVE RADIO IN PRESENCE OF NOISE CORRELATION

[1]K VENKATESH, [2]RAJOO PANDEY

[1,2]Department of Electronics and Communication Engineering, National Institute of Technology, Kurukshetra
E-mail: [1]venky2045@gmail.com, [2]rajoo_pandey@nitkkr.ac.in

Abstract— This paper presents an eigen-value based cooperative spectrum sensing (SS) technique in the presence of noise correlation for Cognitive Radio (CR). In this work, a new Standard Condition Number (SCN) based decision statistics is defined using asymptotic random matrix theory (RMT) for the decision making process. First, the effect of noise correlation under both noise only and signal plus noise hypothesis is defined. Then the new bounds for the correlated noise scenario are defined and a the new SCN based threshold is derived for SS in CR. Simulation results show that sensing with the proposed threshold gives better performance in the presence of noise correlation.

Index Terms—Random Matrix Theory (RMT), Noise Correlation, Standard Condition Number (SCN), Spectrum Sensing (SS).

I. INTRODUCTION

Cognitive Radio (CR) senses the overall spectrum over the wide frequency bands and uses temporally the unoccupied bands for wireless transmission. The CR acts as a Secondary User (SU) and it will not have any primary rights to pre-assign any frequency bands. So, it has to dynamically sense the spectrum to detect the presence of primary user (PU). It is known that the Federal Communications Commission (FCC) has given rights for the opportunistic Spectrum Sharing [1], which led to the formation of IEEE 802.22 working group for developing the standard Wireless Regional Area Network (WRAN) based on the CR technology. WRAN will operate on the unused bands of Very High Frequency (VHF)/ Ultra High Frequency (UHF) (TV broadcasting bands and other wireless microphone bands, which are PUs. WRAN system needs to periodically detect the presence or absence of PU to avoid interference [2].

From the above discussion, it is clear that spectrum sensing (SS) is the fundamental component for a CR system. There are many facts which make spectrum sensing difficult. One of these the important factors is the PU's Signal to Noise Ratio (SNR) received by the secondary receiver, which may be very low. The targeted detection SNR level given by WRAN at worst case is -20dB [2]. Next is the time dispersion and fading of the wireless channel, which complicates the sensing problem. Third is the noise uncertainty, which is caused by the noise/interference level changing with time [3].

In order to address these difficulties, several SS algorithms including energy based detection, matched filter based detection Feature detection, Autocorrelation based detection, Eigen-value based detection, beacon based detection have been investigated [3]. Matched filter based detection, Feature based detection, Beacon based detection are non-blind SS techniques i.e., they requires some specific information about the parameters of the PU signal/system. Energy detection, Autocorrelation Based detection, covariance based detection etc., are blind SS techniques, which do not require any information about the parameters of the PU signal/system. Of all these techniques, energy detection is robust to unknown dispersive channel, but its detection depends on the knowledge of the accurate noise power and its inaccuracy leads to SNR wall and high probability of false alarm [4]-[5]. Thus, it is vulnerable to detect a signal in the presence of noise uncertainty and also it cannot detect the correlated signal. To improve the SS performance, different diversity techniques like cooperative, multi-antenna and oversampling techniques have been introduced. All these techniques use the properties of the received signal. Recent results of the Random Matrix Theory (RMT) [6] are also used. The main advantage of eigen-value based detection is that it requires no prior knowledge of the PU signal and it is better than energy detection technique [4].

In this paper, the problem of Cooperative SS in the presence of noise uncertainty [3] is considered. Here the Standard Condition Number (SCN) of the noise covariance matrix is used to examine and resolve the effect of the noise correlation on the eigen-value based SS. The SCN of a matrix is the ratio of maximum to minimum eigen-value and it is a metric to characterize the asymptotic eigen-value probability detection function (aepdf) support of a random matrix. Then the SCN of the received signal's covariance matrix is used for the decision process. The PU is present, if the calculated SCN is greater than the noise only SCN. In this model, the presence of noise correlation is assumed, which affects the SCN of the noise covariance matrix and as a result the decision metric is affected. To overcome over problem of SS in the presence of noise correlation we employ a method taken from [7]-[8].

Here we consider the asymptotically large matrices where the eigen-values are said to follow Marchenko-Pastur (MP) law, which provides the

convergence of largest and smallest eigen-values of the matrices. Using MP law, a binary hypothesis test under white noise condition is performed in [9], which provides a SCN for the Wishart matrices. But the sample covariance matrix cannot be a Wishart matrix in the presence of correlated noise [4]. In this paper, the noise correlation due to imperfection and oversampling in filtering is considered. Due to the presence of noise correlation, the eigen-value distribution may not follow the MP law and the threshold from [9] will degrade the PU sensing performance. In our paper, a new threshold to carryout the SS in the presence of noise correlation is defined.

The paper is organized as follows. Section II describes the problem. Section III describes the signal model for both white as well as colored noise. Section IV describes the setting of threshold for our problem. Section V provides the Simulation results. Section VI concludes the paper.

Notations: Throughout the paper, boldface lower and upper case letters denotes vectors and matrices, respectively; **E**[.] Denotes expectation; $(.)^T$ denotes the transpose of a matrix; $(.)^H$ denotes the conjugate transpose of a matrix; (.)* denotes the complex conjugate; **I** is identity matrix; $(x)^+$denotes max(0,*x*); $\boldsymbol{R_X}$ denotes the statistical covariance of $\boldsymbol{X}$; $\hat{\boldsymbol{R}}_{\boldsymbol{X}}$ denotes the sample covariance matrix of $\boldsymbol{X}$.

II. PROBLEM DESCRIPTION

Using RMT, many eigen-value based SS techniques have been investigated. But most of the works assume that the noise is white at the CR terminal. Practically, the noise may not be white all the time because the received signal must be passed through a pulse-shaping filter, where a correlation is introduced in the signal. The noise correlation in the CR sensing is due to following two reasons [4].

A. Filtering

CR is a dynamic system and when a white noise is passed through a dynamic system, it is converted to a colored noise, typically a LPF (low pass filter), which is also known as shaping filter. The received signal when passed through shaping filter, which is at the input of the receiver, the noise that is added to the signal before filtering will also pass through the same filter. The noise covariance matrix will depend on the TF (Transfer Function) of the pulse-shape filtering used at the Radio Frequency (RF) front-end of the CR. As a result, the output signal of the filter contains the colored noise and the color of the noise can be tuned by adjusting the shaping filter's parameters.

B. Oversampling

Consider that the bandwidth of the shaping filter is B, which is equal to the bandwidth of the signal. But the sampling rate of the signal is higher than 2B, which leads to the correlation at the sampled output even though the input noise process is white.

Coherent receivers like matched filters are not suitable for the application of SS because no prior knowledge about the PU signal and channel is known. So, for the application of SS in CR, active RC filter with tunable cutoff frequency are proposed. A white noise signal with a power spectral density of $N_0/2$ is given as input to an RC filter having a time constant RC, the noise will be colored after filtering. We assume that the noise correlation effect is dominating the overall effects. We also assume that the RC filter transforms the input autocorrelation function (white noise) into a output autocorrelation function given in [10] $R_y(s) = (N_0/4)RC\exp(-|s|/RC)$ i.e., a exponential correlation model is considered in our paper.

An important research challenge, cooperatively sensing the signal in the presence of the noise correlation, is considered in this paper. A new SCN based decision statistics like other eigen-value based SS techniques [4] is defined. The new SCN based decision to improve the SS performance in the presence of noise correlation is taken from [7]. Also note that, one sided noise correlation model is considered and also an exponential correlation model matrix to define the correlation matrix components is used.

III. SYSTEM MODEL

In the present system model, the main focus is on the cooperative SS in which we have K cooperative SUs and let N be the number of samples that a cognitive user analyzes for making the decision about the presence or absence of a signal. We assume that each SU samples the received signal at the same rate, same instant and during the same interval (neglecting the delay in receiving the PU signal). For detecting the presence or absence of the PU signal, two hypothesis H_0 and H_1 are defined. where H_1 represents the hypothesis for presence of PU signal and H_0 represents the hypothesis for absence of PU signal. It can be shown as follows:

$$\begin{aligned} &H_0 : y_k(i) = \hat{z}_k(i) \quad \text{PU absent} \\ &H_1 : y_k(i) = h_k(i)s(i) + \hat{z}_k(i) \quad \text{PUpresent} \end{aligned} \tag{1}$$

where $y_k(i)$ represents the received signal by the k^{th} cooperative SU at i^{th} instant, i=1,2,3,……N. $s(i)$ represents the PU signal at i^{th} instant, which has to be detected; $h_k(i)$ represents the channel amplitude gain for the k^{th} cooperative SU at the i^{th} instant and $\hat{z}_k(i)$ gives the colored noise for the k^{th} cooperative SU at the i^{th} instant. Assume, the transmitted PU symbols are independent and identical distributed (i.i.d) Gausssian symbols.

As there are K cooperative SUs and each SU analyzes N samples, we can form a *KxN* received signal matrix $\mathbf{Y}$. Let $\mathbf{H}$ denotes the *KxN* channel matrix whose

entries consist of i.i.d coefficients and $\mathbf{H}$ can be represented in matrix form as, $\mathbf{H} \triangleq [\mathbf{h}_1^T \ \mathbf{h}_2^T \ \mathbf{h}_3^T \dots \dots \ \mathbf{h}_K^T]^T$, where $\mathbf{h}_k$ is the column matrix given by , $\mathbf{h}_k \triangleq [h_k(1) \ h_k(2) \ h_k(3) \dots \dots \ h_k(N)]$ with k =1, 2,……..K and also assume that the coherence time of the channel is small so that channel is not correlated.

Let us consider τ as the sensing duration and T_s as the symbol interval. During the sensing process in a cognitive receiver τ and T_s may not be same and will depend on the bandwidth of the signal and the sampling rate at the receiver. So, for the present model, under the hypothesis H_1, the transmitted symbol will remains constant during the sensing period. This case may occur when the rate of sampling at the receiver is much higher than the symbol rate of the transmitter. The received signal can be written as $\mathbf{Y} = \sqrt{p}\mathbf{H}s + \tilde{\mathbf{Z}}$ where s is the constant transmitted symbol, p is the transmitted symbol power, and $\hat{\mathbf{Z}} \triangleq [\hat{\mathbf{z}}_1^T \ \hat{\mathbf{z}}_2^T \ \hat{\mathbf{z}}_3^T \dots \dots \ \hat{\mathbf{z}}_K^T]^T$ with $\hat{\mathbf{z}}_k$ a column matrix $\hat{\mathbf{z}}_k \triangleq [\hat{z}_k(1) \ \hat{z}_k(2) \ \hat{z}_k(3) \dots \dots \ \hat{z}_k(N)]$. Assume the noise variance is normalized to unit value i.e., SNR= p . Therefore, the transmitted signal's sample covariance is $R_s = \mathbf{E}[s^2] = 1$.

Therefore, the received signal can be written as,

$$Y = \begin{bmatrix} \mathbf{y}_1 \\ \mathbf{y}_2 \\ \vdots \\ \mathbf{y}_K \end{bmatrix} = \begin{bmatrix} y_1(1) & y_1(2) & \cdots & y_1(N) \\ y_2(1) & y_2(2) & \cdots & y_2(N) \\ \vdots & \vdots & \ddots & \vdots \\ y_K(1) & y_K(2) & \cdots & y_K(N) \end{bmatrix} \quad (2)$$

Assume that the source signal and noise are independent. Therefore, the covariance matrix of the received signal is given as,

$$\mathbf{R_Y} = \mathbf{E}[\mathbf{Y}\mathbf{Y}^H] = \mathbf{E}[(\sqrt{p}\mathbf{H}\mathbf{S})(\sqrt{p}\mathbf{H}\mathbf{S})^H] + \mathbf{E}[\tilde{\mathbf{Z}}\tilde{\mathbf{Z}}^H]$$
$$= p\mathbf{E}[\mathbf{H}\mathbf{H}^H] + \mathbf{R}_{\tilde{\mathbf{Z}}} \quad (3)$$

Where $\mathbf{R}_{\tilde{\mathbf{Z}}} = \mathbf{E}[\tilde{\mathbf{Z}}\tilde{\mathbf{Z}}^H]$. The sample covariance matrix of noise and received signal are $\hat{\mathbf{R}}_{\tilde{\mathbf{Z}}}(N) = (1/N)\tilde{\mathbf{Z}}\tilde{\mathbf{Z}}^H$ and $\hat{\mathbf{R}}_{\mathbf{Y}}(N) = (1/N)\mathbf{Y}\mathbf{Y}^H$ respectively. The received signal is,

$$\mathbf{Y} = \sqrt{p}\mathbf{H}s + \tilde{\mathbf{Z}} \quad (4)$$

where $\tilde{\mathbf{Z}} \sim$ CN $(0. \hat{\mathbf{R}}_{\hat{\mathbf{Z}}}(N))$is the colored noise. The SCN of noise's sample covariance $\hat{\mathbf{R}}_{\tilde{\mathbf{Z}}}(N)$ will depends on the amount of noise correlation among noise samples.

A. Modeling of Noise Correlation:

In this paper, a single-sided noise correlation model is considered as given in [8]. This model relates colored noise with white noise as shown:

$$\tilde{\mathbf{Z}} = \mathbf{\Gamma}^{1/2}\mathbf{Z} \quad (5)$$

where $\mathbf{Z}$ is a *KxN* matrix with i.i.d Gaussian entries with zero mean and unit variance and represents white noise, and $\mathbf{\Gamma}$ is a *KxK* Hermitian matrix, where it entries corresponds to correlation among the noise samples. In (5) $\mathbf{\Gamma}^{1/2}$ is the square root of $\mathbf{\Gamma}$. $\mathbf{\Gamma}$ is normalized by considering $(1/K)\text{trace}\{\mathbf{\Gamma}\} = 1$, so that it does not affect noise power. The entries of exponential correlation model are taken as described in [11].

$$\phi_{ij} = \begin{cases} \rho^{(j-i)}, & i \le j \\ (\rho^{(i-j)})^*, & i > j \end{cases} \quad (6)$$

where ϕ_{ij} is the (i,j)th element of $\mathbf{\Gamma}$ and $|\rho| \le 1$.

B. Under H_0 Hypothesis:

Under the H_0hypothesis and for correlated noise scenario, $\hat{\mathbf{R}}_{\mathbf{Y}}(N)$ is equal to $\hat{\mathbf{R}}_{\tilde{\mathbf{Z}}}(N)$ and is written as,

$$\hat{\mathbf{R}}_{\mathbf{Y}}(N) = \hat{\mathbf{R}}_{\tilde{\mathbf{Z}}}(N) = \mathbf{\Gamma}^{1/2}\mathbf{Z}\mathbf{Z}^H\mathbf{\Gamma}^{1/2} \quad (7)$$

In the case of white noise, $\hat{\mathbf{R}}_{\mathbf{Y}}(N) = \mathbf{Z}\mathbf{Z}^H$.

C. Under H_1 Hypothesis:

Under the assumption that the signal and the noise are independent and for large values of N, the approximate received signal sample covariance matrix for the white noise case [4] is,

$$\lim_{N\to\infty} \hat{\mathbf{R}}_{\mathbf{Y}}(N) \approx p\mathbf{H}\mathbf{H}^H + \hat{\mathbf{R}}_{\mathbf{Z}}. \quad (8)$$

In this case, $\hat{\mathbf{R}}_{\mathbf{Y}}(N)$ is the sum of two Wishart matrices i.e., $p\hat{\mathbf{R}}_{\mathbf{H}} = p\mathbf{H}\mathbf{H}^H$ and $\hat{\mathbf{R}}_{\mathbf{Z}}$ with the same degree of freedom and having different covariance structures. In this case, MP law holds for both matrices.

Using the same conditions as above, the approximation under correlated noise case is,

$$\lim_{N\to\infty} \hat{\mathbf{R}}_{\mathbf{Y}}(N) \approx p\mathbf{H}\mathbf{H}^H + \hat{\mathbf{R}}_{\hat{\mathbf{Z}}}. \quad (9)$$

where $\hat{\mathbf{R}}_{\mathbf{Y}}(N)$ is the sum of one Wishart matrix $p\hat{\mathbf{R}}_{\mathbf{H}}$ and a correlated Wishart matrix $\hat{\mathbf{R}}_{\hat{\mathbf{Z}}}$. In this case, MP law can be applied for only $p\hat{\mathbf{R}}_{\mathbf{H}}$ and the analysis is carried out for $\mathbf{H_0}$ hypothesis in (7) is applied for $\hat{\mathbf{R}}_{\hat{\mathbf{Z}}}$.

IV. DETERMINATION OF THRESHOLD

To determine the threshold for spectrum sensing under the condition of noise correlated, we use RMT. RMT has many applications in the wireless communications. In the present model, two theorems of RMT, which are useful in determining the threshold for the decision statistics are given below.

Theorem 4.1: [6] Consider an *KxN* matrix **G** whose entries are independent zero mean (real or) complex random variables with variance (1/N) and fourth moment of order $O(1/N^2)$. As $K,N \to \infty$ with $N/K \to \alpha$ $(0 < \alpha < \infty)$, the empirical distribution of eigen values of $(1/N)\mathbf{G}\mathbf{G}^H$ converges almost surely to a non-random limiting distribution with density given by,

$$g_\alpha(\lambda) = (1-\alpha)^+\delta(\lambda) + \frac{\sqrt{(\lambda-a)^+(b-\lambda)^+}}{2\pi\alpha\lambda} \quad (10)$$

where $a = (1-\sqrt{\alpha})^2, b = (1+\sqrt{\alpha})^2$, $\delta(.)$ is a Dirac delta function. (10) is a limiting distribution called as MP law with ratio index α. The parameters a and b in the above distribution defines the support of distribution and corresponds to $\lambda_{\min}$ and $\lambda_{\max}$ respectively. So that

the ratio (b/a) defines the SCN of (1/N)$\mathbf{GG}^{H}$.

The asymptotic eigen-value distribution is obtained from the theorem. But in practice we have only a finite number of samples and the sample covariance matrix $\hat{\mathbf{R}}_{\mathbf{Y}}(N)$ may deviate from that of covariance matrix $\mathbf{R}_{\mathbf{Y}}$ in [4]. In this case, the choice of threshold is difficult to determine for the purpose of SS because the eigen-value distribution of $\hat{\mathbf{R}}_{\mathbf{Y}}(N)$ is complicated due to the consideration of finite parameters in the analysis and also the performance of spectrum sensing algorithms becomes sensitive at the low SNR values. In this paper, an asymptotic analysis is considered to analyze noise correlation effects on the sensing performance because it provides a less complex solution when compared with finite analysis [7]. Under the H_0hypothesis, $\hat{\mathbf{R}}_{\mathbf{Y}}(N)$ is equal to $\hat{\mathbf{R}}_{\mathbf{Z}}(N)$ and is given by (7).

As N$\rightarrow\infty$, $\hat{\mathbf{R}}_{\mathbf{Y}}(N)$ converges to $\mathbf{R}_{\mathbf{Y}}$. For large values of N, the asymptotic analysis holds good. $\hat{\mathbf{R}}_{\mathbf{Z}}(N)$ is nearly a Wishart random matrix in the case of white noise, but it is no longer a Wishart random matrix under correlated noise case. The Wishart matrix is generated using the RMT concept in [12]. In [8], it is given that the asymptotic density of eigen-values of $\boldsymbol{\Gamma}$ can be described as a tilted semi-circular law, which can be a close approximation for the exponential model. The following theorem describes this density:

Theorem 4.2: [8] let $\boldsymbol{\Gamma}$ be a positive definite matrix, whichis normalized as (1/K)trace{$\boldsymbol{\Gamma}$}=1, and whose asymptotic spectrum has a pdf

$$g_{\Gamma}(\lambda)=\frac{1}{2\pi\mu\lambda^{2}}\sqrt{\left(\frac{\lambda}{\sigma_1}-1\right)\left(1-\frac{\lambda}{\sigma_2}\right)} \tag{11}$$

with $\sigma_1 \le \lambda \le \sigma_2$ and $\mu=(\sqrt{\sigma_1}-\sqrt{\sigma_2})/4\sigma_1\sigma_2$. If G is a *KxN* standard complex Gaussian matrix, as defined in Theorem 4.1, then *K,N*$\rightarrow\infty$ with N/K$\rightarrow\alpha(0<\alpha<\infty)$ the asymptotic eigen-value distribution of $\mathbf{W}=\boldsymbol{\Gamma}^{1/2}\mathbf{GG}^{H}\boldsymbol{\Gamma}^{1/2}$ has pdf,

$$g_{\mathbf{W}}(\lambda)=(1-\alpha)^{+}\delta(\lambda)+\frac{\sqrt{(\lambda-\tilde{a})^{+}(\tilde{b}-\lambda)^{+}}}{2\pi\lambda(1+\lambda\mu)} \tag{12}$$

$\tilde{a}$ and $\tilde{b}$ are the parameters and corresponds to $\lambda_{\min}$ and $\lambda_{\max}$ respectively and the SCN of $\mathbf{W}$ is defined by the ratio $\tilde{b}/\tilde{a}$. where the values of $\tilde{a}$ and $\tilde{b}$ are given as,

$$\begin{aligned}\tilde{a}&=1+\alpha+2\alpha\mu-2\sqrt{\alpha}\sqrt{(1+\mu)(1+\mu\alpha)}\\ \tilde{b}&=1+\alpha+2\alpha\mu+2\sqrt{\alpha}\sqrt{(1+\mu)(1+\mu\alpha)}\end{aligned} \tag{13}$$

In (12), the degree of noise correlation is controlled by the parameter μ and it varies the support of the distribution. $\mu$is related to ρ as $\mu=\rho^{2}/(1-\rho^{2})$, given in [8].

In the case of white noise, the presence or absence of signal can be decided by using the deviation of the distribution of the eigen-values from its normal bounds (a,b). The presence of the PU signal can be decided if the eigen-values appear outside these bounds. If the eigen-values lie inside the bounds then the PU signal is absent [9]. In the same way, the presence or absence of PU signal under noise correlation scenario can be decided by sing the new bounds of the eigen-value distribution of the sample covariance matrix. The new bounds are $(\tilde{a},\tilde{b})$ and they depends on the noise correlation parameter μ.

Let us consider that both noise variance and noise distribution are unknown to the detector (practical scenario). Therefore the decision statistic for MP law under the white noise scenario is given as [8],

$$\text{decision}=\begin{cases}\mathrm{H}_0, & if\ SCN\le\dfrac{b}{a}\\ \mathrm{H}_1, & otherwise\end{cases} \tag{14}$$

The values of a and b can be determined from the expressions given in Theorem 4.1. Similarly the decision statistic for the correlated noise case can be determined from the Theorem 4.2. According to it, the decision statistic for the presence or absence of PU signal under noise correlation is given by,

$$\text{decision}=\begin{cases}\mathrm{H}_0, & if\ SCN\le\dfrac{\tilde{b}}{\tilde{a}}\\ \mathrm{H}_1, & otherwise\end{cases} \tag{15}$$

Using the decision statistics given in (14) and (15) we can decide the presence or absence of PU signal under white noise and correlates noise scenarios respectively.

V. SIMULATION AND RESULTS

To study the performance of eigen-value based SS in the presence of noise correlation with the given decision bounds, the probability of detection is used as the performance metric [13]. The channel is considered to be Rayleigh faded and its coefficients are generated from a complex random numbers whose real and imaginary parts are i.i.d Gaussian variables. As a result, $\mathbf{H}\sim \mathrm{CN}(0.\mathbf{I})$.

It can be noted that under the white noise case, the eigen-value distribution of the received signal's covariance matrix follows MP law. Therefore, the decision rule given in (14) is used for sensing of the PU signal in white noise scenario. But under the correlated noise case, the decision rule in (15) is used to sense the presence or absence of PU signal.

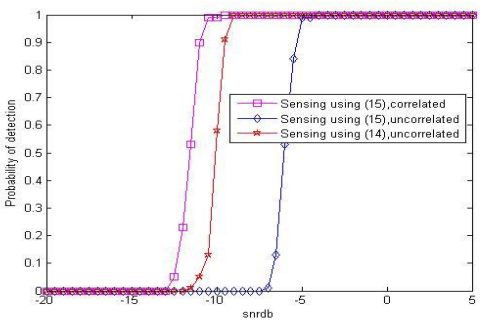

Fig. 1 Probability of detection versus SNR with (14) and (15) ($\alpha=2,\rho=0.5,N=100$ **)**

In the simulation results, the sensing performance is compared with MP–based threshold and the new proposed threshold. Fig.1 shows the probability of detection versus SNR for ρ=0.5, α=2 and N=100. From Fig.1, it can be observed that the performance of sensing using (15) out performs the sensing using (14) under correlated noise scenario. It can also be observed that the sensing of uncorrelated signal using (15) gives poor response. i.e., to decide the threshold correlation should be known. If correlation is zero go for (14), otherwise go for (15). The new threshold gives better response for the correlated noise scenario and if the same is used threshold for white noise case, its performance is poor for low values of SNR as shown in Fig.1.

Fig.2 shows the probability of detection versus the correlation coefficient (ρ) for SNR=-6dB and α=2. It can be observed that as the noise correlation is increasing the sensing performance is decreasing drastically.

From (15), it can be observed that a change in correlation coefficient results in a change in the ratio $(\tilde{b}/\tilde{a})$. Therefore, sensing using (15) for a correlated signal is better for large amount of correlation.

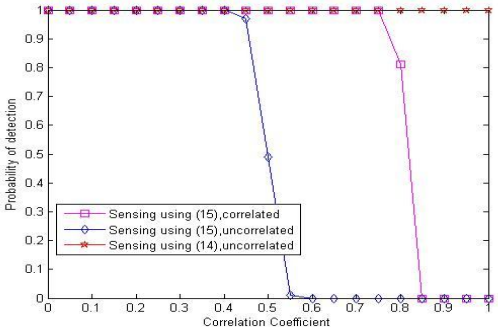

Fig. 2 Probability of detection versus correlation coefficient ($SNR = -6dB, \alpha = 2, N = 100$ **)**

CONCLUSION

In this paper, the presence or absence of PU signal under the condition of noise correlated using eigen-value based cooperative spectrum sensing has been analyzed. A new threshold based on SCN has been used for the improvement of cooperative spectrum sensing performance for this scenario.

From the viewpoint of practical implementations of a CR, the spectrum sensing techniques should work effectively and efficiently where the channel and noise correlation are also present to certain extent. The present work can be extended by considering the presence of channel correlation in addition to the noise correlation and finding new sensing scheme suitable for the conditions.

REFERENCES

[1] FCC, “Facilitating opportunities for flexible, efficient and reliable spectrum use employing cognitive radio technologies, notice of proposed rule making and order,” FCC 03-322, Dec-2003.

[2] Standard for wireless Regional Area Networks (WRAN) – Specific requirements – Part:22 Cognitive Wireless RAN Medium Access Control (MAC and Physical Layer (PHY) Specifications: Policies and procedures for operation in the TV Bands, The Institute of Electrical and Electronics Engineering, Inc. Std. IEEE 802.22.

[3] S. K. Sharma, T. E. Bogale, S. Chatzinotas, B. Ottersten, L. B. Le, and X. Wang, “Cognitive radio techniques under practical imperfections: A survey,” IEEE Commun Surveys & Tutorials., vol. 17, no. 4, pp. 1858-1884, July 2015.

[4] Y. Zeng, and Y. C. Liang, “Eigenvalue-based spectrum sensing algorithms for cognitive radio,” IEEE Trans. On Commun., vol. 57, no. 6,pp-1784-1793, June 2009.

[5] A. Sonnenschein and P. M. Fishman, “Radiometric detection of spread spectrum signals in noise of uncertainty power," IEEE Trans. Aerospace Electronic Systems, vol. 28, no. 3, pp. 654-660, 1992.

[6] A. M. Tulino and S Verdu, “Random matrix theory and wireless communications,” Found. Trends Commun. Inf. Theory, vol. 1, no. 1, pp. 1-182, June 2004.

[7] S. K. Sharma, S. Chatzinotas, and B. Ottersten, “Eigenvalue-based sensing and SNR estimation for cognitive radio in presence of noise correlation,” IEEE Trans. On Vehicular Tech., vol. 62, no. 8, pp-3671-3684, Oct-2013.

[8] X. Mestre, J. R. Fonollosa, and A. P. Zamora, “Capacity of MIMO channels: Asymptotic evaluation under correlated fading,” IEEE Journ. on Selected Areas in Commun., vol. 21, no. 5, June 2003.

[9] L. Cardoso, M. Debbah, P. Bianch,i and J. Najim, “Cooperative spectrum sensing using random matrix theory,” in Proc. 3rd Int. Symp. Wireless Perv. Comput., pp-334-338, May-2008.

[10] S, Haykin, “Communication Systems,” 4th ed. Hoboken, NJ, USA: Wiley 2010.

[11] S. Lokya, “Channel capacity of MIMO architecture using exponential correlation matrix,” IEEE Commun. Lett., vol.5, no. 9, pp. 369-371, Sep. 2001.

[12] N. Raj Rao, and A. Edelman, “Random Matrix Theory,” Cambridge University Press, pp. 1-65, 2005.

[13] S. M Kay, “Fundamentals of Statistical Signal Processing: Detection Theory. Englewood Cliffs, NJ, USA: Prentice Hall, 1998.

★★★

IMPROVED GRADIENT PROFILE SHARPNESS TRANSFORMATION BASEDSUPER-RESOLUTION USING DE-HAZING

[1]A.V.S.DEEPAK, [2]UMESH GHANEKHAR

[1,2]Department of Electronics and Communication Engineering, National Institute of Technology, Kurukshetra
E-mail: [1]deep.adiraj@gmail.com, [2]ugnitk@nitkkr.ac.in

Abstract— This paper presents a Super Resolution (SR)technique considering atmospheric scattering models of hazy images. In which a SR image is considered as combination of radiance of the scene and atmospheric light. This assumption helps us to remove the hazy part in any SR image using dark channel prior. An edge sharpness metric called Gradient Profile Sharpness (GPS) is used in transforming the Low Resolution (LR) image to High Resolution (HR). This results in improved image quality. Extensive simulation results show that proposed method improves the performance of existing SR techniques, in terms of Peak Signal to Noise Ratio (PSNR) and Structural Similarity Index Measure (SSIM).

Index Terms— Super Resolution from single image, Gradient Profile Sharpness transformation, Haze removal, Dark channel prior.

I. INTRODUCTION

The process of generating a High resolution (HR) image from one or many Low Resolution (LR) image(s) is called Super Resolution (SR). These SR techniques can be broadly classified into two categories: (i) classical multi image SR techniques and (ii) Single image based SR techniques.

Classical multi image approach assumes the multiple input images as down-sampled versions of the desired HR image. Then the sub-pixel shifts among LR images are used to estimate HR image.The multi-image Super Resolution approach is a well constrained problem and many methods have been proposed [1].The main drawback of this approach is that the multiple images of same scene are to be presented as input. This may not be possible in many applications like surveillance, remote sensing, etc. Hence, this approach is less preferred by researchers.
In the single image based SR techniques. The single image itself is considered as input. In recent years much work has been done in this area, these works can be classified into three categories: (i) Interpolation based approaches, (ii) learning based approaches and (iii) reconstruction based approaches.In interpolation based approaches speed is key factor which prompts researches to work in this direction and many sophisticated interpolation based models were developed. Butif upscaling ratio is high, these approaches tend to blur high frequency details.

The learning based approaches assume that high frequency details are lost in LR images and these can be hallucinated from dictionary containing image patch pairs. Some of these methods in this approach use dictionary constructed of external data set containing image pairs [2]. But, this makes the performance of these techniques dependent on similarity between input image and the data set. In order to reduce this dependence, self-example based approaches were proposed. These are based on the observation that across different scales of image, patches tend to recur redundantly [3]. Although these approaches are robust, there will be some artifacts in HR image generated and the computational complexity is also very high.
Reconstruction based approaches were developed over the years to tradeoff between performance and computational efficiency of algorithm. As the single image SR is an inherently ill constrained, these approaches enforce a constraint that synthesized HR image is to be consistent with its LR image. To make this problem solvable and to find the best estimated HR image, an effective regularization term is added as a model constraint. Since edges of the image are prominent inits visuality; edge sharpness metrics are often used as regularization terms. The gradient profile isintroduced to describe resolution of edges it is described using three features: (i)magnitude of intensity change, (ii) distance from center pixel which is having maximum gradient to pixel whose gradient magnitude is zero and (iii) the standard deviation of edge profile [4].

This paper proposes a two part model in which first part uses reconstruction based approach to synthesize an HR image using GPS transformation and second part de-hazes itto produce final image which is having higher resolution and is free from scattered atmospheric light.

This remaining paper is organised into four sections. Section II explains the reconstruction based approach using GPS transformation term to synthesize HR image, section III explains how the synthesized image is de-hazed and section IV provides with our experimental results and compares our model's performance with performance of HR image reconstruction using GPS transformation both structurally and visually. The conclusion of our work is given in section V of this paper.

II. RECONSTRUCTION OF HR IMAGE FROM LR IMAGE

This section explains how an HR image can be synthesized from single LR image using reconstruction based approach introduced in section I. This section is segmented into three parts. Part A formulates the problem statement. Part B defines the regularization parameter used in this model i.e. gradient profile sharpness (GPS). Part c details the algorithm used to reconstruct HR image.

A. Formulating the relation between input LR image and HR image

This paper deals with single image super resolution methods. Hence, we focus on problem of estimating $\hat{X}$, the estimate of target HR image X from input image Y. All SR techniques in literature are based on assumption that the available LR images are down-sampled, wrapped, blurred and noisy versions of target HR image. Supposing x, y are vector representations of images X and Y. We can write

$$y = sHx + \eta \tag{1}$$

Where, s represents subsampling operator, H represents blur kernel and η is representation of additive white Gaussian noise (AWGN) added to degrade LR image.

B. Defining regularization term used (GPS)

Equation (1) specifies the relation between input image and target HR image. But the problem is, there can be many HR images which may result same LR image under different blurring and wrapping factors. Hence, there should be a regularization term which ensures that synthesized HR image is consistent with target image. In this paper we use GPS defined in [5]. Gradient profile is described by modeling image's gradient magnitude at edges present in images. Traditionally generalized Gaussian description (GGD) model is used but it tends to cause large fitting errors. Hence triangular and Gaussian mixed model were proposed to model edges. For the ease of description of gradient profile a normalized coordinate system is used for each gradient profile is used. Where, profile peak is located at center.

Triangle model is suited for gradient profiles around short and asymmetric edges. Two sides of center are fitted separately. The linear function can be formulated as

$$m_{TR}(x) = \begin{cases} kd_x + h, & \text{if the value} \geq 0 \\ 0 & \text{otherwise} \end{cases} \tag{2}$$

Where, $m_{TR}(x)$ is the magnitude of gradient at pixel in the model, d_x is the absolute distance of pixel from centre, h is the peak value of profile, k is the slope of edge of triangle and it can be fitted using

$$k = \min_k \sum_{x \in p} [m_{TR}(x) - k.d_x - h]^2 \tag{3}$$

The key features of any description model are its height and spatial scattering.A metric of gradient profile is defined based on eccentricity of gradient profile description models as

$$\eta = {}^{h}/_{d} \tag{4}$$

Where, h is maximum gradient magnitude and d is spatial scattering. For triangle model it is horizontal distance between the center to the point where the gradient magnitude is zero. A larger GPS value means a sharper edge and smaller GPS value means smoother edge and is consistent with human perception of edges.

C. Algorithm used to transform LR image to HR image using GPS transformation

The algorithm of generating a HR image using single image and its GPS value can be divided into four steps. The first step is to extract GPS from the gradient profile description model given in (2).

The second step is to estimate GPS transformation relationship between different image resolutions. To reconstruct HR image we should have its gradient field. Toobtain target gradient field the Gradient profiles in LR image should be transformed into ones in HR image. The gradient transformation model can be formulated only if the relationship of GPSs in various resolutions is known. The parameter in GPS relationship can be estimated using the model in [5]. An up-scaled image (UR) is formed which is of same size as the HR image. After UR image is formed, the edge pixels of the image are found and their corresponding edge pixels in HR image are searched by comparing spatial difference and gradient difference.

$$x_0^{HR} = \arg\min_{x \in N} (d(x, x_0^{UR})^2 + \beta. \left\| \overrightarrow{G_H}(x) - \overrightarrow{G_U}(x_0^{UR}) \right\|^2) \tag{5}$$

Where, the first term $d(x, x_0^{UR})^2$ in (5) correspond to spatial difference and the second term in (5) $\left\| \overrightarrow{G_H}(x) - \overrightarrow{G_U}(x_0^{UR}) \right\|^2$ corresponds to gradient difference. Pair of gradient profiles is extracted from I_{HR} and I_{UR} at the positions of x_0^{HR} and x_0^{UR} then the GPS pairs $(\eta(x_0^{HR}), \eta(x_0^{UR}))$ are calculated according to (4). GPS transformation relation can be written as

$$\eta^{HR} = \alpha.\eta^{UR} \tag{6}$$

Where α determines the degree of enhancement.

The third step is to generate target gradient field in HR image using transformation of gradient profiles. In gradient profile transformation total energy and shape

of original gradient profile are to be preserved. Three constraints are proposed in [5]to keep the transformation consistent. First constraint is there should not be a change in sum of gradient magnitude in a gradient profile. This preserves the luminance difference around the edges. Even with the transformation of gradient profile its shape should not change from its original shape. Shifting of edges should be avoided and to avoid it, the peak in transformed profile should not change its position. Gradient profile transformation models are developed using these three constraints. Weconsidered triangular model, as the shape is fixed and sum of gradient magnitude should also be unchanged, the area should remain unchanged.

$$\begin{cases} h_{TR}^{HR} \cdot d_{TR}^{HR} = h_{TR}^{UR} \cdot d_{TR}^{UR} \\ h_{TR}^{HR} / d_{TR}^{HR} = \alpha^* \cdot h_{TR}^{UR} / d_{TR}^{UR} \end{cases} \quad (7)$$

Where h_{TR}^{HR} and d_{TR}^{HR} are gradient profile's parameters of triangle model in HR image, h_{TR}^{UR} and d_{TR}^{UR} are their counterparts in UR image. Hence we can draw relation between known parameters of gradient profile in UR image and unknown parameters of gradient profile in HR image.

$$\begin{cases} h_{TR}^{HR} = \sqrt{\alpha^*} \cdot h_{TR}^{UR} \\ d_{TR}^{HR} = \sqrt{1/\alpha^*} \cdot d_{TR}^{UR} \end{cases} \quad (8)$$

The slopes of triangle model in HR image can also be calculated as

$$k_{TR_{left}}^{HR} = \frac{-h_{TR}^{HR}}{d_{TR_{left}}^{HR}} = \propto^* k_{TR_{left}}^{UR} \quad (9)$$

Using slope and peak values of a triangle model, the gradient magnitude of each location in gradient profile can be written as

$$\widehat{m}_x^{HR} = \begin{cases} k_{TR_{left}}^{HR} d_x + h_{TR}^{HR} & \text{if } d_x \le d_{Tleft}^{HR} \\ 0 & \text{otherwise} \end{cases} \quad (10)$$

Where, d_x is the distance between current pixel and edge pixel and d_{Tleft}^{HR} is maximum scattering allowed.$k_{TR_{left}}^{HR}$ is the slope of left side of triangular profile,h_{TR}^{HR} is the peak gradient magnitude located at edge.

The final step is HR image reconstruction from estimated target gradient field. Based on transformation models used in [6] target gradient field can be generated from gradients in UR image. This is the prior for HR image reconstruction. When this introduced in HR image reconstruction model, HR image can be found by minimizing reconstruction error in image field and gradient field.

$$I_{HR}^* = \min_{I_{HR}} E(I_{HR}|I_{LR}, \widehat{\nabla I_{HR}}) = \min_{I_{HR}} (E_I(I_{HR}|I_{LR}) + \beta . E_G(\nabla I_{HR}|\nabla \hat{I}_{HR})) \quad (11)$$

Wherethe first term in (11) $E_I(I_{HR}|I_{LR})$implies that there should be consistency between down sampled version of HR image and LR image

$$E_I(I_{HR}|I_{LR}) = \|\downarrow (I_{HR} \otimes G) - I_{LR}\|^2 \quad (12)$$

Second term in (11) $\beta . E_G(\nabla I_{HR}|\nabla \hat{I}_{HR})$ implies that there should be a consistency between HR image and estimated gradients

$$E_G(\nabla I_{HR}|\nabla \hat{I}_{HR}) = \|\nabla I_{HR} - \nabla \hat{I}_{HR}\|^2 \quad (13)$$

III. DE-HAZING OF GENERATED HR IMAGE

This section is dedicated to explain how effect of haze can be removed from image and why is this haze removal necessary. Part A of this section explains the need of de-hazing. Part B of this section gives the standard atmospheric scattering model of scene radiance of hazy image. Part c explains dark channel prior and its calculation. Part D explains how transmission parameter is estimated. Part E explains how original radiance of scene is recovered.

A. Need for De-hazing

Presence of haze or fog in images will degrade the visibility of image.This can become a major problem in many applications like video surveillance, target identification, remote sensing etc. these also are major applications for super resolution. Almost all computer vision algorithms assume that input image's intensity is original radiance of scene. This is not true in the presence of atmospheric light. This assumption leads to inevitable loss of performance is. Hence, to enhance performance of SR techniques haze is to be removed.

B. Atmospheric scattering model of hazy images

The atmospheric scattering model is first proposed in [16] and later developed by Narasimhan and Nayar in [9]. The model can be expressed as following:

$$I(x) = J(x)t(x) + A(1 - t(x)) \quad (14)$$

$$t(x) = e^{-\beta d(x)} \quad (15)$$

It is to be noted that depth of scene$d(x)$ is the key information. As β can be treated like a constant in the conditions of homogenous atmosphere. And the medium of transmission $t(x)$is easily available from (15) if depth of scene is given. The range of depth is [0,∞) as the objects visible in the image can be very distant from the point of observation, and so we have

$$I(x) = A \quad \text{as } d(x) \to \infty \quad (16)$$

Equation (16) shows that the intensity of pixel at infinite depth can be atmospheric light. Hence, we can say if the pixel is sufficiently distant to make the transmission parameter small then the intensity of pixel can be approximately equal to the atmospheric light. We can estimate the atmospheric light by the following equation if a sufficient threshold is given.

$$A = I(x) \quad if\ d(x) > d_{threshold} \quad (17)$$

C. Dark channel prior

The dark channel prior is based on observation on haze-free outdoor images in [10]. The observation made is that in most of local patches not having sky,

one color channel is having very low intensity at some pixels. In other words, the minimum intensity in non-sky patches is very low. We define dark channel as

$$J^{dark}(x) = \min_{C\in\{r,g,b\}}(\min_{y\in\Omega(x)}(J_C(y))) \quad (18)$$

Where $\Omega(x)$ the patch with center at x, $J_C(y)$ is radiance of scene at pixel y. We can say that for non-sky region the intensity of dark channel is quite low and may tend to zero, given that the image is non-hazy. This statistical observation is termed as dark channel prior.

D. Estimating the transmission parameter

As mentioned in part B of this section a haze-free image can be formed from the atmospheric scattering model if the atmospheric light and transmission parameter are known. The atmospheric light can be found using (16) or (17). Now to estimate the transmission parameter we use the atmospheric light and the dark channel prior. We assume that transmission parameter $t(x)$ is constant locally. Taking the min operator on (14) we get:

$$\min_{y\in\Omega(x)}(I^C(y)) = \tilde{t}(x)\min_{y\in\Omega(x)}(J^C(y)) + (1-\tilde{t}(x))A^C \quad (19)$$

This operation is performed on all three color channels separately and operation in each color channel is independent of other color channels. Hence the min operation operating on each color can be written as

$$\min_C(\min_{y\in\Omega(x)}(\frac{I^C(y)}{A^C})) = \tilde{t}(x)\min_C(\min_{y\in\Omega(x)}(\frac{J^C(y)}{A^C})) + (1-\tilde{t}(x)) \quad (19)$$

But from dark channel prior the first term in right hand side of equation tends to zero.

$$J^{dark}(x) = \min_C\left(\min_{y\in\Omega(x)}\left(J^C(y)\right)\right) = 0 \quad (20)$$

This gives the estimate of transmission parameter as:

$$\tilde{t}(x) = 1 - \min_C(\min_{y\in\Omega(x)}(\frac{I^C(y)}{A^C})) \quad (21)$$

Even though the dark channel prior does not apply to sky regions, this equation still holds good because the color of sky is approximately equal to the atmospheric light and the second term in (21) tends to one. And the transmission parameter tends to zero, which is consistent with atmospheric scattering model when distance tends to infinity. But in practice, the atmosphere is never absolutely free of ant particle. In fact, according to the phenomenon called aerial perspective, the presence of haze is cue for human to perceive depth. If haze is removed thoroughly, the obtained image may seem unnatural and perception of depth may be lost.Hence we may add small amount of haze for distant objects by introducing a constant parameter in (21):

$$\tilde{t}(x) = 1 - \omega\min_C(\min_{y\in\Omega(x)}(\frac{I^C(y)}{A^C})) \quad (22)$$

Where, ωallows preserving haze adaptively. The value of ω is application specific.

E. Recovering radiance of scene

With the transmission map the radiance of scene can be recovered using (22). But the direct attenuation term may be zero when transmission parameter tends to zero. The transmission parameter is restricted to a lower bound t_0. Which means for high dense haze regions a small amount of haze is preserved. Equation (14) can be written in its modified form as

$$J(x) = \frac{I(x)-A}{\max(t(x),t_0)} + A \quad (23)$$

The aim of lower bound t_0 is to make sure that the denominator in (22) never equals to zero.

IV. EXPERIMENTAL RESULTS

This paper generates HR image from an LR image. We collected standard images in pairs. One image is of higher resolution and other is decimated version of the first one. We are using magnification factor of three. So the decimation factor should also be three. The color image is first converted into YCBCR formand Super resolution is applied on Luminance channel only. To reduce color distortion in generated HR image. We have used triangular gradient profile description model. To de-haze generated HR image, we consider t_0 = 0.1 and ω is set to 0.95.The simulation is run on MATLAB r2013a, running on Windows 10 backed by Intel i5 processor. We compare the results of our technique with the results produced by reconstructing HR image alone.

The list of images used in testing is

Fig 1: The input images taken to test our algorithm (1) Baboon, (2) Baby, (3) Barbara, (4) Bird, (5) Bridge, (6) Coastguard, (7) Face, (8) Comic, (9) Flowers, (10) Lena, (11) man, (12) Monarch, (13) Pepper, (14) Woman ,(15) Zebra

Their corresponding HR images are shown in figure 2

Fig 2: The HR images synthesized by our algorithm (1) Baboon, (2) Baby, (3) Barbara, (4) Bird, (5) Bridge, (6) Coastguard, (7) Face, (8) Comic, (9) Flowers, (10) Lena, (11) man, (12) Monarch, (13) Pepper, (14) Woman ,(15) Zebra

The merit of a SR technique is given by comparing the generated HR images with ground truth. The comparison can be done qualitatively and structurally. Picture to Signal Noise Ratio (PSNR), gives qualitative analysis and Structural Similarity index (SSIM), gives structural analysis. We now compare the values of PSNR and SSIM obtained only when HR reconstruction (using GPS transformation) is used and those values obtained when the de-hazing is also applied. They are tabulated in table (1) where, image number corresponds to the respective image mentioned in fig (1).

Table 1: comparison of PSNR and SSIM values (a) HR reconstruction without de-hazing (b) HR reconstruction with de-hazing

Image	(a) HR reconstruction without de-hazing		(b)HR reconstruction with de-hazing	
	PSNR	SSIM	PSNR	SSIM
1	23.45	0.8989	28.05	0.902
2	23.58	0.9047	29.01	0.9277
3	23.46	0.9269	29.84	0.9270
4	24.46	0.6837	30.80	0.7961
5	23.41	0.9355	26.22	0.9364
6	23.42	0.9238	27.84	0.9045
7	23.34	0.9394	27.21	0.9328
8	24.54	0.6636	27.93	0.6961
9	23.60	0.8359	26.47	0.8222
10	23.52	0.9264	25.78	0.8850
11	24.05	0.8470	27.74	0.8764
12	23.42	0.9413	24.18	0.9001
13	23.77	0.8797	29.75	0.8914
14	24.01	0.8172	24.91	0.8478
15	23.71	0.9436	29.54	0.9666

CONCLUSION

The proposed algorithm uses a haze removal technique to improve performance of SR. The images were enhanced both visually and structurally. It is worth mentioning that haze removal method is based on dark channel prior which may fail for images containing large sky regions. This work can be extended by using improved haze models and advanced priors like color attenuation prior.

REFERENCES

[1] Tsai and Huang R. Y. Tsai and T. S. Huang, “Multiframe image restoration and registration,” tech. rep., Greenwich, CT, 1984.

[2] S. Mallat and G. Yu, “Super-resolution with sparse mixing estimators,” IEEE Trans. Image Process., vol. 19, no. 11, pp. 2889–2900, Nov. 2010

[3] M. Ebrahimi and E. R. Vrscay, “Solving the inverse problem of image zooming using ‘self-examples,”’ in Image Analysis and Recognition. Berlin, Germany: Springer-Verlag, 2007, pp. 117–130.

[4] J. Sun, J. Sun, Z. Xu, and H.-Y. Shum, “Gradient profile priorand its applications in image super-resolution and enhancement,”IEEE Trans. Image Process., vol. 20, no. 6, pp. 1529–1542,Jun. 2011.

[5] Qing yan, Yi Xu Xiaokang Yang, Nguyen “Single image super resolution using gradient profile sharpness”, IEEE Transactions on Image Processing.,vol.24 , no: 10 pp 3187-3202 19 march 2015.

[6] M. Ebrahimi and E. R. Vrscay, “Solving the inverse problem of image zooming using ‘self-examples,”’ in Image Analysis and Recognition. Berlin, Germany: Springer-Verlag, 2007, pp. 117–130.

[7] M. Bevilacqua, A. Roumy, C. Guillemot, and M.-L. Alberi Morel, “Single-image super-resolution via linear mapping of interpolated selfexamples,” IEEE Trans. Image Process., vol. 23, no. 12, pp. 5334–5347, Dec. 2014.

[8] E. J. McCartney, Optics of the Atmosphere: Scattering by Molecules and Particles. New York, NY, USA: Wiley, 1976

[9] S. G. Narasimhan and S. K. Nayar, “Vision and the atmosphere,” Int. J. Comput. Vis., vol. 48, no. 3, pp. 233–254, Jul. 2002.

[10] H. Kaiming, S. Jian, and T. Xiaoou, "Single image haze removal using dark channel prior," Processing of 2009 IEEE Conference on Computer Vision and Pattern Recognition (CVPR). 2009, pp. 1956-1963.

★★★

MULTIPLE RESPONSES PROCESS PARAMETERS OPTIMIZATION OF TURNING AL-TICp METAL MATRIX COMPOSITES

[1]V. NAGA PRASAD NAIDU, [2]R. RAMA CHANDRA, [3]P. HUSSAIN BABU

[1]Professor & Principle, Intell Engineering College, Anantapur.
[2]Professor & Principle, S.k.d Engineering College, Gooty.
[3]Assistant Professor, Intell Engineering College, Anantapur.

Abstract— This investigation is proposed to investigate the Machining response of Al-TiC_P metal matrix composites. Aluminum alloy is considered as a matrix metal composite. The reinforcing phase considered is TiC_P Metal matrix composites will be fabricated using stir casting techniques. The number of process parameters considered in this investigation is spindle speed, Feed rate, Depth of cut grain size of TiC_P and cutting tool material. Experiments will be planned and conducted according to DOE (Design of Experiments).The machining responses considered are surface roughness, cutting force, cutting power & tool wear. In order to predict the output responses within the range of process parameters modeling will be done using response surface methodology and artificial intelligence systems viz. Fuzzy logic / Neural Networks; Grey relational analysis is used for optimization of multiple response characteristics. Finally analysis of variance and confirmation test will be done in next step to validate the developed models.

Keywords – Stir Casting, Machining, Optimization.

I. INTRODUCTION

In presents days every organization or Industry should depends upon composite materials because of more consistent with high stability, low density and high specific strength to wear ratio. These materials are widely used in Aerospace, Automotive, Electrical & Electronics, and Metallic & Medical Industries.

Al based metal matrix composite materials are one of the important composites easily available with low cost. These Al base composites improved Strength, Stiffness, and Wear Resistance over unreinforced alloys. However the final conversion of these composites into engineering products is always associated with machining by turning operation is circular in machine industries where work-piece is rotated along its axis and cut in form of chips by cutting tools with considering cutting parameters, for instance speed, and feed, depth of cut. Despite of that it is difficult even to skilled operator to carry out the job with optimum parameters which avail better characteristics and excellent qualities. For the record optimization is the best suite technique to draw optimum values which reveals to accomplished optimum scenario of economy, performance hence overall profit.

The turning is controlled by cutting and the geometry parameters. The cutting parameters include cutting speed, feed and depth of cut. Hence there is a need to optimize the process parameters. The objective is study to find out optimization of the process for minimization of surface roughness, power consumption and machining time of turning. Design of experiments (DOE) will be adopted and optimize combination of process parameters chosen using response surface methodology. Optimization of the process parameters using Genetic Algorithm optimization. The Response Surface Methodology (RSM) and genetic algorithm are the tools to measure the performance and calculate most suitable optimistic values.

II. RELATED WORK

This emphasis basically on the number of materials and the fabrication methods of composites. Metal matrix composites (MMC) are advanced materials resulting from a mixture of two or more materials in which superior properties are realized. They are acknowledged significant attention in recent years because of their high strength, stiffness, low density.

III. MATERIALS

A wide variety of matrix cast aluminum & titanium alloy are used to fabricate composites based on different reinforcement materials depend upon on their application in industries. Aluminum and Titanium metal matrix composites are mainly used in defense, military, automobile and general engineering purpose because of their superior properties.

Composites are manufactured with great achievement by the use of fiber reinforcement materials in metal matrix metallic materials. The aim concerned in designing MMC materials is to unite the attractive attribute of metals and reinforcement. In reinforced MMC, reinforcement particle is mixed to the matrix of the mass material to boost its stiffness and strength. Applications which are subjected to serious loads, or tremendous thermal variations, such composite is superior to any machining process.

IV. CUTTING PARAMETERS

Speed

Speed always refers to the spindle and the work piece. When it is stated in revolutions per minute (rpm) it tells their rotating speed.

$$v = \frac{\pi DN}{1000} \frac{m}{min}$$

Here, V is the cutting in turning,
D is the initial diameter of the work piece in mm
N is the spindle speed in RPM.

Feed

Feed always refers to the cutting tool, and it is the rate at which the tool advanced along its cutting path.

$F = fN$ mm/ min^{-1} ---------- (2)

Here, F is the feed in mm per minute,
f is the feed rate in mm/rev and
N is the spindle speed in RPM

Depth of Cut

Depth of cut is practically self-explanatory. It is the thickness of the layer being removed (in a single phase) from work piece or distance from the uncut surface of the work to the cut surface.

Here, D and d represent initial and final diameter (in mm) of the job respectively.

Depth of cut = (D-d) /2 mm ---------- (3)

Surface Roughness

Roughness is a measure of the texture of a surface.

Material Removal Rate

The material rate (MRR) in turning is the volume of material/material that is removed per unit time in mm^3/min. For each revolution of the work piece, a ring shaped layer of material is removed.

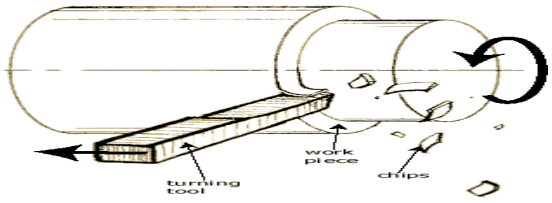

Fig- Material Removal Rate in Turning

$$MRR = \left[\frac{\pi D^4}{4} - \frac{\pi d^4}{4}\right] X\ F\ X\ rpm \quad ---(4)$$

Where,
D = diameter of work piece before cutting
d = diameter of work piece after cutting

Manufacturing Methods

A number of composite fabrication have been developed that can be placed under. The following categories. They are (1) Stir Casting (2) powder metallurgical techniques (3) liquid Metallurgy (4) squeezes casting.

Among the number of techniques existing for metal matrix composites, stir casting techniques usually accepted as a namely promising way, at present practiced commercially. Its advantages are simplicity, flexibility and applicability to large quantity production. It allows a conventional composites fabrication is route to be used, and therefore minimize the final cost of the product. Metal matrix composites are usually fabricated by liquid metallurgy route or stir casting technique. A comparison of different fabrication methods are below table 1.

In stir casting the particulates phase are mechanically mixed in the liquid phase before solidification of the melt. Parameters such as unusual particle sizes, density, geometries, pour or the progress of an electrical charge throughout mixing may direct to agglomeration. In this method incorporation of matrix and reinforcement is a vital step to get a homogenous distribution of reinforcing particles in matrix. The reinforcement particles were mixed in a calculated mixer by stirring for few minutes and cast in a steel mold or sand mould. Magnesium (1%) addition during the stirring

Improves the wettability of reinforcement with the melt aluminum. The molten degasses in completely liquid condition with (Na-CL and KF) blend then skimmed, followed with degassing by pure argon for 30 to 40 seconds. Stirring, the molten metal composites are poured into the permanent mould, which was preheated to 200^{o}c.

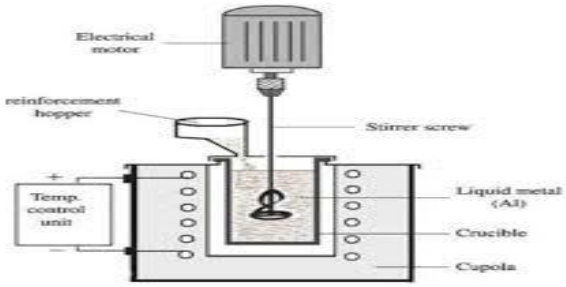

Fig.1 A schematic diagram of Stir Casting Technique

V. THE POWDER METALLURGY PROCESS

The concept of making parts from metal powder is simple and straight forward; however, the techniques employed can be very sophisticated, requiring a high level of technical competence and a substantial investment in capital equipment. The process consists of three steps: blending, compacting, and sintering.

Blending

Blending is the process of powder agitation for the purpose of homogenizing the particle sizes. Mixing also takes place and serves to intersperse powders of different chemical compositions. Alloyed powders are produced by combining a homogeneous mixture of carefully weighed and blended powders.

Lubricants are added to the powder to reduce friction between the particles as

They are being compacted, as well as to reduce die wear. Stearic acid, lithium stearate, or powdered graphite is the principal lubricants used. Blending is almost universally done dry; however, in some finely divided aluminum powders, to reduce dust and the danger of explosion or fire, the process is done wet.

Compacting

After the metal powders have been blended to achieve various desired properties, they are pressed or compacted to the required shape, size, and density.

Metal powders present problems of internal friction when pressed in the die. Both density and strength decrease in the powder mass as the distance from the punch increases. To minimize this condition, punches are used at both ends of the die as shown in fig. the use of lubricants improves the density, minimizes the load required, and increases life, particularly by easing part ejection. However, lubricants can create problems in reduced green strength, in feeding the powder into the die, and in lubricant reaction. Lubricants must be driven off by a low temperature stage heating before sintering,

For high volume production, tungsten carbide is used as the die material.

Although the cost is higher, it will outwear the normally used tool steels by a ratio of

About 10:1. Some carbide dies can be used to produce a million parts before tolerances are exceeded. High pressures, sometimes in excess of 50 tons/in2. (689.5Mpa) are used to cause mechanical interlocking between the irregularities of the particles.

The compaction operation consolidates and dandifies the powders into what is commonly termed a green compact. The compact will be very close to the size, shape, density of the finished part. After ejection from the die the part can be handled, but is relatively fragile in the green state and if dropped will probably crack.

There are two main methods of compacting metal powders: (1) with a punch and Die (2) is statically. Part geometry is the major factor in determining which method is to be used. If the part shape is simple, mechanical pressing is likely to be used. Parts with intricate configurations can be made by isostatic compaction discussed later.

Die Compaction: Die compaction is limited to vertical motions only, so parts with back angles are undercuts cannot be made. For a mechanical press operating on powder fill/ compaction/ejection cycle of 3 to 4 seconds, approximately 1000 components can be produced per hour. For simpler parts, these outputs can be increased with multi station rotary presses, where multiple sets of tools are mounted on a rotary table. Punch motions are actuated by fixed, horizontal cam tracks or rollers, and the presses are capable of very high output rates in the order of 35,000 parts per hour.

Mechanical and Hydraulic Presses. Both mechanical and hydraulic types of Presses are used for compacting. The advantages and limitation of each are briefly as follows.

Mechanical presses are of lower tonnage (usually 200 tons or less) and have faster cycles. Normally no dwell time is possible, although newer presses have clutches. Compacting is done to given height, not to a given pressure or density.

Hydraulic presses are of higher tonnage (usually 500 tons or more), have slower Cycle time, even with accumulators, and have infinitely variable dwell time. Parts may be pressed to a given load to provide good density control. Limit switches may be used for height control.

VI. SINTERING

Sintering is the third step in producing powdered metal parts. The green compacts are heated in muffle type or wire mesh conveyer belt furnace. Special atmosphere, such hydrogen or dissociated ammonia, are required for sintering of ferrous metal to control both carburization and de carburization of iron and iron rich compacts.

Furnace temperature vary with the sintering requirements; for brass, a temperature of 1600^{o} to 1615^{0}F (870^{o} to 880^{o}C) is satisfactory, and for stainless steel, 2000^{o} to 2350^{o}F (1100^{o} to 1300^{o}C) is used. The temperature must remain between 60% to 80% of the melting point of the principle constituent. The sintering time may range from 20 minutes to an hour or more. The lubricants that were originally blended with the powders are permitted to burn off in a special chamber before the parts reach the high heat zone of the furnace.

VII. LIQUID METALLURGY ROUTE

Liquid state processes include stir casting or compo casting, infiltration, spray casting and in situ (reactive) processing. The selection of the processing route depends on many factors including type and level of reinforcement loading and the degree of micro structural integrity desired.

VIII. SQUEEZE CASTING

The squeeze casting process is actually a combination of casting and forging. A precise amount of molten metal is poured into the bottom half of a preheated die set and allowed to partially solidify. An upper die then descends applying pressure throughout the duration of solidification. Intricate shapes can be produced at that are far less than would normally can required for hot or cold forging. Both retractable and disposable cores can used to create holes and internal passages. Gas and shrinkage porosity are substance reduced and mechanical properties are enhanced. The process can be applied to both ferrous and nonferrous alloys and both wrought and cast alloy be processed.

An adaptation of the process can be used to produce metal matrix composites by forcing the pressurized liquid around formed or fiber reinforced that have been positioned in the mold. Another modification involves the use of thixotropic semi solid material. Here the need to introduce a precise amount of molten metal into the die is eliminated by starting with chucks of metal that have been heated into the semisolid range. Thixotropic material can be handled mechanically, like a solid, but shaped at low pressure because it flowed like a liquid when agitated or

squeezed. The absence of the turbulent flow minimizes the gas pickup and entrapment. Since the material is already partially solid, solidification shrinkage and related porosity is reduced. Cooling while under pressure completes the solidification, while simultaneously producing high quality intricate parts with good finish and precision

Table.1.Comparative evaluations of the different techniques used for MMCs fabrication.

Method	Range of shape and size	Metal Yield	Range of volume fraction	Damage to reinforcement	Cost
Liquid metallurgy(Stir Casting)	Wide range of shapes; up to 500kg	Very high,>90%	Up to 0.3	No damage	Least expensive
Squeeze casting	Limited to perform shape	Low	Up to 0.45	Severe damage	Moderately expensive
Powder metallurgy	Wide range; restricted size	High	-	Reinforcement fracture	Expensive
Spray casting	Limited shape; large size	Medium	0.3-0.7		Expensive
Lanxide technique	Limited by pre-form shape; restricted size	-	-	-	expensive

IX. LITERATURE REVIEW

The following review given us an idea of the techniques used for fabricating, Wear Analysis, Machining of Turning & Optimization of aluminum and titanium carbide powder metal matrix composites.

Raidu et al, (2010) developed a fuzzy logic based model for selecting cutting parameters in turning tool and die steel with cemented carbide, ceramic and sintered PcBN cutting tool during hard turning operation.

M.Subramanian et al, (2013) In this metal matrix composites (AL 7075-T6) they developed a statistical model a predict cutting force on terms of machining parameters such as cutting speed, feed rate and axial depth of cut Responses surface methodology experimental design was use for conducting experiments. The tool was shoulder mill with two carbide insert the cutting force were measured using three axis milling tool dynamometer. The second order mathematical model in terms of machining parameters was developed for predicting cutting force; the optimization of shoulder mill machining parameters to acquire minimum cutting force was done by Genetic Algorithm (GA)

C.Dileep Kumar et al, (2014) the effect of cutting parameters on surface finishes and optimizes them for better surface finish and material removal rate (MMR) during turning of Ti-6Al-4V. A combined Taguchi method and grey relational analysis is used for the optimization. Analysis of variance (ANOVA) is employed to find out contribution of each at three level and is designed by using Taguchi's L9 Orthogonal array (OA) MINITAB statistical software is employed to create the plan carrying out the analysis.

K.Krishna et al. (2015) They study the prediction of material removal rate (MMR) of CNC turning using back propagation neural network (BPNN) machining operation have been performed in AL work piece by carbide insert over a range of cutting parameters of BPNN & MRR, spindle load has been use as output of the network, And they inclusion of cutting speed, fee rate, depth of cut as an input parameters lead to better training of the network. And they performance of the Artificial Neural Network (ANN) has been found.

Girish Kant et al,(2015) it develops a predictive an optimization model b coupling the two artificial intelligence approaches- artificial neural network (ANN) and genetic algorithm (GA)-as an alternative to conventional approaches in predicting the optimal value of machining parameters(cutting speed, feed rate, depth of cut and flank wear) leading to minimum surface roughness. A real machining experiment has been referred in this to study to check the capability of the proposed model for prediction and optimization of surface roughness.

Arezzo et al, developed an expert system to select cutting tools and cutting conditions of turning operations using Prolog. The system can select the tool holder, and the insert and cutting conditions, such as cutting speed, feed rate and depth of cut. Dynamic programming was used to optimize the cutting conditions.

R.Arularasan et al, (2015) they study titanium alloy composites the non conventional optimization technique, Genetic algorithm (GA) results were compare with taguchi optimization technique. Te process variable considered for optimization are speed, feed & depth of cu

CONCLUSION

Based on the above investigation, it is conclude that there are number of techniques which are used to prepare composite material, the Stir casting Technique is best way to fabricate the MMC's. In this research the optimization of machining condition

with corresponding surface Roughness, Cutting Power & Tool wear rate, In this field the turning parameters optimization using Grey Relational Analysis, Neural Network method but there is a lack in studies in the field of vibration optimization in turning operation which is very important. The performance of quality of surface and optimization of cutting parameters with aid of DOE, Grey Relational Analysis Neural Network, optimization is one of the goals of manufacturing systems also it is simple to use and are increasingly used to solve inherently intractable problems quickly. However many studies are concentrated on optimization of surface roughness and cutting parameters.

ACKNOWLEGEMENT

Finally I Wish special thanks to all authors & my guides to give excellent path of my investigation in Al based composites.

REFERANCE

[1] K.Saravana Kumar et al,''Optimization of CNC turning process on INCONEL718 using genetic algorithm'', IRACST-Engineering science and Technology an international journal (ESTIJ), 2:532-537, (2012).

[2] Rasool Mokhtari Homami et al,''Optimization of Turning process Using artificial intelligence technology'', International Journal of Advanced Manufacturing Technology (2013).

[3] M.Subramanian et al, ''Optimization of Cutting Parameters for Cutting Force in Shoulder Milling of Al7075-T6 Using Response Surface Methodology and Genetic Algorithm''. International Conference on Design and Manufacturing, Proceia Engineering 64 pp690-700, (2013).

[4] Y.Muhammad et al, ''Surface Quality Chip Formation in Turning of LM6 Aluminum Alloy and Particulate Reinforced Metal Matrix Composites''. Journal Of Material Science Forum Vols. 773-774 (2013) pp894-901.

[5] D.Sai Chaitanya Kishore et al. Investigation of cutting force, Surface roughness an flank wear in turning of In-situ Al6061-TiC metal matrix

★★★

EXPERIMENTAL INVESTIGATIONS ON PARTIAL REPLACEMENT OF STEEL SLAG AS COARSE AGGREGATES AND ECO SAND AS FINE AGGREGATE

[1]Y. ANAND BABU, [2]SURI NANDINI

[1]Associate Professor, Civil, [2]M.Tech Scholar, Civil Engineering Department,
MVR College of Engineering and Technology, Paritala, Andhra Pradesh, India

Abstract— Concrete is the 2nd highest using material in this world. Continuous utilization of coarse and fine aggregates for concrete we are facing different problems like lack of availability of these aggregates with good quality. To overcome this problem replaced the aggregates with eco-sand and steel sag. The primary objective of the project is to increase the strength of the concrete by replacing coarse aggregate by steel slag and also 30% replacement of eco sand as fine aggregate. As of from literature steel slag is replaced for 0,15,30,45,60,75,90 % which indeed gives us 7 mixes (M1, M2, M3, M4, M5, M6, M7) totally. After conducting various tests we can arrive to conclusions of mixes M1, M2, M3, M4 are relatively good strength than conventional mix. Particularly the mixes M3, M4 which consists of 30 & 45 % of slag has high strength in all tests. It is evident that 50 % or more is not feasible as the strength found is very low compared to conventional mix.

Keywords— eco-sand, steel sag, replacement of aggregate, strength comparison.

I. INTRODUCTION

1.1. General

Concrete is a mixture of cement, water and aggregates with or without admixtures. It is a composite material composed of granular materials like aggregates embedded in a matrix and bound together with cement or binder which fills the space between the particles and glues them together. Concrete is unique among major construction materials because it is designed specifically for particular civil engineering projects. Thus the concept of replacement of coarse aggregate with steel slag and fine aggregate with Eco-sand seems to be promising. The issue of environmental degradation and need for aggregates demands for the usage of any other alternative source

1.2. Existing Problems

- India has an enormous growth in the Steel Industries and Steel slag a byproduct of the same has to be disposed of properly; else they may cause environmental hazards to the surroundings.
- River sand poses the problem of acute shortage in many areas due to large requirements in construction industry.
- Rapid and prolonged sand mining causes scouring of river beds and also the loss of natural minerals present in the river leads to environmental effects.
- The unit cost of sand increases day by day and there is a need for an alternative material.
- Thus, this study aims at using byproducts of steel and cement industry, which will be cost effective and also a better way for managing its disposal.

1.3. Research Significance

- A new concrete with more strength and durability could be found.
- The behaviour of concrete under various tests can be noted.
- The significant research of whether replacements are resistible is being done.

1.4. Objectives and Scope of the Study

1.4.1. General

Steel slag as partial coarse aggregate replacement and Eco-sand as partial fine aggregate replacement entails economical, technical and energy saving benefits. To ascertain its technical feasibility to incorporate in concrete production, a study on its strength is needed.

1.4.2. Objective

The objective of the present study is

1. To study the broader use of the eco-sand in concrete as fine aggregate.
2. To study the possibility of using steel slag as coarse aggregate replacement in concrete.
3. To study the feasibility of utilization of eco-sand as fine aggregate replacement material along with steel
   a) Compressive strength
   b) Split Tensile strength
   c) Flexural strength
4. To investigate the strength of replaced concrete with that of conventional concrete.

1.4.3. Scope of the Study

This project aims mainly to study the mechanical and durability characteristics of the concrete with steel slag as coarse aggregate replacement and Eco-sand as fine aggregate replacement, by conducting compressive strength test, split tensile strength test, flexural strength test, water absorption test and thus

comparing the results obtained with normal conventional concrete using M30 & M50 grade of concrete.

- A much more extensive study on the properties and behaviour of concrete with eco-sand can be made
- Investigation may be done for higher grades of concrete and with different water cement ratios with same materials
- Study on concrete with full replacement of steel slag as coarse aggregate can be done.

II. METHODOLOGY

The following figure shows the methodology involved in the entire project work.

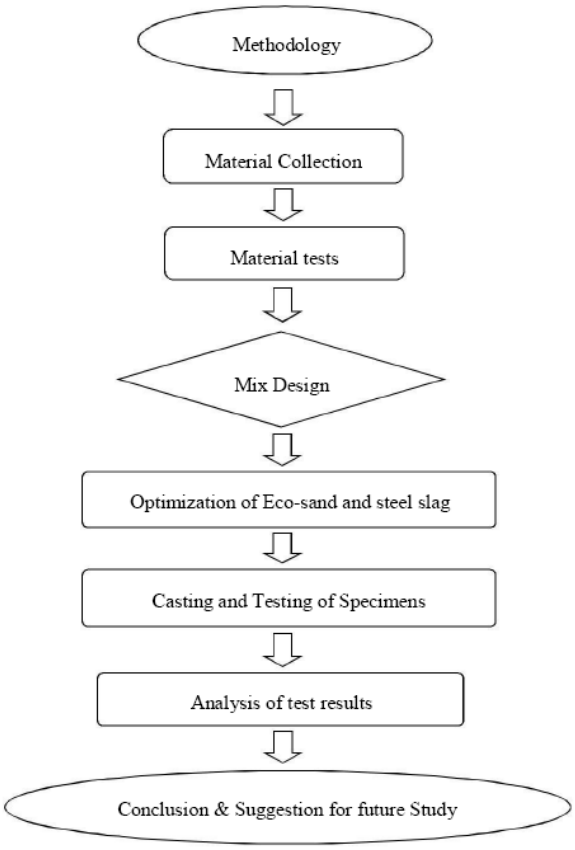

Figure 2.1 Methodology involving entire project

III. MATERIALS AND PROPERTIES

All the materials which are to be used that is normal fine aggregate, normal coarse aggregate, steel slag, eco sand, and OPC of 53 grades were tested to find their properties.

3.1. Steel Slag

Steel slag is an industrial byproduct obtained from the steel manufacturing industry. It is produced in large quantities during the steel-making operations which utilize Electric Arc Furnaces (EAF). Steel slag can be used in the construction industry as aggregates in concrete by replacing natural aggregates. Natural aggregates are becoming increasingly scarce and their production and shipment is becoming more difficult. Steel slag is currently used as aggregate in hot mix asphalt surface applications, but there is a need for additional work to determine the feasibility of utilizing this industrial by-product more wisely as a replacement for both fine and coarse aggregates in a conventional concrete mixture. Steel slag is a by-product of steel making, is produced during the separation of the molten steel from impurities in steel-making furnaces.

3.1.1. Physical Properties

Steel slag aggregates are highly angular in shape and have rough surface texture. They have high bulk specific gravity and moderate water absorption (less than 3 percent). Table 3.1.1 lists some typical physical properties of steel slag.

Table 3.1.1 Typical physical properties of steel slag

Property	Value
Specific Gravity >	3.2 - 3.6
Unit Weight, kg/m^3 (lb/ft^3)	1600 - 1920 (100 - 120)
Absorption	up to 30%

3.1.2. Chemical Properties

The chemical composition of slag is usually expressed in terms of simple oxides calculated from elemental analysis determined by x-ray fluorescence. Table 3.1.2 lists the range of compounds present in steel slag from a typical base oxygen furnace. Virtually all steel slag's fall within these chemical ranges but not all steel slag's are suitable as aggregates. Of more importance is the mineralogical form of the slag, which is highly dependent on the rate of slag cooling in the steel-making process.

Table 3.1.2 Typical steel slag chemical composition

Constituent	Composition (%)
CaO	40 - 52
SiO_2	10 - 19
FeO	10-40 (70 - 80% FeO, 20 - 30% Fe_2O_3)
MnO	5 - 8
MgO	5 - 10
Al_2O_3	1 - 3
P_2O_5	0.5 - 1
S	< 0.1
Metallic Fe	0.5 - 10

3.1.3. Mechanical Properties

Processed steel slag has favorable mechanical properties for aggregate use, including good abrasion resistance, good soundness characteristics, and high bearing strength. Table 2.1.3 lists some typical mechanical properties of steel slag.

Table 3.1.3 Typical mechanical properties of steel slag

Property	Value
Los Angeles Abrasion (ASTM C131), %	20 - 25
Sodium Sulfate Soundness Loss (ASTM C88), %	<12
Angle of Internal Friction	40° - 50°
Hardness (measured by Moh's scale of mineral hardness)*	6 - 7
California Bearing Ratio (CBR), % top size 19 mm (3/4 inch)**	up to 300

* Hardness of dolomite measured on same scale is 3 to 4.
** Typical CBR value for crushed limestone is 100%.

Slag is a co-product of the iron and steel making process. The use of steel slag aggregates in concrete by replacing natural aggregates is a most promising concept. Steel slag aggregates are already being used as aggregates in asphalt paving road mixes due to their mechanical strength, stiffness, porosity, wear resistance and water absorption capacity.

Table 3.2 Steel aggregate properties

S.no	Property	Value
1	Specific gravity	2.61
2	Water absorption	1.05%
3	Flakiness Index	8.5%
4	Elongation Index	4.5%
5	Impact strength	19.5%
6	Crushing Strength	19%

3.3. Eco-Sand

Eco-sand is very fine particles, a by-product from cement manufacturing semi-wet process, a product by ACC cements. It is finely powdered crystalline silica which can replace up to 50% of conventional sand usage in concrete and mortars. Its micro-filling effect reduces pores in concretes and provides better moisture resistivity and thus durability. It has more consistent grading than many extracted aggregates. The use of Eco-sand rather than extracted or dredged natural sand will help designers and contractors address issues of sustainability. The Eco-sand has various advantages such as energy efficient, fire resistant, reduction of dead load, environmentally friendly, durable, light weight, low maintenance and low construction cost. The non-absorbent nature and smooth surface texture benefits workability and reduces water requirement. The cost is about Rs.24 per cubic feet whereas river sand is about Rs.35 to Rs.40 per cubic feet approximately. The cost of Eco-sand is less than river sand, yet its behavior and characteristics has to be studied.
Its specific gravity is 2.63 and the particle size is less than 15 μm sieve.

3.4. Cement

It is defined as a material with adhesive and cohesive properties which make it capable of binding material fragments into a compact mass. Cement is obtained by burning calcareous and argillaceous materials by partial fusion at a high temperature of about 1450ºC. The Ordinary Portland Cement is generally classified into three grades, they are 33 grade, 43 grade and 53 grade. In this study OPC 53grade has been used. Brand used is Coromandel King OPC 53grade cement. Its chemical composition is as given in Table 3.3.1; its physical properties are as follows.

Table 3.4.1 Chemical composition of OPC (53 grade)

Properties	Values obtained	Requirements as per
Lime saturation factor	0.9	0.8-1.02
Alumina Modulus	1.23	0.66 (min)
Insoluble residue (%)	0.25	4 (max)
Magnesia (%)	1.1	6 (max)
Sulphuric anhydrideSO3 (%)	1.5	3 (max)
Loss on ignition (%)	0.8	4 (max)
Alkalies	.	.
Chloride (%)	0.002	0.1 (max)
C3A Content	7	.
Temperature during Testing	27±2	27±2
Humidity (%)	90±5	90±5

3.5. Coarse Aggregate

Coarse aggregate consists of river gravel, crushed stone or manufactured aggregate with particle size equal to or greater than 4.75mm. It shall comply with the requirements of IS383-1970. For the coarse aggregates, the following test has been carried out conforming to IS2386 (part 1) 1963. In this study coarse aggregate of maximum size 12.5 mm was used and the physical properties are as follows.

3.5.1. Physical Properties

Specific gravity : 2.71

3.6. Fine Aggregate

Aggregates are the major ingredients of concrete, as they constitute 70-75% of the total volume, provide a rigid skeleton structure for concrete, and act as economical space fillers. In India river sand is used as fine aggregate. The sand was washed and screened at site to remove deleterious materials and tested as per the procedure given in IS: 2386-1963 and the test results should comply with the requirements of IS383-1970. The results are as follows

3.6.1. Physical Properties

Table 3.*6.1* Physical properties of fine aggregate

S. No	Property	Value
1	Sieve Test	Separate analysis is done
2	Specific gravity	2.45
3	Fineness Value	2.98%
4	Bulk density	10.2%

3.7. Water

For this study portable water available in the campus with pH value 7 and conforming to the specifications of IS456-2000 is used for concreting as well as curing of the specimens.

IV. EXPERIMENTATION

This chapter presents the details of experimental investigations carried out on the test specimens to study the strength related properties of high performance concrete using steel slag and Eco-Sand. Here, an attempt was made to study the strength development at different replacement levels at different ages with Eco-sand and the results were compared. It is found from the past researches that optimum replacement level of steel slag for cement is 0 to 100% by means of weight. So in all the mixes fine aggregate was replaced with 30% of Eco-sand. The strength related properties such as compressive strength, splitting tensile strength, flexural strength were studied. Minimum three specimens were tested for each mix for each test. The entire tests were conducted as per specifications required.

4.1. Test Result

4.1.1. Compressive Strength

The casted cubes have been tested and the compressive test results are listed in the Table 4.1.1

Table 4.1.1 Determination of compressive strength

Mix Combination	7Days strength (Mpa)	14Days Strength (Mpa)	28Days Strength (Mpa)
Control Mix	24.68	32.18	39.68
Eco sand 30% and Steel slag 0%	27.61	33.852	38.2
Eco sand 30% and Steel slag 15%	28.80	34.212	40.21
Eco sand 30% and Steel slag 30%	30.22	35.77	41.32
Eco sand 30% and Steel slag 45%	32.4	37.6	42.8
Eco sand 30% and Steel slag 60%	27.34	31.77	36.2
Eco sand 30% and Steel slag 75%	26.20	31.0	35.8
Eco sand 30% and Steel slag 90%	27.79	29.52	34.78

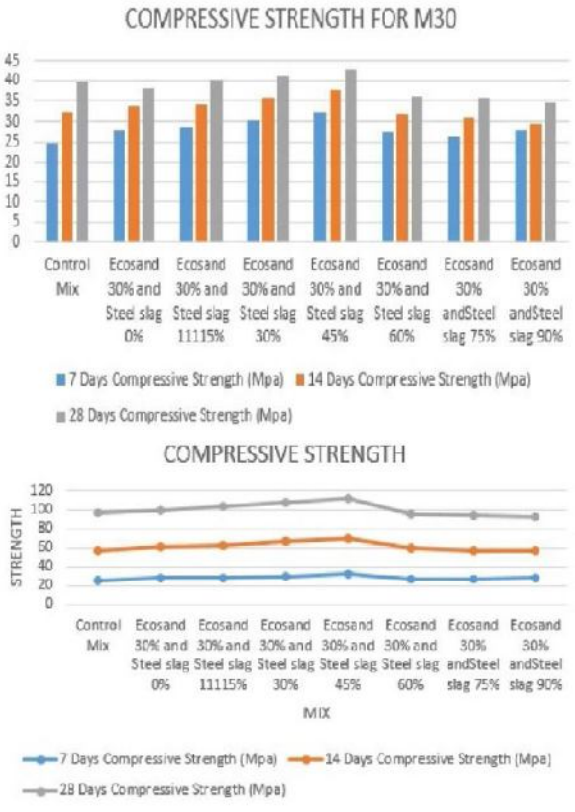

4.1.2. Split Tensile Test

The spilt tension test has been carried out for cylinders and the results are stated in the Table 4.1.2

Table 4.1.2 Determination of Split Tensile Strength

Mix Combination	28 Days Split Tensile Strength (Mpa)
Control Mix	2.62
Eco-sand 30% and Steel slag 0%	2.75
Eco-sand 30% and Steel slag 15%	2.89
Eco-sand 30% and Steel slag 30%	2.70
Eco-sand 30% and Steel slag 45%	3.14
Eco-sand 30% and Steel slag 60%	3.29
Eco-sand 30% and Steel slag 75%	3.52
Eco-sand 30% and Steel slag 90%	4.36

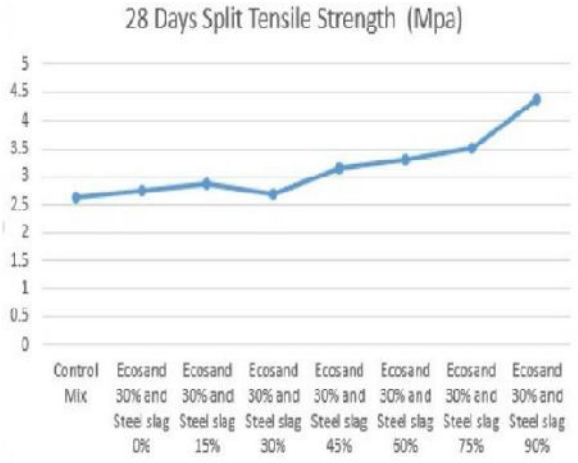

4.1.3. Flexural Strength Test

The flexural strength test for beam has been carried out and the results have been tabulated in the Table 4.1.3

Table 4.1.3 Determination of flexural strength

MIX ID	% OF STEEL SLAG	% OF ECO SAND	ULTIMATE LOAD (kN)	FLEXURAL STRENGTH AT 28 DAYS IN N/mm^2
MC	0	0	28	11.2
M1	0	30	35	13.6
M2	15	30	37	14.0
M3	30	30	43	14.8
M4	45	30	48	17.2
M5	60	30	31	19.2
M6	75	30	27	12.4
M7	90	30	24	10.8

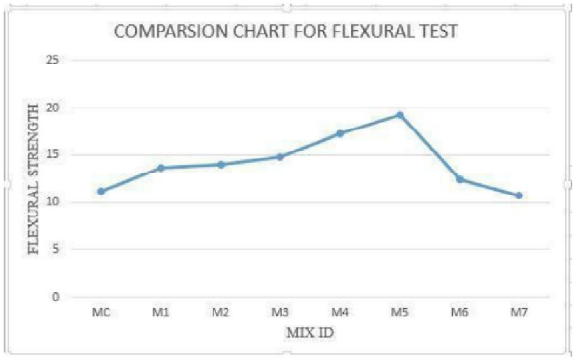

From the Fig 4.1.3 we can arrive that the maximum flexure strength is obtained for mix M4and that of minimum strength is obtained for mix M6.

4.1.4. Test results for Beams

A total of 27 beams are tested and following are the deflection and stiffness for conventional and various other Mixes. The conventional beam results are kept as reference and comparative study is done. It is expected that an increase around 30% strength is gained by adding steel slag and Eco-sand in an incremental basis.

4.1.5. Conventional Beam

The deflection and stiffness values are tabulated for control mix in Table 4.1.4.1. The load is give from 0-35 kN and their corresponding deflection shown below.

Table 4.1.4.1 Conventional Beam Results

Load (kN)	Deflection (mm)	Stiffness (kN/mm)
0	0	0
5	0.53	9.43
10	1.02	9.80
15	2.6	5.76
20	2.88	6.94
25	3.52	7.10
30	3.76	7.97
35	4.22	8.29

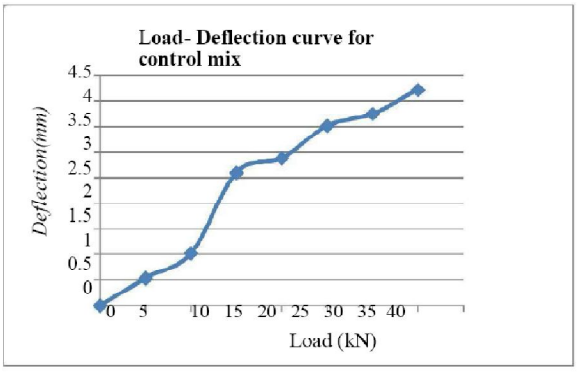

4.1.6. Mix M7 (Eco-sand 30% and steel slag 90%)

The deflection and stiffness values are tabulated for mix M5 in Table 4.1.4.2 and load vs. deflection curve is shown below

Table 4.1.4.2 M7 Beam results

Load (kN)	Deflection (mm)	Stiffness (kN/mm)
0	0	0
5	0.82	6.09
10	1.83	5.46
15	3.02	4.96
20	3.82	5.23
25	4.75	5.26
30	4.87	6.16
35	5.12	6.83
40	5.95	6.722

The main objective of this research was to utilize the steel slag aggregate in the concrete mixture and identify the mechanical and flexural properties of the mixture. The experimental study started by replacing the percentage of the volume of natural aggregates, normally used in the manufacture of concrete , with steel slag in increments of 10% until all the natural aggregates were replaced by the steel slag to find the possible optimum replacement level for the steel slag in concrete.

4.2. Comparison of Results

Now comparing the results for 28 days strength for M30 & M50 grades.

4.2.1. Comparison of Compression Strength for M30 & M50 Grades

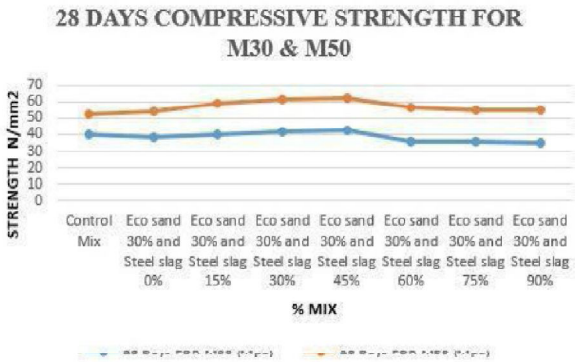

Graph shows 28 days compressive strength

4.2.2. Comparison of Split Tensile Strength for M30 & M50 Grades

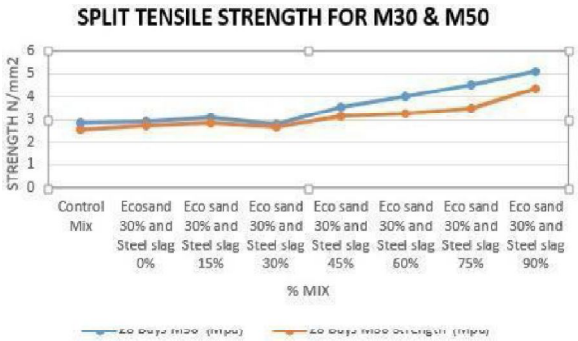

Graph shows comparison of split tensile strength for 28 days

4.2.3. 28 days Flexural Strength for M50 & M30

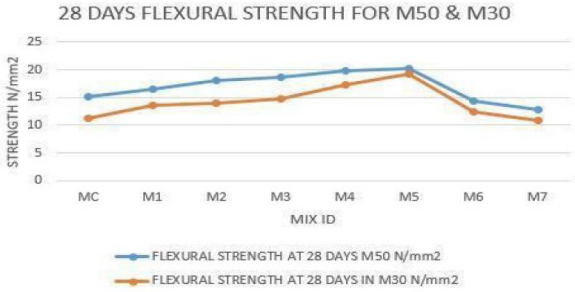

Graph shows comparison of Flexural tensile strength for 28 days

4.2.4. Mix Design Calculation

TYPE OF MIX	Cement Kg/m^3	Fine Aggregates (sand + 30% eco sand)Kg/m^3	Coarse Aggregate (% replacement slag)kg/m^3	Water l/m^3
MC	400	593.3	1154.4	180
M1	400	415.31 +177.9	1154.4	180
M2	400	415.31 +177.9	981.24+173.16	180
M3	400	415.31 +177.9	808.08+346.32	180
M4	400	415.31 +177.9	634.92+519.48	180
M5	400	415.31 +177.9	461.76+692.64	180
M6	400	415.31 +177.9	288.6+865.8	180
M7	400	415.31+177.9	115.44+1038.96	180

CONCLUSION

- Optimum level of replacement for Eco-sand is found as 30%. Increase in strength initially is attributed to particle size effect and decrease in strength beyond 30% is attributed to water absorption capacity of Eco- sand.
- Optimum level of replacement for steel slag is found as 60%. Increase in strength initially is attributed to shape effect and decrease in strength beyond 60% is attributed to porosity of steel slag.
- The combination, 30 percent replacement of Eco-sand and 60 percent replacement of steel slag is fixed for study and it gave compressive strength of above 40Mpa and 60Mpa for concrete mixes M30 & M50, split tensile strength and flexural strength were also found to be comparatively higher.
- Replacing the conventional granite coarse aggregate by steel slag aggregate in conventional concrete enhances the compressive strength when the replacement level is up to 60 percent, for further replacements compressive strength is found to decrease.
- The increase in strength for the replacement of coarse aggregate by steel slag up to 60 percent may be due to shape, size and surface texture of steel slag aggregates, which provide better adhesion between the particles and cement matrix.
- From the test results obtained it may be concluded that ES30St60 combination is the optimum and most suitable for areas not exposed to marine conditions.
- At 75% and 90% replacement of sand in M50 grade ,the strength of the concrete is decreased ,so to overcome this admixtures like silica fume or fly ash are added to cement to increase the strength.

5.1. Scope for Further Study

- A much more extensive study on the properties and behavior of concrete with Eco-sand can be made.
- Investigation may be done for higher grades of concrete and with different water cement ratios with same materials.
- Study on concrete with full replacement of Eco-sand as fine aggregate can be done.
- Further investigation on resistance of concrete with steel slag aggregates to attack by sulfates, acid, and alkali silica reactions, carbonation,

harmful chemicals and resistance to high temperatures can be carried out.

- Fire resistance capacity of steel slag aggregate concrete may be investigated. Due to presence of several dangerous heavy metals and salts in the steel slag aggregates, leaching tests can be carried out to verify its environmental compatibility.
- A broad study can be done on durability characteristics of concrete with steel slag and Eco-sand as coarse and fine aggregate replacements. Age maturity concept and corrosion studies can be carried or further as the normal aggregate is replaced with steel slag in concrete.

REFERENCE

[1] Abdulaziz I. Al-Negheismish, Faisal H. Al-Sugair and Rajeh Z. Al-Zaid (1996), 'Utilization of Local Steelmaking Slag in concrete', Journal of Environmental science of sustainable society, Vol. 1, pp. 39-55,

[2] Anastasiou E. and Papayianni I. (2006), 'Criteria for the Use of Steel Slag Aggregates in Concrete', Measuring, Monitoring and Modeling Concrete Properties.

[3] Barry M.S., Ibrahim M., Maslehuddin M., Al farabi M.S., Shameem M., (2002), 'Comparison of properties of steel slag and crushed limestone aggregate concretes', Construction and Building Materials, Vol. 17, pp 105-112.

[4] Biju Mathew, Dr Freeda Christy C, Dr. Benny Joseph and Anuragi.P, An Experimental Study on Properties of Cement Mortar by Replacement of Natural Sand with Manufactured Sand. *International Journal of Civil Engineering and Technology (IJCIET),* 7(4),2016, pp.483–490.

[5] Dubravka Bjegovic´, Goran Vrhovac, Ivanka Netinger, (2011), 'Utilization of steel slag as an aggregate in concrete', Materials and Structures.

[6] Emery J J (1980), 'Pelletized lightweight slag aggregate' Journal of Environmental engineering, Vol. 24, pp 111-116.

[7] Juan M Manso, Juan A Polanco, and Javier J Gonzalez (2004), 'Electric Arc Furnace Slag in Concrete',

[8] Journal of Materials in Civil Engineering, Vol. 16.pp 639-645.

[9] Juan M Manso, Juan A Polanco, Milagros Losanez and Javier J Gonzalez (2006),'Durability of Concrete made with EAF Slag as Aggregates' Cement and Concrete Composite, pp 528-534.

[10] IS: 2386:1963, "Methods of test for Aggregates for concrete", Bureau of Indian standards, New Delhi, India.

[11] IS 10262: 1982, "Concrete mix proportioning guidelines (First Revision)", Bureau of Indian standards, New Delhi, India.

[12] Ananthayya M.B. and Prema Kumar W. P., Influence of Steel Fibers and Partial Replacement of Sand by Iron Ore Tailings on the Compressive and Splitting Tensile Strength of Concrete. *International Journal of Civil Engineering and Technology (IJCIET),* 5(3),2014, pp.117–123.

[13] IS 456: 2000, "Code practice for Plain and cement concrete (Fourth Revision)", Bureau of Indian standards, New Delhi, India.

★★★

ORAL MICROBIOTA IN HEALTHY THAI ADULTS IN BANGKOK AND NEARBY PROVINCES

[1]MATANEE PALASUK, [2]PATCHAREE RITPRAJAK, [3]NARAPORN SOMBOONNA

[1,3]Department of Microbiology, Faculty of Science, Chulalongkorn University.
[2]Department of Microbiology, Faculty of Dentistry, Chulalongkorn University.
E-mail: [1]matanee13@gmail.com, [2]patcharee.r@chula.ac.th, [3]naraporn.s@chula.ac.th

Abstract— Oral cavity is a complex organ containing several parts such as teeth, tongue, gingival and cheeks, that have a variety of bacteria. More than 700 species of bacteria have been reported in oral cavity. Dysbiosis in oral microbiota can increase a risk of oral disease and may lead to systematic disease. Oral microbiota diversity could be indicated oral health and there have many factors that affect to oral microbiota composition such as ages, gender and race. Next-generation sequencing is a technique that used to study all microorganisms including non-culturable microorganisms. In this study, we collected saliva and oral rinse from 20 healthy Thai adults. metagenomic DNA were amplified V4 region of the 16s rRNA gene using universal primers. The number of OTUs and alpha-diversity index by Chao (richness) between saliva and oral rinse were significantly different, but by Shannon (diversity) ware similar. Then, we separated into 5 groups according ages. The results demonstrated that community richness only between 20s and 30s groups was significantly different in saliva, whereas in oral rinse the 20s group was all significantly different when compared with all other groups. However, a community diversity between age remained similar in both sample types. Abundant bacterial phyla were Proteobacteria, Firmicutes, Bacteroidetes, Actinobacteria and Fusobacteria. Yet, compared with 30s, Firmicutes increased markedly in 50s in saliva (*P*-value = 0.047), and in oral rinse this difference significant since between 20s and 30s, 20s and 50s (*P*-value = 0.039 and 0.022, respectively). Then, Non-metric multidimensional scaling to visualize the closeness of bacterial composition structures between age ranges, the results showed that 30s was likely separated from older groups. In conclusion, our results suggested that ages may change bacteria diversity, and represented a preliminary oral microbiota information of Thai individuals in Bangkok and nearby provinces.

Keywords— Oral, Microbiota, 16S rRNA.

★★★

International Conference on

Business, Economics, Social Sciences & Humanities (ICBESH - 2019)

&

Applied Science, Management & Technology (ICASMT - 2019)

Bangkok, Thailand

28th May, 2019

Event Partner:

Conference Alert 360

www.conferencealert360.com

Publisher

International Institute of
Academic Research & Publications
L/1483, HB Colony, Phase - II, Dumduma
Bhubaneswar, Odisha, India, 751019
E-mail : info@iiarp.org
Visit for upcoming Conferences - **www.iiarp.org**

ISBN

978-81-939606-0-8